Center for Experimental
Nuclear Physics and
Astrophysics
University of Washington

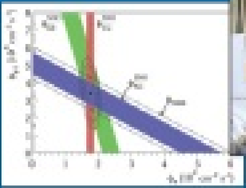

ANNUAL REPORT 2002

INTRODUCTION

CENPA pursues a broad program of research in nuclear physics, astrophysics and related fields. Research activities are conducted locally and at remote sites. The current program includes "in-house" research on nuclear collisions and fundamental interactions using the local tandem Van de Graaff, as well as local and remote non-accelerator research on fundamental interactions and user-mode research on relativistic heavy ions at large accelerator facilities in the U.S. and Europe.

Our Phase I determination of the astrophysical S-factor for the ^{7}Be(p,γ)^{8}B reaction has been completed and published. Phase II measurements are currently underway, and will result in a more accurate value and will provide additional data at lower proton energies.

The first analysis of the neutral-current-induced breakup of deuterium by ^{8}B solar neutrinos was completed for the pure heavy water phase of SNO operation (November 1999 to May 2001). A clear 5.3 σ excess of neutral-current events above what can be attributed to electron neutrinos was found, consistent with flavor transformation, neutrino oscillations, and mass.

The data from the pure heavy water phase was also analyzed with respect to day and night rates and a slight asymmetry of night over day for the charged current signal ($14 \pm 7\%$) was found. In a global two-flavor analysis incorporating the total spectral shape (NC + CC) in night and day from SNO as well as other solar-neutrino data, the LMA solution is strongly favored at more than the 99.5% confidence level.

Hadronic interactions of muons and their secondaries have now been incorporated into the SNO data analysis code.

Electronics for the neutral-current detector array have been completed, tested and shipped to Sudbury. Data-acquisition and analysis code has been written and is under test.

The upgrade to the emiT detector for investigation of time-reversal invariance violation in neutron beta decay has been completed, with new high-voltage withstand capability, analog fiber-optic links from the proton detector arrays, new surface-barrier detectors with thin and stable dead layers, and new preamplifiers.

Initial tests of an experiment to search for the ground state decay of ^{8}B were carried out, with expected production of a magnetically analyzed radioactive beam of ^{8}B at a few ions per second.

Study of lead perchlorate as a Čerenkov medium has been completed and the technique has been adopted for use by the OMNIS supernova detector.

Initial attempts to dissolve ^{100}Mo in liquid scintillator are encouraging. We are within a factor of two of developing a viable technique for use in a search for neutrino-less double beta decay of ^{100}Mo.

The hardware for welding and deployment of the NCD array has been completed and is being prepared for shipping to SNO.

The UW Electroweak Interactions group joined an international collaboration that has begun to build "KATRIN" (KArlsruhe TRItium Neutrino project), a next generation experiment aimed at making a precise determination of or limit on the mass of ν_e from tritium beta decay.

CENPA faculty have been involved in efforts to establish a National Underground Science Laboratory (NUSL) in the United States. A proposal for building the laboratory at the Homestake Mine in Lead, SD was submitted in June 2001 to the National Science Foundation.

Our short-range tests of the Newtonian inverse-square law, which test "large extra dimensions" and "fuzzy graviton" scenarios, have made substantial progress during the last year. We recently reported an upper limit of 200 micrometers on the maximum size of the largest extra dimension that couples to gravity. We are currently analyzing results taken with a new instrument that has about 50 times higher sensitivity. An even more sensitive instrument has been designed and should be taking data by the middle of the summer.

A major upgrade of the ^{199}Hg EDM experiment has been completed and should yield a factor of three improvement in a new EDM search now ready to begin.

Our event-by-event analysis of STAR data has revealed the development of complex correlation structures with strong centrality dependence in Au-Au collisions at RHIC energies, in contrast to results at CERN SPS energies. The dominant source of charge-independent correlation structure appears to be initial-state scattering, and centrality dependence seems to indicate the growth of a dissipative medium for more central events. Charge-dependent correlation structures are consistent with a possibly-related source opacity for the more central events.

The initial HBT results from STAR have produced several surprises, which the physics community has come to call "The HBT Puzzle". In particular, the source radius ratio R_{Out}/R_{Side}, expected for dynamical reasons to have a value between 2 and 10 reflecting long-duration pion source emission, instead has a value very close 1 over the whole range of the measurements, reflecting a very short emission duration and suggesting a very "hard" equation of state for the expanding system.

As always, we encourage outside applications for the use of our facilities. As a convenient reference for potential users, the table on the following page lists the capabilities of our accelerators. For further information, please contact Prof. Derek W. Storm, Executive Director, CENPA, Box 354290, University of Washington, Seattle, WA 98195; (206) 543-4080, or storm@npl.washington.edu. Further information is also available on our web page: http://www.npl.washington.edu.

We close this introduction with a reminder that the articles in this report describe work in progress and are not to be regarded as publications or to be quoted without permission of the authors. In each article the names of the investigators are listed alphabetically, with the primary author, to whom inquires should be addressed, underlined.

Derek Storm, Editor　　　　Barbara Fulton, Assistant Editor

TANDEM VAN DE GRAAFF ACCELERATOR

A High Voltage Engineering Corporation Model FN purchased in 1966 with NSF funds, operation funded primarily by the U.S. Department of Energy. See W. G. Weitkamp and F. H. Schmidt, "The University of Washington Three Stage Van de Graaff Accelerator," Nucl. Instrum. Meth. **122**, 65 (1974). Recently adapted to an (optional) terminal ion source and a non-inclined tube #3, which enables the accelerator to produce high intensity beams of helium and hydrogen isotopes at energies from 100 keV to 5.5 MeV.

Some Available Energy Analyzed Beams

Ion	Max. Current (particle μA)	Max. Energy (MeV)	Ion Source
^{1}H or ^{2}H	50	18	DEIS or 860
^{3}He or ^{4}He	2	27	Double Charge-Exchange Source
^{3}He or ^{4}He	30	7.5	Tandem Terminal Source
^{6}Li or ^{7}Li	1	36	860
^{11}B	5	54	860
^{12}C or ^{13}C	10	63	860
$*^{14}$N	1	63	DEIS or 860
^{16}O or ^{18}O	10	72	DEIS or 860
F	10	72	DEIS or 860
* Ca	0.5	99	860
Ni	0.2	99	860
I	0.001	108	860

*Negative ion is the hydride, dihydride, or trihydride.

Additional ion species available including the following: Mg, Al, Si, P, S, Cl, Fe, Cu, Ge, Se, Br and Ag. Less common isotopes are generated from enriched material.

BOOSTER ACCELERATOR

See "Status of and Operating Experience with the University of Washington Superconducting Booster Linac," D.W. Storm *et al.*, Nucl. Instrum. Meth. A **287**, 247 (1990). The Booster is presently in a "mothballed" state.

TANDEM VAN DE GRAAFF ACCELERATOR

A High Voltage Engineering Corporation Model FN purchased in 1966 with NSF funds; operation funded primarily by the U.S. Department of Energy. See W.G. Weitkamp and F.H. Schmidt, "The University of Washington Three Stage Van de Graaff Accelerator," Nucl. Instrum. Meth. **122**, 65 (1974).

Some Available Energy Analyzed Beams

Ion	*Max. Current* *(particle* m *A)*	*Max. Energy* *(MeV)*	*Ion Source*
^{1}H or ^{2}H	50	18	DEIS or 860
^{3}He or ^{4}He	2	27	Double Charge-Exchange Source
^{3}He or ^{4}He	30	7.5	Tandem Terminal Source
^{6}Li or ^{7}Li	1	36	860
^{11}B	5	54	860
^{12}C or ^{13}C	10	63	860
* ^{14}N	1	63	DEIS or 860
^{16}O or ^{18}O	10	72	DEIS or 860
F	10	72	DEIS or 860
* Ca	0.5	99	860
Ni	0.2	99	860
I	0.01	108	860

* Negative ion is the hydride, dihydride, or trihydride.

Additional ion species available include the following: Mg, Al, Si, P, S, Cl, Fe, Cu, Ge, Se, Br and Ag. Less common isotopes are generated from enriched material.

Contents

1 Fundamental Symmetries and Weak Interactions

Weak Interactions

1.1 Status of the emiT data acquisition system

M. A. Howe and J. F. Wilkerson

The emiT data acquisition (emiTDAQ) software that will be used for the second run of the emiT experiment is rapidly evolving into its final form. It is written in C++ and is compiled with the MetroWerks compiler for running on Macintosh computers. The emiTDAQ software uses much of the code base of the successful SHaRC program (see Section 2.8) that has been in routine operation at SNO for several years. The emitDAQ application is composed of object-oriented software modules that represent each of the emiT electronic hardware modules, a control task that coordinates the actions of those modules, and dialogs for initializing, controlling, and monitoring the emiT experiment.

A number of new software modules were developed for this run of emiT because the electronic hardware set has changed substantially. New hardware modules include a CEAN 755 TDC and a CEAN 862 QDC for acquisition of PMT data with timing information provided by a CENPA-built 100MHz latched clock. For digital control functions an Acromag IP320 I/O module and an Acromag IP220 DAC module have been added. The new modules enable the experiment to be run using only VME hardware instead of the mixture of CAMAC and VME hardware that was used in the first run of the experiment. Since each of these hardware objects is represented by a self contained object-oriented software object, it was possible to do systematic testing of the interaction of the various subsystems of the detector as the emitDAQ application was being developed. The figure below shows emiTDAQ being used during system validation testing.

The main control object of emitDAQ is a task that coordinates the activities of all of the software modules. One of the main modules the task is a well developed run control system for testing event readout of data in the current system. As well as providing a 'one-button' start run capability, it also provides controls for setting the length of a run and whether a run is to be repeated. In the developmental phase of the hardware/software the run control also provides controls for taking data with sub-parts of the system, i.e. just proton singles data, just TDC data, data with or without using the latched clock, etc. As the emiTDAQ matures, this part of the event readout software will be moved into an embedded processor which will read out the data

In addition to run control, the main dialog for the system shows a layout of the emiT hardware and is active in the sense that it shows a lot of information about the current state of the detector and the data rates. Maximum data rates are shown in bar graphs, but in the pictorial representation of the detector the rate for each channel is shown color coded in the place where that detector channel actually is in the detector. Clicking on a particular channel brings up a dialog that can be used to adjust the constants for that channel. By

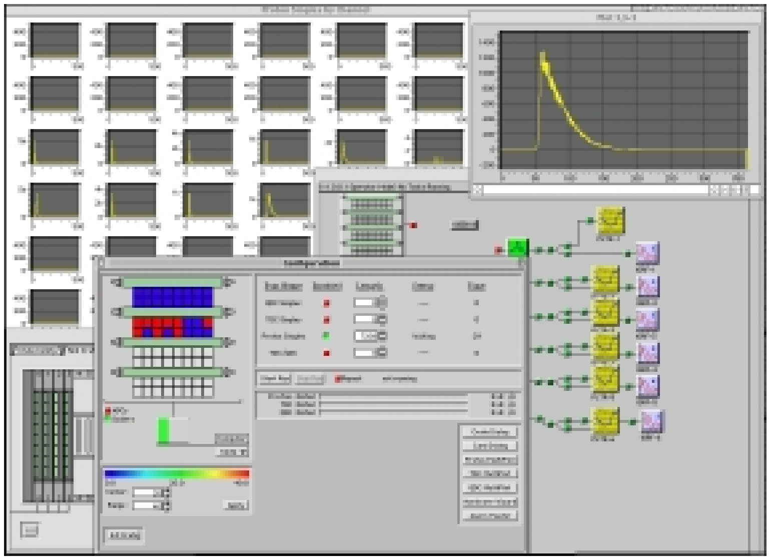

Figure 1.1-1. A screen dump of emiTDAQ during software validation tests.

clicking on other parts of the picture, dialogs for controlling or visualizing other parts of the detector can be displayed.

For monitoring the data, a multi-plot object was developed that shows a histogram of the data for every ADC channel on one page. There are also multi-plots for the TDC and QDC data. These allow the operator to quickly visualize the overall state of the detector, find dead channels, gain/threshold problems, etc. The multi-plot can also dump the data from each channel into a disk file for offline analysis.

The final data path is now under development. In this phase the actual event readout will be moved off the Mac and into an embedded eCPU running in the VME crate. The eCPU will monitor the latched clock for signals to proceed, read out hardware as required, bundle the data together with the timing information from the latched clock, and finally place the data into dual memory for access by the Mac for monitoring and storage.

1.2 Final preparations for a second run of the emiT experiment

L. Grout,* H. P. Mumm, A. W. Myers, P. Parazzoli,† R. G. H. Robertson, K. Sundqvist,‡ T. D. Van Wechel, D. I. Will and J. F. Wilkerson

The emiT experiment is a search for time-reversal (T) invariance violation in the beta decay of free neutrons. Current observations of CP(T) violation in the Kaon and B-meson systems can be accommodated within the standard model of particle physics. However, baryogenisis and attempts to develop unified theories indicate that additional sources are required. The standard model predicts T-violating observables in beta decay to be extremely small (second order in the weak coupling constant) and hence are beyond the reach of modern experiments.[1] However, potentially measurable T-violating effects are predicted to occur in some non-standard models such as those with left-right symmetry, exotic fermions, or lepto-quarks.[2,3] Thus a precision search for T-violation in neutron beta decay provides an excellent test of physics beyond the Standard Model.

The emiT experiment probes the T-odd P-even triple correlation between the neutron spin and the momenta of the neutrino and electron, $D\vec{\sigma}_n \cdot \vec{P}_e \times \vec{P}_\nu$, in the neutron beta-decay distribution. The coefficient of this correlation, D, is measured by detecting decay electrons in coincidence with recoil protons from a polarized beam of cold (2.7 meV) neutrons. Four electron detectors (plastic scintillators) and four proton detectors (large-area diode arrays) are arranged in an alternating octagonal array concentric with the neutron beam. The protons produced in the decay have a relatively low energy ($\leq$ 751 eV). While this allows for a delayed coincidence trigger between the proton and electron it increases the complexity of the detection scheme by requiring that the protons be accelerated using high voltage electrodes.

During the first run, high voltage related problems damaged electronic components, led to high background rates and ultimately produced a non-symmetric detector. Systematic effects were less effectively canceled due to the lack of full detector symmetry and a more complex data analysis scheme was required. The result, $D = -0.1 \pm 1.3 \times 10^{-3}$, represents a small improvement over the current world average.[4]

We have used an electrostatic modeling program to fully redesign the proton focusing assembly. The aim was to maintain focussing efficiency while reducing high field regions and minimizing the associated field emission, the dominate background during the first run. We have successfully constructed and tested four new electrodes based on this design. Initial tests indicate an accidental coincidence rate of approximately 10^{-5} Hz compared to an estimated signal of 20 Hz.

---

*Presently at MIT Lincoln Labs, Lexington, MA 02420.

†Presently at Los Alamos National Laboratory, Los Alamos, NM 87545.

‡Presently at Physics Department, University of Washington, Seattle, WA 98195.

[1] M. Kobayashi and T. Maskawa, Prog. Theor. Phys. **49**, 652 (1973).

[2] P. Herczeg, *Progress in Nuclear Physics*, W.-Y. P. Hwang, ed., Elsevier Sciences Publishing Co. Inc. (1991) p. 171.

[3] E. G. Wasserman, *Time Reversal Invariance in Polarized Neutron Decay*, Ph.D. thesis, Harvard University, (1994).

[4] L. J. Lising *et al*, Phys. Rev. C **62**, (2000) 055501.

To reduce dead-layer proton energy-loss we have decided to use surface barrier detectors having a thickness of 20 μg/cm^2 Au, a depletion region of 300 microns and an active area of 300 mm^2 for the second run. As cooling of these detectors is critical to achieving acceptable energy resolution, we have installed a new liquid nitrogen based system. The system enables cooling of the detectors to approximately -50 C with the minimal requirement that the dewar be refilled once a day. In addition, fabrication of redesigned low-power preamps is nearing completion.

To test the performance of our hardware a series of measurements using low energy gammas from a ^{133}Ba source have been made. These have demonstrated an energy resolution as good as 3 keV full width at half maximum and a background around 9 keV. Due to the complexity of the system, however, the average performance is typically around 6 keV FWHM.

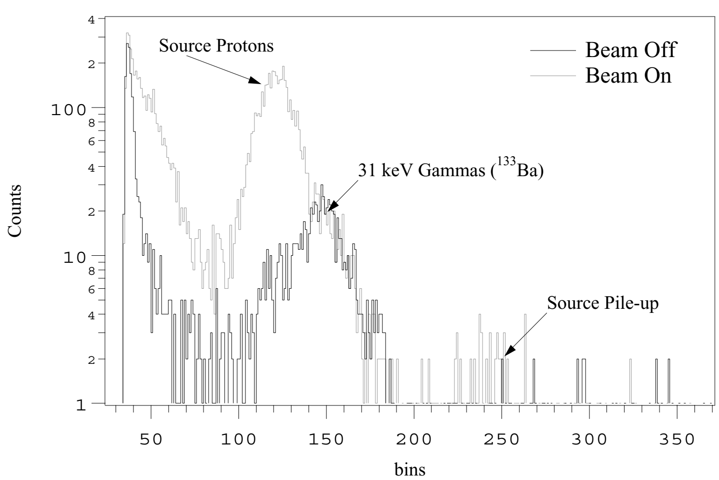

Figure 1.2-1. ^{133}Ba spectrum and proton source with electrode bias at -30 kV

We have also constructed a low energy, < 800 eV, low-intensity proton source to facilitate *in situ* characterization of our detectors[5] (see figure). Using this source we have directly measured detector thickness allowing a comparison with previous measurements using alpha particles.[6]

Considerable progress has been made on an upgrade and simplification of the data acquisition system. Code that allows detailed control and monitoring of much of the hardware is nearing completion (see previous section). In addition we have chosen to time-stamp individual proton and electron events allowing the use of a slow-software coincidence trigger. To this end a custom timing board with 10 ns precision has recently been constructed and tested. See Section 6.1.

Beam-line preparations for the second run are currently underway at NIST. Initial measurements indicate that the reactor upgrade has yielded the expected factor of 1.8 increase in flux. We estimate that emiT will begin collecting data in the middle of May 2002, likely reaching the goal of D $< 5 \times 10^{-4}$ during the fall of 2002.

[5]F. Naab, Nucl. Instrum. Methods, to be submitted.
[6]CENPA Annual Report, University of Washington (2001) p. 13.

1.3 Search for second-class currents in the mass-8 system

M. Beck,* R. Hazama, K. A. Snover and D. W. Storm

We are searching for second-class currents in the mass-8 system by comparing the weak magnetism plus second-class tensor form factors in beta decay with the isovector M1 matrix element for the photon transitions in ^{8}Be. CVC relates the isovector M1 and weak magnetism. The beta decay data were measured previously.[1] The form factors are extracted from the measured energy dependence of angular correlation coefficients. Preliminary results have been reported,[2] but there are remaining questions about the beta detector response functions. The detectors are plastic scintillator, consisting of a large cylinder preceded by a thin, smaller diameter paddle, and surrounded by a veto annulus.

We modeled the detectors' response to electrons and to positrons using GEANT. Before including any effect of photon statistics, we find (see Fig. 1.3-1) the electron response to be described by a narrow Gaussian with a low energy tail. The positron response, as expected, shows an additional high energy peak from annihilation radiation which registers in the detector. We have parameterized the GEANT response functions with a set of energy dependent parameters. Using these response functions, we plan to reanalyze the beta-decay

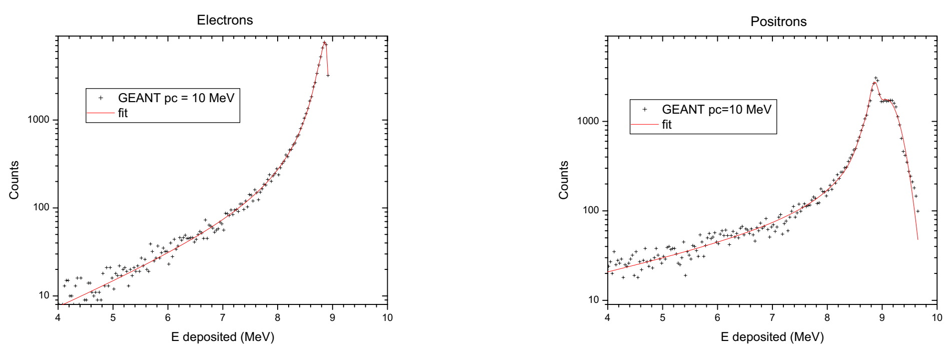

Figure 1.3-1. Spectra from the large plastic cylinder, for 10 MeV/c particles that pass through the paddle and do not register in the veto. Points are calculated with GEANT and the curves are the parameterized detector response functions.

data to obtain the sum of weak magnetism and second-class tensor form factors.

To obtain the isovector M1 matrix element for the analog transition in ^{8}Be, we have measured γ-spectra at three angles as a function of excitation energy in ^{8}Be. The ^{8}Be is made as a resonance with ^{4}He incident on a ^{4}He target, as has been described previously.[3,4]

The details of this analysis have been described previously,[3] and we are presently attempting to resolve some discrepancies in the data analysis.

*Presently at Katholieke Universiteit, Leuven, Belgium.

[1]Nuclear Physics Laboratory Annual Report, University of Washington (1998) p. 8.

[2]M. Beck *et. al.*, *Proc. 6th Conf. on the Intersections of Particle and Nuclear Physics*, 1997. AIP Conference Proceedings 412, 416.

[3]CENPA Annual Report, University of Washington (2001) p. 14.

[4]L. De Braeckeleer *et. al.*, Phys. Rev. C **51**, 2278 (1995).

1.4 Search for a permanent electric dipole moment of ^{199}Hg

W. C. Griffith, M. D. Swallows,* M. V. Romalis† and E. N. Fortson*

The measurement of a finite permanent electric dipole moment (EDM) on an atom or elementary particle would reveal a new source of CP violation beyond the standard model. Currently, the most precise limit on an EDM is given by our search for the EDM of ^{199}Hg. In the experiment, spin polarized Hg vapor, contained in quartz cells, is placed in parallel magnetic and electric fields, and the Larmor spin precession frequency is measured. The direction of the electric field is frequently reversed, and a nonzero EDM would manifest itself as a frequency shift correlated with the direction of the electric field. Our result of $|d(^{199}\mathrm{Hg})| < 2.1 \times 10^{-28}\, e$ cm,[1] was obtained using a two vapor-cell setup, which allowed for cancellation of frequency noise due to magnetic field fluctuations common to both cells. We have since been developing a four vapor-cell version of the experiment. The additional cells will allow for cancellation of magnetic field gradient noise, and will also improve our understanding of systematic effects by allowing us to measure magnetic fields due to charging and leakage currents.

All upgrades to the apparatus allowing it to accommodate four vapor cells have been completed. These included constructing new electrodes and a larger cell-holding vessel, and setting up optics and detectors for the additional light beams. Also, the data acquisition and analysis software was modified to accommodate the additional signals.

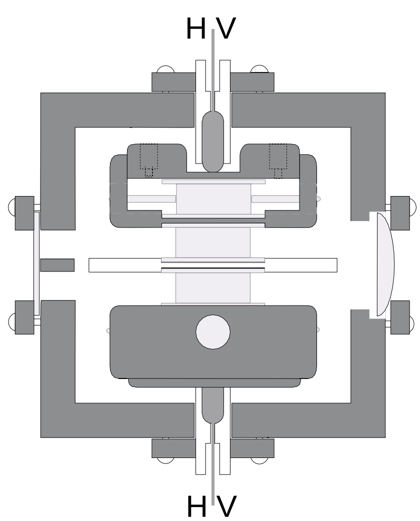

Figure 1.4-1. Cutaway view of the cell-holding vessel. High voltage ($\pm$ 10 kV) is applied to the middle two cells with the ground plane in the center, so that the electric field is opposite in the two cells. The outer two cells are enclosed in the HV electrodes (with light access holes shown for the bottommost cell), and are at zero electric field. A uniform magnetic field is applied in the vertical direction.

*Physics Department, University of Washington, Seattle, WA 98195.
†Princeton University, Princeton, NJ 08544.

[1] M. V. Romalis, W. C. Griffith, J. P. Jacobs and E. N. Fortson, Phys. Rev. Lett. **86**, 2505 (2001).

Several batches of new Hg-vapor cells have been prepared for use in the experiment. The cells used in our previous measurement contained a buffer gas composition of 90% N_2 and 10% CO and their spin coherence time tended to degrade after long term UV exposure. This was probably caused by damage to the paraffin cell wall coating from collisions with Hg atoms in the metastable 6^3P_0 state. While CO is effective in quenching Hg to the ground state, N_2 tends to quench to the metastable state. To avoid this behavior, the new cells use pure CO buffer gas, which has led to longer and more stable spin relaxation times.[2]

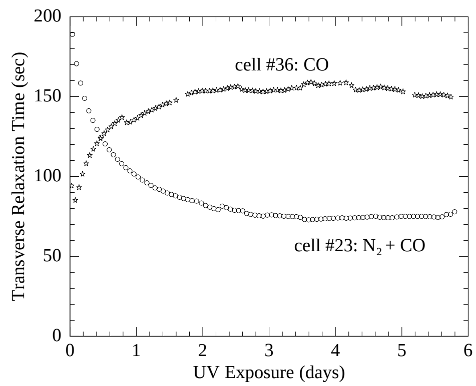

Figure 1.4-2. Effect of UV exposure on transverse spin relaxation time. The relaxation time for the cell containing 90% N_2 and 10% CO quickly drops below 100 seconds, while in the cell containing pure CO the relaxation time initially increases and then is stable.

We also investigated a possible source of noise due to light shifts affecting the atomic magnetization direction. Spin polarization is achieved through optical pumping with circularly polarized light directed perpendicular to a magnetic field of 20 mG and chopped at the Larmor frequency of the ^{199}Hg spins. If the chopping frequency does not match the Larmor frequency exactly, then a small amount of Hg magnetization is rotated into the vertical direction (parallel to the magnetic field) due to the Zeeman light shift. Later, the probe beam, which is linearly polarized but acquires a small circular polarization by passage through the spin polarized vapor, produces a light shift that rotates the vertical magnetization back into the plane of precession, but phase shifted from the main component of magnetization, leading to a change in the measured Larmor frequency. We combat this effect by taking several steps to reduce the buildup of vertical magnetization. We installed a lock system for the laser that allows us to set the wavelength of the pump light at the point of zero light shift. Furthermore, we have taken measures to ensure that the chopper frequency better matches the Hg Larmor frequency in each of the four cells. Previously, the frequencies in the four cells differed by a part in 10^4 due to magnetic field gradients. We have installed gradient compensation coils so that the four precession frequencies match to a part in 10^6. The chopper frequency is then set precisely to the measured Larmor frequency using a function generator.

Overall, these improvements have resulted in a factor of three improvement in our statistical sensitivity per unit time, and we are presently preparing to start accumulating data towards a new measurement of the EDM of ^{199}Hg.

[2] M. V. Romalis and L. Lin, submitted to Phys. Rev. A.

Torsion Balance Experiments

1.5 Sub-mm test of Newton's inverse-square law

E. G. Adelberger, M. C. Feig, J. H. Gundlach, B. R. Heckel, C. D. Hoyle,*
D. J. Kapner, U. Schmidt† and H. E. Swanson

Since our last report,[1] we have continued testing the gravitational inverse-square law at even shorter distances. Our experiments are principally motivated by higher-dimensional string theories that predict deviations from the gravitational inverse-square law at short distances,[2] and by attempts to understand the observed cosmological constant that speculate about similar modifications.[3] These deviations are typically parameterized as an addition of a Yukawa term to the Newtonian potential,

$$V(r) = -G(\frac{m_1 m_2}{r})(1 + \alpha e^{-r/\lambda}). \tag{1}$$

The basic geometry of our experiment has remained the same, consisting of a thin metal disc with an azimuthally symmetric array of holes, suspended from a 20μm diameter tungsten fiber. A thin attractor disc, with a geometry similar to that of the pendulum disk rotates beneath the pendulum. A third, thicker disc, is attached to the bottom of the thin attractor so that its holes are out of phase with the upper attractor, canceling the Newtonian torques between the thin attractor and the pendulum.

To improve the sensitivity of our experiment to these potential deviations, we consider the following simplified scaling of the torque produced by a Yukawa potential term.

$$\tau_y \propto \frac{\alpha G \rho_1 \rho_2 A \lambda^4 e^{-s/\lambda}}{s} \tag{2}$$

where ρ_1 and ρ_2 are the densities of the two thin discs, A is the total area of the holes in a disc, and s is the vertical separation between the pendulum and attractor. To increase the signal from a Yukawa interaction, we can increase the densities of the discs, increase the areas of the holes, and decrease the separation. We have done all of these things.

By using molybdenum for both the pendulum and attractor, we increased the product of the densities by a factor of four over our published result.[4] We added a second row of holes to the pendulum and attractor to increase the interacting area, and installed a class 10,000 clean room to reduce the dust contamination that was limiting our vertical separation.

We have also come up with a satisfactory way to eliminate electrostatic potentials in our experiment. We have always isolated our pendulum and attractor electrostatically by stretching a $10\mu m$ thick gold-coated beryllium-copper membrane between them. In the past

*Presently at University of Trento, Italy.
†Presently at Physikalisches Institut, Heidelberg, Germany.
[1]CENPA Annual Report, University of Washington (2001) p. 2.
[2]See, for example, N. Arkani-Hamed *et al.*, Phys. Lett. B **429**, 263 (1998).
[3]G. Dvali *et al.*, hep-th/0202174 v1.
[4]C. D. Hoyle *et al.*, Phys. Rev. Lett. **86**, 1418 (2001).

we have deposited a gold coating via resistive evaporation onto the pendulum surface to eliminate any electrostatic wells that may exist between the pendulum disc and the membrane. For our most recent data, we did not deposit this coating on the molybdenum, as we feared that the chromium adhesion layer might introduce some unknown magnetic effect.

Without this gold coating, we noticed two effects. First, our pendulum period varied with height above the membrane, belying a height-dependent electrostatic potential. This is to be expected, as there is a small contact potential difference between molybdenum and gold. We found that we could eliminate this effect by applying a reverse voltage. A less benign effect was the increase in noise as we moved our pendulum very close to the membrane. This could be due to small motions of the pendulum relative to the membrane. The reverse voltage served to reduce this effect as well.

To avoid this problem, we now gold coat our pieces with a sputtering technique. By first sputtering our substrate ("etching"), we remove any thin oxide layers, the usual culprit in poor adhesion. We then sputter gold onto this fresh surface. We have found that sputtered layers of gold are more durable on our substrates than those from resistive evaporation.

With existing data taken with a 22-fold symmetric system, we have improved our sensitivity substantially; pending analysis should show our experiment to be sensitive to large extra dimensions with sizes as small as $100\mu m$.

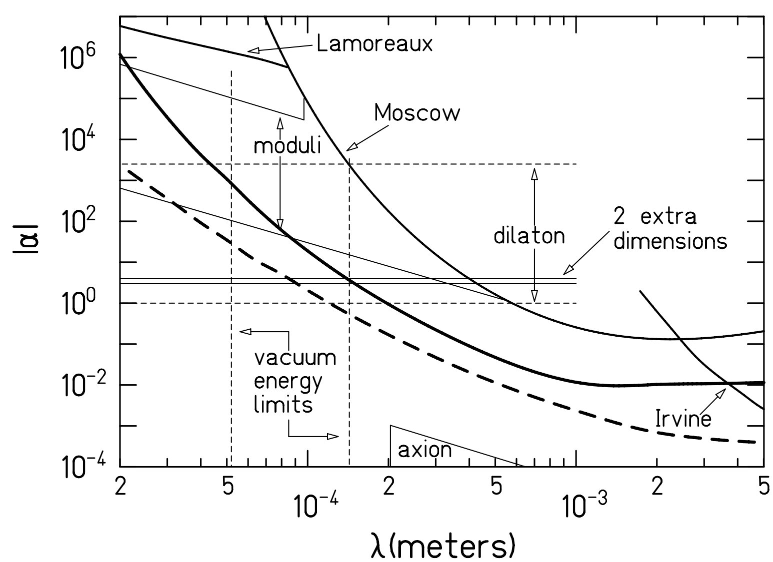

Figure 1.5-1. (α,λ) Parameter space.The heavy solid line shows existing Eöt-Wash limits, while the dashed line shows our expected sensitivity from existing data, if a null result is found.

1.6 A new equivalence principle test

E. G. Adelberger, T. W. Butler, K.-Y. Choi, J. H. Gundlach, B. R. Heckel,
D. J. Kapner, S. M. Merkowitz,* U. Schmidt† and H. E. Swanson

Practically every attempt at formulating quantum gravity, as for example string, or M-theory, predicts new, subtle, gravitational effects. Precision experimental tests of gravity, as for instance equivalence principle (EP) tests, have therefore emerged as important tests of fundamental physics. Theoretical predictions for an EP-breakdown are tantalizingly close to the sensitivity of modern torsion balances.

We have over the past few years constructed a new continously rotating torsion balance. The instrument is in operation undergoing systematic tests. Its key features include the following:
High rotation rate: A fast rotation rate will minimize statistical noise which has predominantly 1/f-character. The instrument is rotated with a direct-driven air-bearing turntable, stabilized with a tight feedback loop to a high-resolution angle encoder. For angle encoder non-linearities of up to the 9th harmonic of a revolution, we establish a correction function by operating the turntable at two different speeds. From the response of the pendulum at these two speeds we calculate the harmonic correction function.

Tilt elimination: A turntable rotation axis misalignment from vertical produces a rotation of the pendulum at the signal frequency. We eliminate the axis tilt using an active leveling mechanism.[1] The system functions well, leaving an unresolved periodic tilt of less than 3 nrad.

Vibration isolation: The balance's day-time noise performance is worsened by vertical building vibrations. We built a vibration isolater for the torsion-fiber top attachment with 3 leaf springs. An eddy current damper damps the vertical motion and pendulum motion. Day and nighttime noise performances are now equal.

New pendulum design: We have built an aluminum pendulum with eight 5-g test bodies, seated in cones and held on by a small screw. The repeatability of the vertical test body placement is better than <5 μm. We have sets of Al, Be and Ti test bodies.

Gravity gradient compensation: The instrument is surrounded by precisely machined compensators to eliminate the ambient gravity gradient with l=2, m=1,2 and l=3, m=1. The uncompensated gravity gradients were measured with special test bodies that augmented the corresponding pendulum moments. To minimize the pendulum's gravitational moments, the compensators were rotated about the pendulum so that they add to the ambient gradient.

We are currently operating the instrument with a composition dipole. Once the instrument has come into an equilibrium state, our statistical uncertainty in one day of operation is $\approx$2 nrad, corresponding to 1.2×10^{-12} cm/s^2.

---

*Presently NASA/GSFC, Greenbelt, MD 20771.

†Presently at Physikalisches Institut, Heidelberg, Germany.

[1] CENPA Annual Report, University of Washington (2001) p. 4.

1.7 Numerical calculation for the short-range inverse-square law test

E. G. Adelberger, B. R. Heckel, D. J. Kapner and U. Schmidt*

Our short-range test of Newton's inverse-square law requires a high precision calculation of the expected Newtonian torques acting on our pendulum. The "test bodies" of our pendulum and attractor are azimuthally symmetric arrays of holes in flat metal discs. To calculate the torques on our pendulum, we must start by calculating the gravitational force between two cylinders. In our planar geometry, it is the x-component of the force between the cylinders that produces a torque along the axis of our torsion fiber. This component is computed as the six-dimensional integral:

$$F(dx, dz)_x = G\rho_1\rho_2 \int d^3r_1 \int d^3r_2 \frac{x_1 - x_2}{[(x_1 - x_2)^2 + (y_1 - y_2)^2 + (z_1 - z_2)^2]^{3/2}} \tag{1}$$

where the limits for r_1,r_2 are the physical boundaries of the two cylinders. We work in a Cartesian system; the x and z integrations are performed analytically, while the y integrations are performed numerically using a Romberg integration scheme. The results of two independent calculations of F_x vs. dx, one written in Mathematica, one written in C, agree within their fractional precisions ($< 10^{-6}$).

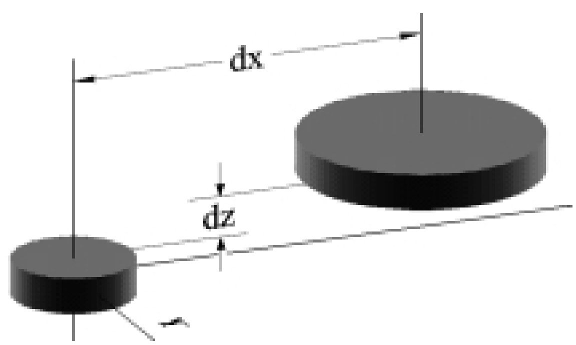

Figure 1.7-1. Coordinate System for Calculating the Force between two cylinders.

Knowing F_x, we then calculate the harmonic components of the torque on the pendulum as a function of attractor rotation angle. For our current geometry, a 22-fold azimuthally symmetric system, our *first harmonic* occurs with a frequency 22 times that of the attractor rotation, while the *second harmonic* has twice that frequency, *etc.*

Our attractor actually consists of two stacked discs. The upper, thin, disc produces a Newtownian torque on the pendulum, plus whatever torque arises from a short-range Yukawa force. The lower, thicker attractor has holes that are placed out of phase with the upper attractor, serving to cancel Newtonian torques on the pendulum. The cancellation is not perfect, but reduces the expected Newtonian signal by a factor of 50.

Several parameters are needed to calculate these harmonics. For each plate, the parameters are the hole radii in the discs, the vertical spacing to the pendulum (dz), and the

*Presently at Physikalisches Institut, Heidelberg, Germany.

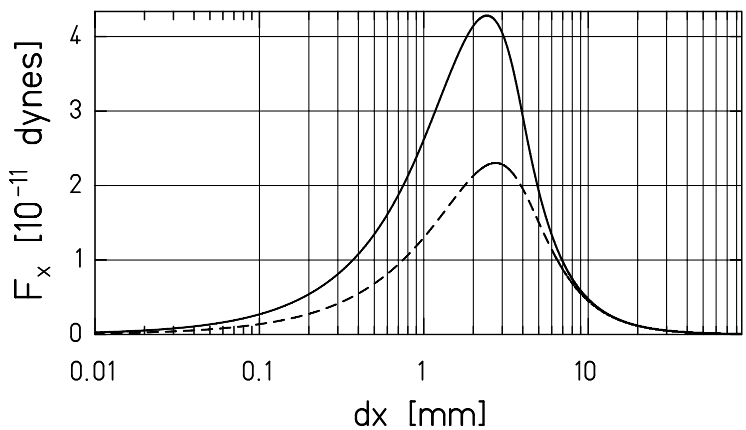

Figure 1.7-2. The x component of the force between two Molybdenum cylinders of radii 2.4 and 1.6mm as a function of dx. The solid line is for $dz = 50\mu m$ while the dashed line is for $dz = 1050\mu m$.

horizontal offset between the pendulum and attractor axes (dR). To combine the torques from the two plates, we have additional parameters: the gap between the attractor discs (t), and the angle between the hole patterns of the two discs (θ). We then have the Newtonian torque,

$$\tau_N(r_p, r_{ua}, r_{la}, t, \theta, dR, dz) \tag{2}$$

where r_{ta}, r_{ba} are the radii of the holes of the upper and lower attractor.

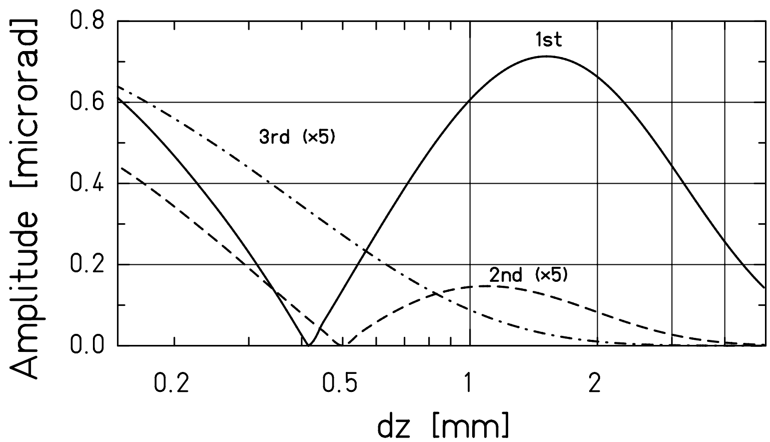

Figure 1.7-3. The first three harmonic components of the torque for ideal parameters of our 22-fold symmetric system.

1.8 Computer controlled torsion fiber damping routine

E. G. Adelberger, S. Beckman,* M. C. Feig, B. R. Heckel, D. J. Kapner and H. E. Swanson

Because the pendulum fiber for the sub-millimeter experiment is so weak, even small influences such as seismic effects, pressure bursts, or accidental contact with the attractor plate can cause the pendulum to twist wildly. The energy in the twist motion must be damped out and the pendulum brought back onto the detector before data taking can resume. The damping can be done manually, but the process is tedious and time consuming. Greatly complicating matters is the fact that the detector is only 0.1 degrees wide, but the pendulum often acquires an amplitude several times this value. We have written a C program to perform the damping more efficiently and accurately.

The damping program interacts with the apparatus in two ways. First, it reads information from the detector for one full period of the pendulum to determine its current motion. This portion of the code is very similar to the data acquisition routines used during experiments except that the sampling rate is set much higher, 20 points per second, to account for the higher speed of the pendulum. Second, the program can alter the pendulum's motion via a motor that rotates the point of suspension of the fiber. The motor does not directly affect the current angular position of the pendulum, but rather changes the equilibrium angle of the oscillation.

The most complicated portion of the code is the motion fitting routine. The data are handled in a variety of different ways depending on two parameters: the number of good data points and the number of times the pendulum crosses through the detector during the period. Using whichever method, a fit is performed to determine the amplitude and phase of the oscillation and the offset of the equilibrium position. From this information, two adjustments are calculated, one to be made at the maximum of the oscillation and one at the minimum, which should return the pendulum to a stationary position centered on the detector. These changes are then sent to the motor.

The damping program has been tested out in a variety of situations and is typically able to reduce the amplitude by a factor of 50, and thus the energy by a factor of 2500, in a single run. If the initial oscillation is especially large, the program can be run iteratively until the motion is damped sufficiently. The limiting factor is the step size of the motor, 0.001 degrees. This is more than adequate, however, to ensure that the pendulum remains on the detector for the entire period.

A single run of the damping routine takes approximately two periods, one period for data taking and one period for the adjustments at the maximum and minimum. Depending on the specific fiber used, the pendulum period is about 500 seconds, so the program can effectively damp the pendulum in eight to 16 minutes. And since the process is automated, the only time commitment for the user is to begin a run and check back on the results at the end.

*Department of Physics, University of California, Berkeley, CA.

1.9 Finite element analysis of capacitance for pendulum in $1/r^2$ test

E. G. Adelberger T. W. Butler and D. J. Kapner

We are in the process of using finite element analysis to calculate the capacitance between the short-range torsion pendulum and the thin beryllium-copper screen that electrostatically isolates it from the attractor mass. This calculation will be used to determine more accurately the separation between the pendulum and attractor mass.

The short-range experiment tests the gravitational inverse square law by monitoring the interaction between the pendulum and attractor mass at a number of different heights. Consequently, the height of the pendulum above the attractor is one of the most significant parameters in the experiment. The height is obtained from measurements of the capacitance between the pendulum and electrostatic screen. In order to use these measurements to obtain heights, we must know the functional dependence of capacitance on height. Capacitance measurements were made at a number of different heights above the screen. While we were unable to directly measure the absolute height of the pendulum, the measurements did give the shape of the capacitance versus height (CH) curve. The absolute height was then determined by a fitting procedure. The fitting procedure relied on an analytical expression for the functional dependence of capacitance on height that included a number of approximations to account for edge effects and finite thickness. In addition, the expression assumed that any contribution to the capacitance resulting from the pendulum support frame and the surrounding electrostatic shield was independent of the separation between the pendulum and the screen that is held at equipotential with the beryllium-copper screen. Thus it is desirable to verify the result determined from this semi-empirical procedure in an independent manner. It was proposed that finite element analysis (FEA) could be used to calculate an absolute CH curve for the pendulum and electrostatic screen. The advantage of FEA is that it requires much less geometric approximation than analytical methods.

I have begun an effort to use ANSYS, a widely distributed commercial FEA program, to make calculations of the capacitance of the short-range geometry. I have been able to use ANSYS to reproduce capacitance values of geometric configurations that admit exact analytical solutions. I have also constructed an accurate model which includes the short-range pendulum, the pendulum support frame, the beryllium-copper screen, and the surrounding electrostatic shield. ANSYS is able to take advantage of the 22-fold symmetry of the pendulum, which greatly reduces computational time and increases the accuracy of the calculations. Preliminary calculations have been made which show good agreement with the semi-empirical capacitance values.

1.10 Torsion balance test of CPT and Lorentz symmetries

E. G. Adelberger, B. R. Heckel, J. H. Gundlach and M. White

The standard model of particle physics is invariant under Lorentz and CPT symmetries. However, in an extended theory that combines the standard model with gravity, Lorentz and CPT symmetries may be spontaneously broken. Colladay and Kostelecky[1] have developed a consistent picture of new particle couplings that arise if CPT and Lorentz symmetries are broken. They pointed out that torsion balance measurements with a spin polarized pendulum provide the most sensitive test for these symmetry violations in the electron sector of their model.

In previous work, we developed a spin-polarized pendulum by stacking four rings of permanent magnets.[2] Each ring had the form of a hollow octagon with four consecutive magnets made from Alnico V material and the remaining four from $SmCo_5$. The magnetization in the Alnico comes entirely from electron spin polarization while that in SmCo has a substantial contribution from the orbital magnetization of the Sm ions. The assembled octagons were magnetized as a unit, forcing the magnetization to run inside the octagon, leaving only a small leakage magnetic field outside of the octagon. The stacked octagons were placed inside of a magnetic shield to complete the spin pendulum. We estimated that there were 8×10^{22} uncompensated spins in the assembled pendulum, with a leakage field of less than 0.2 mGauss outside of the shield. The pendulum was operated in the EotWash II apparatus to search for new pseudo-scalar fields.

To search for CPT and Lorentz symmetry violation, we have rebuilt the spin pendulum. The octagon segments were magnetized individually to the same level of magnetization, making the leakage field from the assembled stack small enough to eliminate the need for an entire magnetic shield. Instead, two layers of magnetic shielding foil now encircle the pendulum, resulting in a reduction by over a factor of two of the pendulum mass. The leakage field from the new spin pendulum is 0.7 mGauss at a distance of 3 cm from the pendulum. The 120-g pendulum is now supported by a 30-micron diameter W fiber, increasing the sensitivity to torques by a factor of 7 over our original spin pendulum. The largest systematic error in the original experiment came from spurious signals associated with the tilt of the rotation axis of the apparatus. The "feetback" leveling system, described in the 2001 Annual Report[3] has eliminated tilt as a limitation for the new measurements.

The new spin pendulum has been mounted in the EotWash II apparatus and data collection has begun. The signature of CPT and Lorentz symmetry violation is a torque on the pendulum that couples to an axis fixed in space. We rotate the entire apparatus with a period of 1600 sec. to produce a signal that would have the same period. Preliminary data exceeds our original sensitivity by a factor of five and we anticipate an overall increase by a factor of 30 for this measurement, corresponding to an anomalous coupling to spin of less than 10^{-21} eV.

[1] D. Colladay and V. A. Kostelecky, Phys. Rev D. **55**, 6760 (1997); *ibid.* **58**, 116002 (1998).
[2] M. G. Harris, Ph.D. thesis, University of Washington, 1998.
[3] CENPA Annual Report, University of Washington (2001) p. 4.

2 Neutrino Research

SNO

2.1 Solving the solar neutrino problem at SNO: Evidence for the flavor transformation of solar ^{8}B neutrinos

K. M. Heeger and the SNO Collaboration

For more than 30 years, experiments have detected neutrinos produced in the thermonuclear fusion reactions which power the Sun. These reactions fuse protons into helium and release neutrinos with an energy of up to 15 MeV. Data from these solar neutrino experiments were found to be incompatible with the predictions of solar models. More precisely, the flux of neutrinos detected on Earth was less than expected, and the relative intensities of the sources of neutrinos in the sun were incompatible with those predicted by solar models. With the recent measurements of the Sudbury Neutrino Observatory (SNO), it has finally become possible to test the solar model predictions and the particle properties of neutrinos independently.

The measurements at the Sudbury Neutrino Observatory (SNO) show that the neutrino flux produced in the $^8\mathrm{B} \rightarrow {}^8\mathrm{Be}^* + \mathrm{e}^+ + \nu_e$ beta-decay reaction in the Sun contains a significant non-electron type component when measured on Earth. This measurement is the first direct evidence for the flavor transformation of solar neutrinos. This neutrino flavor conversion indicates that neutrinos have mass. Together with the oscillation signature in atmospheric neutrino studies, these results are strong evidence for mixing in the lepton sector and new physics beyond the Standard Model.

Located 2-km underground in an active nickel mine in Sudbury, Ontario, the Sudbury Neutrino Observatory is a water Čherenkov detector specifically designed to study the properties of solar neutrinos. It consists of a spherical acrylic tank filled with 1000 tonnes of heavy water and surrounded by 7000 tonnes of light water to shield it from b ackgrounds. The choice of D_2O as a target material makes the SNO detector unique in comparison with other solar neutrino detectors. It allows SNO to measure both the total flux of solar neutrinos as well as the electron-type component of the neutrino flux produced in the Sun.

Solar neutrinos from the decay of ^{8}B are detected via the charged-current reaction on deuterium ($\nu_e + d \rightarrow p + p + e^-$) and by elastic scattering off electrons ($\nu_x + e^- \rightarrow \nu_x + e^-$). Some 9,500 photomultiplier tubes (PMTs) are used to record the Čherenkov signature of these neutrino interactions. The charged-current reaction is sensitive exclusively to ν_e while the elastic-scattering reaction also has a small sensitivity to ν_μ and ν_τ. Neutrinos also interact through the neutral-current reaction ($\nu_x + d \rightarrow p + n + \nu_x$). The neutron produced in the NC interaction thermalizes in the heavy water and captures on deuterium, emitting a characteristic 6.25-MeV γ. All three interaction rates have been measured in SNO.

SNO has been online since November 1999 taking production data, calibration data, and background measurements. The current SNO results are based on 306.4 live days of data taken between November 2, 1999, and May 27, 2001. Using the characteristic radial and

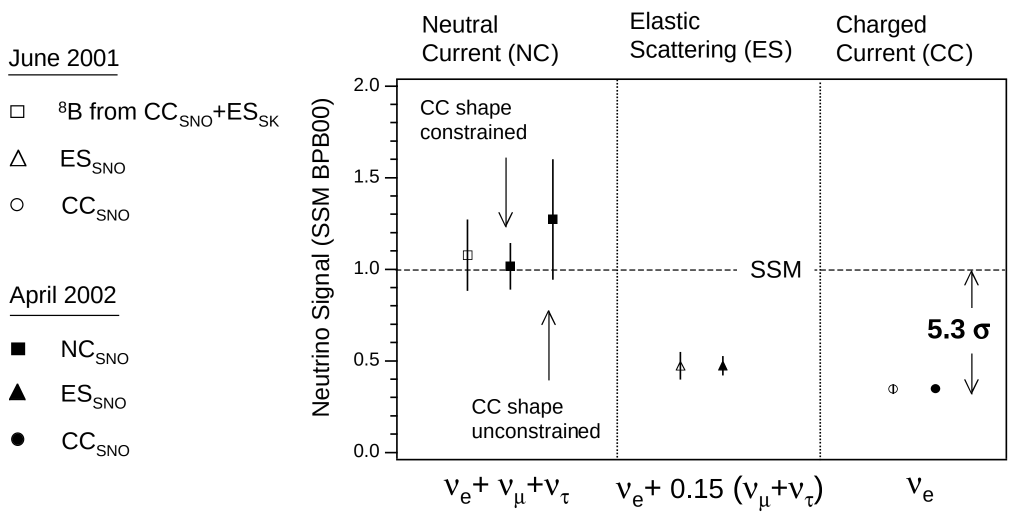

Figure 2.1-1. SNO's solar neutrino flux measurements in units of standard solar model predictions (BPB00). About 2/3 of the active solar neutrino flux consists of flavors other than ν_e. The difference between the total flux of ^{8}B neutrinos and the ν_e flux provides evidence at the 5.3 σ level for the flavor transformation of solar neutrinos.

solar angle distributions as well as the energy spectrum of γ's from neutron capture events on deuterium, the neutrino candidate event set is resolved into contributions from charged-current interactions, elastic scattering, and neutron events. Backgrounds from radioactivity in the D_2O and H_2O are measured by regular low-level radioassays of U and Th decay chain products and from a lower-threshold neutrino signal analysis. In common with all previous solar neutrino experiments, SNO observes a reduced flux of ν_e from the Sun compared to solar-model predictions.

A comparison of the charged-current and neutral-current interaction rates is used to test the hypothesis of neutrino flavor transformation. The charged-current reaction on deuterium is sensitive exclusively to ν_e while the neutral-current interaction is sensitive to ν_μ and ν_τ, as well as ν_e. Under the assumption of no spectral distortions in the CC spectrum the difference between the CC and NC interaction rates is more than 5.3 σ. This is clear evidence for the non-electron flavor component of the solar neutrino flux. Without the constraint on the CC spectrum SNO makes a model-independent determination of the ^{8}B flux. The measured total flux of solar ^{8}B neutrinos is in good agreement with solar model predictions. We note that the total ^{8}B neutrino flux deduced in June 2001 from SNO's measurement of the charged-current interaction and Super-Kamiokande's measurement of the elastic scattering of ^{8}B neutrinos is in excellent agreement with SNO's neutral-current measurement published this year. The results of this work are summarized in Fig. 2.1-1 and have been submitted for publication.[1]

[1] Q. R. Ahmad *et al.*, LANL arXive, nucl-ex/0204008, nucl-ex/0204009.

2.2 Muon spallation neutrons at the Sudbury Neutrino Observatory

Q. R. Ahmad,* J. A. Formaggio, R. Hazama, J. L. Orrell, R. G. H. Robertson, M. W. E. Smith and J. F. Wilkerson

Muons produced by cosmic-ray interactions in the Earth's atmosphere reach the SNO detector even at its 6010 m water equivalent depth. Muons both Čerenkov radiate and interact electromagnetically with nuclei as they pass through the SNO detector. Continuing previous work,[1] spallation neutrons produced by the passage of high energy muons have been studied.

The passage of muons through the SNO detector is distinct from the neutrino interactions. The amount of Čerenkov light produced by a muon is orders of magnitude greater than that produced by the resultant electrons of neutrino interactions. This higher energy signal allows for easy separation of the muons from neutrinos. The ability to separate out the muons allows for the selection and/or removal of muon spallation products which produce subsequent events. It has been shown that the muon spallation products are predominately neutrons by comparing the events which follow muons with single neutron Monte Carlo calculations and also with data from neutron calibration sources.

The capture of a neutron on a deuteron, $d(n,\gamma)t$, produces a mono-energetic gamma ray with an energy of 6.25 MeV. This mono-energetic gamma can be used as a calibration source. Spallation neutrons provide a constant, uniformly distributed, and container-less calibration source which has been used to study SNO's low energy response for both energy scale and temporal variations.

One use of this neutron data set is as a "blindness" tool. Once the spallation neutrons are flagged, they can be reinserted into the neutrino data set. This has the effect of increasing the apparent neutral current (NC) component of the solar neutrino flux. This blindness scheme was instituted for the current salt phase of SNO as one way of hiding the true NC number from the analyzers.

Muon spallation neutrons have also been studied in support of a day *vs.* night neutrino analysis.[2] The goal of the study was to determine if there are day-night asymmetries in the rate of muon induced spallation neutrons. It was determined that the spallation neutron rate had a day-night asymmetry $A = 2(\phi_D - \phi_N)/(\phi_D - \phi_N) = 2.2 \pm 5.9\%$, which is consistent with zero. These neutrons were also used to compare the low energy response of the detector day vs. night - another potential asymmetry.

Recent work has begun the process of comparing theoretical predictions of neutron production from muons to that which SNO measures. In addition Monte Carlo algorithms are in the early stages of integration in the SNO Monte Carlo and analysis code framework. It is expected that muons and their spallation products will remain a fertile non-neutrino physics topic.

---

*Presently at Sapient Corporation, Cambridge, MA 02142.
[1] CENPA Annual Report, University of Washington (2001) p. 23.
[2] arXiv.org pre-print: nucl-ex/0204009.

2.3 Electron antineutrino studies at the Sudbury Neutrino Observatory

S. R. Elliott, C. E. Okada,* J. L. Orrell, R. G. H. Robertson and J. F. Wilkerson

Electron antineutrinos, $\bar{\nu}_e$, interact in SNO's heavy water via a charged-current weak interaction with deuterium nuclei, d:

$$\bar{\nu}_e + d \rightarrow e^+ + n + n \qquad Q = -4.03 \text{ MeV} \qquad (\mathrm{CC}_{\bar{\nu}_e})$$

The positron, e^+, and neutrons, n, produced by this reaction can give detectable signals in SNO. If the positron has sufficient energy, it will Čerenkov radiate as it passes through the heavy water. Each neutron can capture on another deuterium nucleus releasing a 6.25 MeV gamma-ray which will also produce a detectable signal. Reaction $\mathrm{CC}_{\bar{\nu}_e}$ provides a distinctive signature which is separable from the "background" of other processes occurring in the SNO detector. The distinctive signature is the time coincidence of SNO events due to each of the three product particles.

In Table 2.3-1 we list sources of electron antineutrinos and give a preliminary estimate of the $\mathrm{CC}_{\bar{\nu}_e}$ event rate in SNO.[1] One background to the $\mathrm{CC}_{\bar{\nu}_e}$ signal is an accidental coincidence

$\bar{\nu}_e$ Source	# $\mathrm{CC}_{\bar{\nu}_e}$ $(\mathrm{kT{\cdot}Yr})^{-1}$	Comment
Atmospheric	10	Potential 1st $\Phi^{\mathrm{atmo}}_{\bar{\nu}_e}/\Phi^{\mathrm{atmo}}_{\nu_e}$ measurement
Nuclear Power Reactors	2	Precisely calculable
Supernova Relic	0.1	
Terrestrial	0	Below $\mathrm{CC}_{\bar{\nu}_e}$ threshold
Solar	*<100*	*Based on current best limits*

Table 2.3-1. Preliminary estimates of the $\mathrm{CC}_{\bar{\nu}_e}$ rate in SNO.

of uncorrelated SNO events. The accidental coincidence rates are given by

$$r_{\mathrm{acc.},2} = r^2 t_w \qquad r_{\mathrm{acc.},3} = r^3 {t_w}^2 \qquad (\text{for } rt_w \ll 1)$$

where $r_{\mathrm{acc.},2}(r_{\mathrm{acc.},3})$ is the rate of accidental coincidences of 2(3) SNO events in a given time window, t_w, with a single event rate r, after instrumental cuts are applied. A preliminary analysis determined that the SNO single event rate (after cuts) was 2.61×10^{-4} events/second. The neutron's mean capture time on deuterium in pure heavy water is ≈40 ms. The coincidence window, t_w, is chosen to be large compared to the mean neutron capture time and 500 ms is a good preliminary choice. Using these values we determine the accidental coincidence rates:

$$r_{\mathrm{acc.},2} = 3.4 \times 10^{-8} \quad \mathrm{Hz} \qquad r_{\mathrm{acc.},3} = 4.4 \times 10^{-12} \quad \mathrm{Hz}$$

These values support the belief that an electron antineutrino search in SNO's data is feasible even though the expected $\mathrm{CC}_{\bar{\nu}_e}$ event rate is low.

---

*Institute of Nuclear and Particle Astrophysics and Nuclear Science Divison, Lawrence Berkeley National Laboratory Berkeley, CA.

[1]References: The atmospheric & nuclear power reactor numbers are internal SNO calculations, the supernova relic numbers are from M. Kaplinghat *et al.*, Phys. Rev. D **63**, 043001 (2001), and the solar number is based on a limit from M. Aglietta *et al.*, JETP **63**, 791 (1996).

2.4 Neutron backgrounds from cosmic rays and atmospheric neutrinos in SNO

Q. R. Ahmad,* J. A. Formaggio, R. Hazama, J. L. Orrell, R. G. H. Robertson,
M. W. E. Smith and J. F. Wilkerson

The Sudbury Neutrino Observatory (SNO) is a unique second-generation solar neutrino experiment specifically designed to measure both the energy and flavor composition of neutrinos emanating from the sun. By using heavy water as its primary target, SNO is able to distinguish between charged-current and neutral-current neutrino interactions and thus uniquely determine the flavor content of solar neutrinos in a model-independent way.

SNO is sensitive to the neutral-current reaction via the capture of neutrons on deuterium (^{2}H(n,γ)^{3}H), releasing a gamma ray of 6.25 MeV. Because the detector is sensitive to all free neutrons within it, a precise determination of all neutron-induced background is essential in measuring the neutral-current rate in SNO. The majority of background events come from low-level radioactivity present in the detector; mainly uranium and thorium decay-chain daughters (^{214}Bi and ^{208}Tl). However, a non-negligible background comes from external sources, such as cosmic-ray activity, nuclear reactor neutrinos, and atmospheric neutrinos.

Spallation productions from high-energy cosmic-rays constitute a potentially serious background to the neutral-current measurements, since a large number of neutrons are released as a muon passes through the detector. Current measurements estimate a neutron production rate of approximately 4.14 $(E_\mu/\mathrm{GeV})^{0.74} \times 10^{-6}$ neutrons/(μg cm^{-2}).[1] Most of the muons which produce spallation products are tagged by the Čerenkov light produced. However, muons which travel through and/or interact in the surrounding rock have no tagged signature and constitute a potential silent background to the neutral current measurement. An additional background arises from atmospheric neutrinos interacting in the detector. These events are indistinguishable from solar neutrinos and represent an irreducible background.

Muon spallation, muon interactions in the rock, and atmospheric neutrinos typically involve interactions above 20 MeV. To properly model neutrons and hadrons produced in these interactions, a full high-energy hadron transport scheme was added to the SNO Monte Carlo.[2] Simulations of silent backgrounds determined that atmospheric neutrino events in the heavy water are the most significant, producing about 14.6 ± 2.8 neutrons per year that capture on deuterium. This translates into a $0.7 \pm 0.2\%$ contribution to the total neutral current signal.

The utilities developed to access this background have a wide range of other uses in SNO physics. The hadron transport code will be used also in atmospheric neutrino measurements, muon spallation measurements, and exotic neutron-anti-neutron oscillation searches.

---

*Presently at Sapient Corporation, Cambridge, MA 02142.

[1] Y.-F. Wang *et al.*, Phys. Rev D **64**, 013012 (2001).

[2] Applications and Software Group, CERN, "GEANT: Detector Description and Simulation Tool," CERN Program Library Report Q123.

2.5 Search for solar hep neutrinos in the Sudbury Neutrino Observatory

K. M. Heeger and the SNO Collaboration

The Sudbury Neutrino Observatory (SNO) is designed to measure the flux of solar neutrinos and to determine the shape of the solar neutrino spectrum. Neutrinos from the beta-decay of ^{8}B dominate the solar neutrino spectrum between 5-15 MeV. The shape of the neutrino energy spectrum from a single beta-decaying source is well known and independent of solar physics to an accuracy of 1 part in 10^6. A measurement of the shape of the solar neutrino energy spectrum is a direct test of the minimal electroweak model and can be used to constrain models of neutrino flavor transformation.

Near the ^{8}B endpoint the solar neutrino spectrum is very sensitive to any underlying background, including instrumental effects and neutrinos with energies above 15 MeV from other sources than ^{8}B-decay. In a rare branch of the pp-chain in the Sun, ^{3}He and proton fuse forming the reaction $^3\text{He} + \text{p} \rightarrow {}^4\text{He} + \text{e}^+ + \nu_e$. This *hep* process produces the highest energy solar neutrinos with an energy of up to 18.77 MeV. Fig. 2.5-1 shows Monte-Carlo simulations of the observed energy spectrum of ^{8}B and *hep* neutrinos in the SNO detector as predicted by Standard Solar Model calculations. The number of photomultiplier hits, NHIT, is the basic energy measure of events.

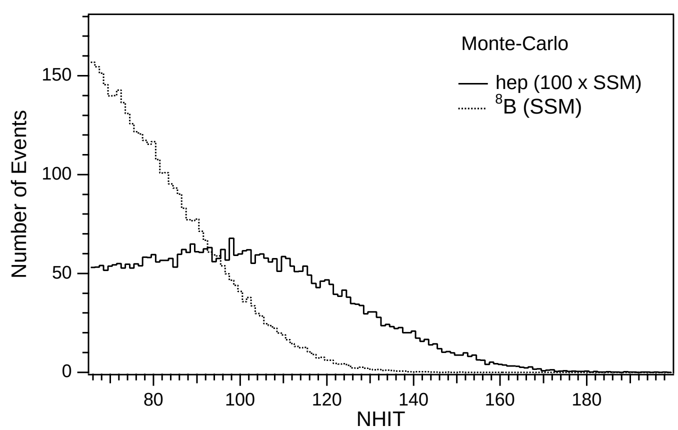

Figure 2.5-1. Energy (NHIT) spectrum of ^{8}B neutrinos and *hep* neutrinos in the Sudbury Neutrino Observatory as predicted by Standard Solar Model calculations. The *hep* spectrum is scaled by a factor of 100. With a maximum energy of 18.77 MeV, neutrinos produced in the $^3\text{He} + \text{p} \rightarrow {}^4\text{He} + \text{e}^+ + \nu_e$ (*hep*) reaction are the highest energy solar neutrinos.

In the past, the measurements of the energy distribution of recoil electrons created by ^{8}B and *hep* neutrinos scattering off electrons in the Super-Kamiokande detector raised significant experimental and theoretical interest in the observation and calculation of the *hep* neutrino flux.[1] One possible interpretation of the Super–Kamiokande measurement suggested a flux of hep neutrinos ≥ 20 times larger than the best theoretical estimate at the time. Standard Solar Model (SSM) calculations for the flux of *hep* neutrinos predict a flux of 9.3×10^3 cm^{-2}

[1] J. N. Bahcall *et al.*, Phys. Lett. B **436**, 243 (1998).

s^{-1} compared to 5.05×10^{10} cm^{-2} s^{-1} for the much more abundant ^8B neutrinos. The SSM predictions of the *hep* flux are based on low-energy cross-section calculations with an S-factor of $S^{SSM}(hep) = (2.3 \pm 1.3) \times 10^{-20}$ keV-b. The rate of the *hep* reaction is so small that it does not affect solar modeling and other solar model predictions.

The reliable estimation of the *hep* cross-section has been a long-standing challenge in nuclear physics. Modern evaluations of this S-factor using approaches based on effective field theory (EFT)[2] or standard nuclear physics approaches (SNPA)[3] yield S-factors in the range between $8.6 - 10.1 \times 10^3$ cm^{-2} s^{-1}. These calculations yield a *hep* flux prediction that is ~ 4 times higher than Standard Solar Model calculations. Therefore, a measurement of the flux of *hep* neutrinos at the Sudbury Neutrino Observatory is of interest to astrophysics and nuclear physics alike. It is also an important part of a detailed shape analysis of the solar neutrino energy spectrum measured at SNO.

In the first phase of the experiment, SNO has measured the interaction rates of solar neutrinos with pure D_2O. The results deduced from SNO's measurements include the total active flux of ^8B neutrinos. It was found to be in good agreement with Standard Solar Model predictions. Low backgrounds and the efficient discrimination of instrumental effects have also allowed SNO to measure the energy spectrum of solar neutrinos and to perform a rare event study in the energy region between 15-30 MeV. Above the ^8B endpoint high energy backgrounds and instrumental backgrounds are estimated to contribute less than 0.8% and 0.5% to the measured interaction rate. The physics background from atmospheric neutrino interactions is estimated to be small in comparison.

As part of the SNO solar neutrino analysis, we have analyzed data from the pure D_2O phase for high-energy solar neutrinos as well as lowest-energy atmospheric neutrinos. Calibration of the solar neutrino energy spectrum is based on a tagged 6.13-MeV ^{16}N γ-source below the ^8B endpoint and 19.8-MeV γ's from a pT source above the ^8B endpoint. Using analysis techniques similar to the ones developed for the measurement of the interaction rates of ^8B neutrinos with deuterium the flux of *hep* neutrinos in the Sudbury Neutrino Observatory has been determined. Candidate events for atmospheric-neutrino induced muons are found and techniques for the robust and unique identification of low-energy atmospheric neutrino events are under development. The results of this work are being prepared for publication.

[2] T. S. Park *et al.*, LANL arXive, nucl-th/0110084.
[3] L. E. Marcucci et al., Phys Rev C **63**, 015801 (2001).

2.6 Seasonal variation of the muon flux at SNO in the deepest underground laboratory

R. Hazama and the SNO Collaboration

SNO is the most northerly underground neutrino detector in the world (the geographical position is 46.5° N (57.2° N magnetic) in latitude) and the geomagnetic field guides cosmic rays into the earth's atmosphere and determines the minimum momentum of cosmic ray primaries that can reach the top of the atmosphere above the detector (the geomagnetic cutoff is 40 GeV/c for protons).[1] Besides, SNO lies under rock overburden of 6010 m water equivalent. Hence, the muon energy threshold at the SNO site is ∼4 TeV and larger than at all the other sites, such as MACRO (1.3 TeV)[2], Super-Kamiokande (1.7 GeV), and AMANDA (500 GeV). For high energy muons, air expansion caused by an increase in atmospheric temperature (see Fig. 2.6-1) leads to increased decay of the parent mesons and thus to a positive correlation between muon intensity and atmospheric temperature. As the atmospheric temperature increases, the height of the atmosphere increases, density of the air decreases, and fractionally more pions/kaons decay to muons before interacting. SNO's great depth is the most appropriate for this correlation study. At shallow depths, this correlation is small because the threshold energy is so low that interactions are unimportant in the cascades. This seasonal variation is the observation of a known phenomenon and is thus a test of the achievable stability of the SNO detector. Further, it can be used as a continuous monitor during the entire day and night running time without any disruption to normal data taking, unlike deployable devices.

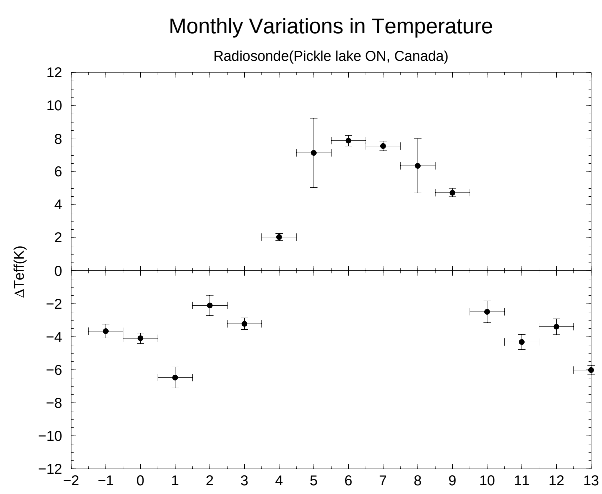

Figure 2.6-1. Monthly variations in the effective temperature, $\triangle T_{eff} = T_{eff} - < T_{eff} >$, where T_{eff} is the mean of the monthly effective temperature distribution and $< T_{eff} >=$ 219.4 K is the mean effective temperature for the data set (Nov'99-Dec'00). The temperature data of the upper atmosphere were provided by the nearest available meteorological observatory to SNO; Pickle Lake site (51.4° N −90.2° E). You can see a ±4% variation.

[1] C. E. Waltham, Initial Observation of Through-Going Muons in SNO, SNO internal report.
[2] M. Ambrosio *et al.*, Astropart. Phys **7**, 109 (1997).

2.7 The day-night asymmetry of the solar neutrino flux measured at SNO

M. W. E. Smith and the SNO Collaboration

As solar neutrinos pass through the earth, matter effects might enhance the oscillation from one flavor to another. This effect is insignificant when the sun is above the horizon (day) but can be quite substantial when the sun is below the horizon (night). One can quantify the effect by forming the day-night asymmetry parameter

$$A = 2\frac{\phi_N - \phi_D}{\phi_N + \phi_D}$$

where ϕ_N and ϕ_D are the measured night and day neutrino fluxes.

The flux of electron neutrinos is measured primarily by the charged-current interaction with deuterium, although some additional sensitivity is provided by the elastic-scattering (ES) reaction. The total flux of all active neutrinos is measured primarily by the neutral-current reaction with deuterium, with the ES reaction again providing a little information. If the electron neutrinos are oscillating only to active flavors then the asymmetry in the total neutrino flux A_{tot} is expected to be zero.

Allowing A_{tot} to float, SNO has measured[1] $A_e = 12.8 \pm 6.2^{+1.5}_{-1.4}\%$, $A_{tot} = -24.2 \pm 16.1^{+2.4}_{-2.5}\%$, with a correlation of -0.602 between the two measurements. The joint confidence ellipses for A_e, A_{tot} are shown in Fig. 2.7-1.

We note that at $\approx 68\%$ c.l., the measurements permit $A_{tot} = 0$. By forcing this constraint, SNO measures $A_e = 7.0 \pm 4.9 \pm 1.3\%$.

The previous measurement from the SuperK experiment used only the ES reaction, which constrains only a linear combination of A_e and A_{tot}. This result is shown as a diagonal band in Fig. 2.7-1. The width of the band is determined by the SuperK error, while the slope of the band is determined by SNO data.

[1] The SNO Collaboration, nucl-ex/0204009.

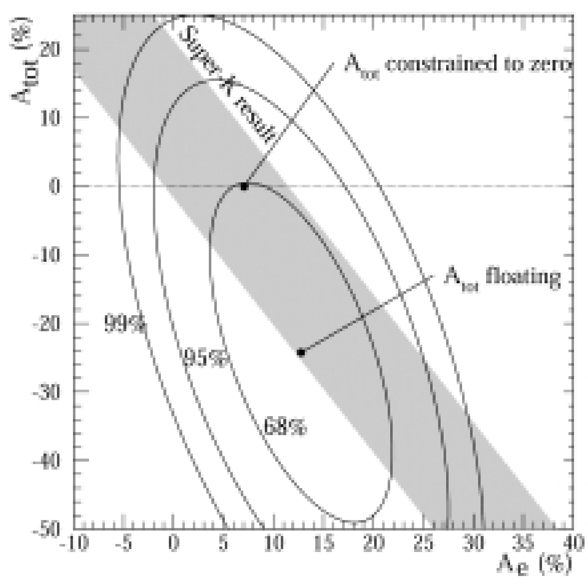

Figure 2.7-1. Joint probability contours for $\mathcal{A}_e$ and $\mathcal{A}_{tot}$. The points indicate the results when $\mathcal{A}_{tot}$ is allowed to float and when it is constrained to zero. The diagonal band indicates the 68% joint contour for the Super-K $\mathcal{A}_{ES}$ measurement.

2.8 Status and updates to the SNO data acquisition system

A. A. Hamian,* M. A. Howe, P. Harvey† and J. F. Wilkerson

The Sudbury Neutrino Observatory data acquisition (SNO DAQ) system is designed to provide continuous readout of the detector's photomultiplier tubes (PMTs) with a minimum of dead time. Since the SNO DAQ system has been described extensively in past annual reports,[1] only a brief overview of the most significant updates is provided here.

In August 2001, the computer running the SNO Hardware Acquisition Real-time Control program (SHaRC) failed and was replaced with one of the spare monitoring computers. As it was becoming clear that the DAQ computers were rapidly aging, it was decided to retire all of the 250MHz PPC Macs and replace them with newer models. Four machines were shipped to site, two 733MHz G4s and two 450 MHz G3s. The faster machines were used to replace both the underground DAQ system and the above ground test stand DAQ system. The other two are being used as the operator control stations. In addition, the SBS 617 PCI to VME controller was replaced with a SBS 622 controller. The new controller has the advantage of using fiber optics to decouple the VME crate from any electronic noise generated by the DAQ computer. The upgrades were carried out in December 2001.

To run SHaRC on the new G4s the code that probes the bus for cards and builds the device registry was rewritten from the ground up to work with the new G4 bus structure. It is now more robust against future changes and is backward compatible with older machines.

After SHaRC begun running on the G4, a number of eCPU/Mac VME hardware exceptions began to occur during periods of intense Mac-VME bus activity. Since the issue was resolved, no VME hardware exceptions have be reported and the overall stability of the DAQ system running on the new machines has been excellent.

Another enhancement to SHaRC was the introduction of the capability to edit the standard run types directly from within SHaRC and to save the run types into files which can be reloaded on demand. This capability extends to the different sources, so that each source can have multiple custom setup files. This has proven to be extremely helpful for the calibration group which regularly adjusts the trigger thresholds.

In addition, a new type of ECA calibration task was added which allows the operator to use an external pulser to generate very low rate pedestal pulses for doing calibrations during normal running to help diagnose various hardware/calibration problems. The PMTs in the pedestal set can be set from a group of randomly selected tubes or can be specified from a file.

The SNO DAQ system continues to perform reliably, and there are no major upgrades foreseen in the coming year.

---

*Presently at Avocent Corporation, Redmond, WA 98052.

†Queens's University, Kinston, Ontario, Canada.

[1]Nuclear Physics Laboratory Annual Report, University of Washington (1997) pp. 20-23; (1998) pp. 18-20; (1999) pp. 16-18; (2000) p. 19; CENPA Annual Report (2001) p. 25.

SNO NCDs

2.9 NCD data taking and analysis

T. V. Bullard, G. A. Cox, S. R. Elliott, K. M. Heeger, A. Hime,* R. G. H. Robertson, M. W. E. Smith, L. C. Stonehill, J. F. Wilkerson and J. M. Wouters*

With the recent installation of the nearly complete NCD electronics and data acquisition system, we are now taking data on 30 of the 96 channels available. In comparison to the 4 channels of data that were previously being acquired, the amount of data we are now able to take has significantly increased for the "cooldown" phase of the NCD's. With this increase in data and the new structure of the data stream, a number of changes have been made, and are currently being made, to the software analysis routines. Among these changes was the development of a new program called AnalystConv, which reads in the new data stream and converts it into a file containing the digitized data and other parameters that the Analyst program uses to analyze the data. A zero level cut has also been implemented to cut out non-ionizing events that are caused by electronic noise. This cut is based on the maximum time gap between two consecutive baseline crossings in an event. A cut of 0.6 microseconds has shown to have zero sacrifice of neutron and alpha events, about 98% efficiency in cutting out microphonic and oscillatory noise events, and 100% efficiency in cutting out baseline and noise spike events. Its efficiency for cutting out micro-discharge events has not been fully characterized, but it is estimated to be about 80% with the ability to cut out more if additional cut parameters are implemented.

The data analysis projects that have been in progress this year attempted to address the contamination issues of both the "background-free" neutron region of phase space and the region targeted for determining the bulk alpha activity in the counters due to the ^{238}U and ^{232}Th content in the NCD's. The first of these projects involved the assembly of two short counters with high levels of ^{210}Po contamination. One counter has a high ^{210}Po level in the end cap region, while the other has it in the mid-body of the counter. The goal of this study was to characterize the risetime vs. energy distributions of alphas originating from the end cap region where the electric field is weak, which might mimic neutron events that would otherwise be distinct from the distributions of bulk and surface alphas. It was determined that end-effect alpha events do indeed contaminate both the neutron region and the bulk alpha region. A conservative upper limit of 0.14 end effect events per day will occur in the neutron region at the estimated time of deployment (March 2003). This limit would give 18 events over the first year of running the entire NCD array, resulting in a contamination that is a few percent of the expected neutral current signal. The contamination of the bulk alpha region will require further studies and data taking with the end effect counters now that the ^{210}Po contamination has decayed away and can be separated from the bulk activity.

The second data analysis project was the "Water Wall" study. In this experiment, data was taken from a few NCD strings that were set up in a water enclosure underground at SNO to measure and compare the thermal and fast components of the neutron flux from

*Los Alamos National Laboratory, Los Alamos, NM 87545.

the surrounding norite rock. In performing this analysis, we encountered and identified a number of problems with the current analysis procedures that become more apparent at lower energies, and we have not been able to get conclusive results about the data. The problems with the current data analysis methods that have been identified are mostly attributed to the log-amp calibration procedures and parameters used, as well as to the method used to determine the onset time and duration of an ionizing event. An automated log-amp calibration routine is currently being designed and implemented to address the first issue. Studies are also underway to create a more robust method of determining the onset time and duration of an event, as well as to implement a "moments analysis" to provide more complete information about each event. Once these problems are resolved, data analysis will resume.

The priority for data analysis during the remaining time in the cool-down phase of the NCD's is to determine the intrinsic backgrounds that will affect our ability to measure the neutral current signal in SNO using the NCD's. The data taking will also be geared towards verifying and characterizing the electronics and data acquisition system. Both of these characterizations will provide a large part of the information needed to assess readiness for deployment.

2.10 Status of the NCD DAQ for SNO

G. A. Cox, M. A. Howe and J. F. Wilkerson

The data acquisition system for the Neutral Current Detectors (NCDDAQ) at the Sudbury Neutrino Observatory (SNO) is near full data taking capability and complete system monitoring. The NCDDAQ, written in C++ , is based on the SNODAQ software within the SHaRC framework.[1] The main goal of the NCDDAQ is to provide real–time system monitoring and initialization for the entire array of NCD electronics,[2] data acquisition controls, and an output data stream, all within an intuitive graphical interface. The NCDDAQ features single–button run–initialization, a Hardware Wizard for simple setup, high-voltage controls, individual low-level electronic component controls, an alarm system, and a database for electronic information storage.[3] Below is a figure of the NCDDAQ main control window along with some monitoring tools

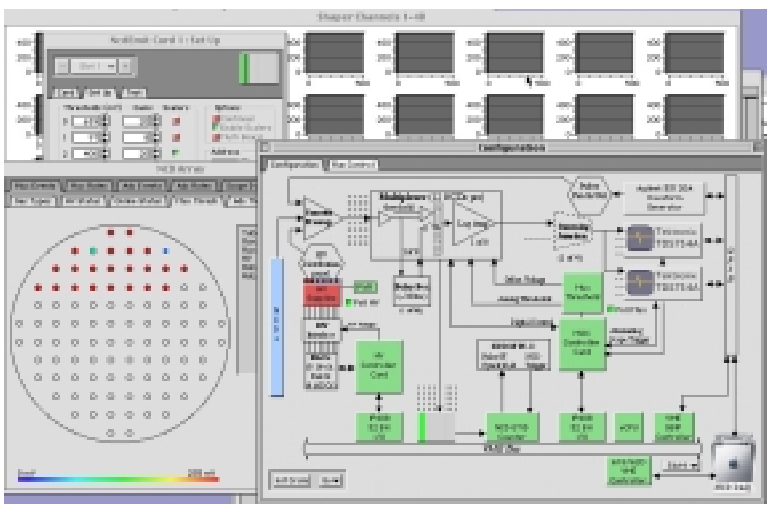

Figure 2.10-1. A screenshot of the NCDDAQ

The NCDDAQ now has an output data stream, which, after full development, will be inserted into the main SNO data stream. In the final configuration, most of the data-taking processes will be handled by an eCPU in the VME crate. The eCPU will load the data stream into dual port memory where it can be dispatched to analysis and monitoring tools. The data stream includes data from three main sources: the ADC Shaper cards, the NCD Multiplexers (MUX), and two digital oscilliscopes. The NCDDAQ can correlate data between the MUX and the oscilliscopes and combines them into a single event. The inclusion of the ADC data will occur with finalization of the GTID board and related software.

Other minor additions to NCDDAQ include a replay function, data stream filters, pulse generator control over GPIB, improved digital oscilloscope controls, NCD array monitoring

[1]Nuclear Physics Laboratory Annual Report, University of Washington (1997) pp. 20-23; (1998) pp. 18-20; (1999) pp. 16-18.
[2]CENPA Annual Report, University of Washington (2001) pp. 32-33.
[3]CENPA Annual Report, University of Washington (2001) pp. 34-35.

tools, multiple ADC Shaper data monitoring, and other areas to improve ease of use and configuration. The replay tool allows the user to replay an entire data file as if it were happening in real–time. The data filters parse data from the stream as specified by user input. The pulse generator will be used extensively in future calibration routines. Once fully developed, a multitude of calibration waveforms will be programmable into the pulse generator. The added NCD monitoring tools allow visual inspection of information on the array of NCD strings, such as event rates, thresholds, and gains.

2.11 NCD cable repair and testing

T. H. Burritt, P. J. Doe, S. R. Elliott, J. A. Manor and R. G. H. Robertson

SNO Neutral Current Detectors are to be to be deployed in the heavy water in an array of 96 strings. Each string is connected to the data acquisition system by a custom made coaxial cable of eight to fifteen meters length. These cables were designed to be slightly positively buoyant in heavy water, to match the impedance of the detector strings and were constructed of carefully chosen, low-radioactivity material. The cable is attached to the detector strings by way of a bell-shaped, nickel coupler. The cable end is inserted into the nickel bell and the shield braid is soldered to the nickel. Voids in the bell were then filled with silicone potting compound and adhesive heat shrink was applied to the junction between the nickel and the cable. The complete wet-end assembly is shown in figure Fig. 2.11-1. The heat shrink and the potting compound form primary and secondary water barriers. Due to the unique design of the cable and bell connections, tests are currently being conducted to ensure their long-term integrity at high voltage while underwater.

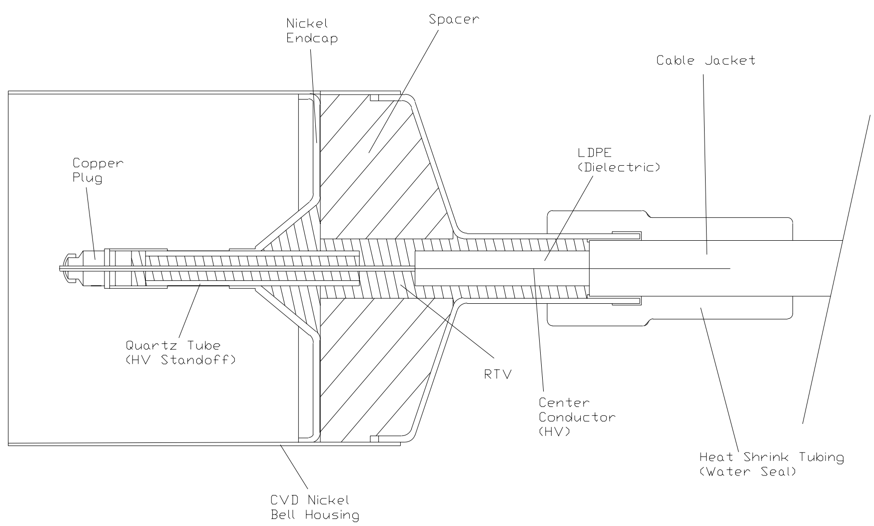

Figure 2.11-1. The cable wet-end showing the nickel bell housing. The silicone potting and heat shrink that form the water barrier can also be seen.

The cables must satisfy stringent requirements. They must withstand a minimum of 5 years exposure to the ultra-pure heavy water and must be electrically very quiet at their operating voltage of 1.835 kV. Spurious electrical discharges could represent a source of background to the anticipated neutron capture signal of 10 events per day. To ensure that the cables satisfy these criteria we devised the following series of tests.

One form of electrical noise, micro-discharge at high voltage, can mimic the signal of a neutron capture in the ^{3}He detector. The completed cable assemblies are therefore being micro-discharge tested at 2.4kV for a minimum of 12 hours. A cable with a micro-discharge rate of less that 0.25 per hour is considered acceptable. Studies have shown that this will result in a spurious trigger rate for the whole array of approximately 12 per hour, at the operating voltage of 1.835 kV. This rate is compatible with our ability to identify and reject micro-discharge events.

After passing the micro-discharge tests, the cables are placed in a water tank. The water in this tank is purified until it has a resistance of 10 MΩ, degassed, chilled to 11 °C, and raised to 2 atmospheres pressure. These conditions approximate those of the heavy water in which the cables will be deployed. When placed in the tank the cables are bent to a 10-inch diameter. This represents the most strenuous forces that any part of the cable will be subjected to once it is installed in the SNO detector. The cables are required to remain watertight during a 2-week exposure in the water test tank and to pass a subsequent micro-discharge test.

Before deployment of the array, all 96 cables will have to pass these tests.

2.12 Neutral current detector electronics commissioning status

G. A. Cox, P. J. Doe, C. A. Duba, A. W. Myers, R. G. H. Robertson, L. C. Stonehill, T. D. Van Wechel and J. F. Wilkerson

The Sudbury Neutrino Observatory (SNO) has the ability to probe both the neutral- and charge-current neutrino flux through the use of heavy water. SNO needs to differentiate between neutrons and other events in order to distinguish potential neutral-current neutrino flux. The Neutral Current Detector (NCD) array is set to be placed within SNO in less than a year and has the potential to provide extremely accurate neutron recognition. The low expected rate of neutral-current events generated by solar neutrinos necessitates event-by-event recognition while the high potential neutron rate from galactic supernovae requires a fast data acquisition system.

The NCD electronics were designed and built with both of these goals in mind. Dual data paths provide the low-rate scenario with digitized data while allowing for high-rate data taking. Each string of NCD counters has a pair of independent thresholds, one level for low-rate pulse digitization and one for high-rate signal integration. The NCD electronics also provide 8 individually controllable high voltage power supplies for selective distribution amongst the NCDs 96 strings.

The bulk of construction and shipping is complete, and the NCD electronics has entered its commissioning phase as we bring the NCD array online in preparation for deployment. Currently, there are two complete running NCD systems, the primary one underground at SNO, and the secondary one at UW. A redundant third system, planned for above-ground placement in Sudbury, will be completed and shipped shortly.

The underground system at SNO is currently running with 30 strings hooked into 5 NCD Shaper/ADC cards, 3 multiplexer (MUX) boxes, and two digitizing scopes. An SBS 618 VME controller connects the Shaper/ADCs to the control computer, whereas the scopes are in direct GPIB communication. After acquiring an event, the control computer saves the events to disk in a platform-independent data format. At the end of each run, the control computer then ships the data record back to CENPA.

At this time, the underground system is mostly monitoring background events from the cavity wall of the SNO control room. With the help of several specially designed counters and a protective water encasement, we are exercising the full running of the system while we quantify expected background rates. During this phase, we are also sensitive to time-dependant neutron fluxes, such as might indicate or mimic a nearby supernova.

In the upcoming months before deployment, the primary system will be constantly monitoring the array, acquiring data, and shipping it for analysis at CENPA. During this commissioning phase, we will be finalizing software modules that facilitate simple array operation and monitoring. We will also use this time to calibrate the sensitivity and backgrounds of the NCD array.

2.13 Underground NCD welding prior to deployment

J. F. Amsbaugh, T. A. Burritt, P. J. Doe and B. Morissette*

As reported last year,[1] we have completed construction and testing of the laser welding equipment needed for neutral current detector (NCD) deployment in the Sudbury Neutrino Observatory (SNO) detector. Some minor improvements and modifications have been made to aid in the use of the equipment and handling of the NCDs.

The NCD welding will occur in two stages. First the so called pre–deployment welding, in which individual NC detectors are welded into the largest segments that will fit into the room above the SNO detector. The NCD anchors and cable ends are also welded to the segments during pre–deployment. It is conservatively estimated that pre–deployment welding will take about 3 months. The goal is to minimize the time the SNO detector is off for the second stage, NCD deployment. The NCDs will likely be deployed in spring 2003.

Before any technical activity is allowed at the SNO detector, a review is required to satisfy the SNO Project Site Policies and Procedures.[2] A review panel has been formed and has begun work. Equipment documentation, safety reports, assembly procedures, welding procedures, electrical inspection, and manpower schedules have been submitted. These will be finalized and approved by the review. A test concerning the electrical interference (EMI) of the laser welder on the SNO detector will be done. Any EMI will have to be eliminated, since the pre–deployment welding occurs while the SNO detector is running.

A roll-around rack for transporting the NCD to and from the NCD storage area is already underground. It will be used to rearrange the NCDs in the storage rack in the proper order for the pre–deployment welding in April 2002. Also at this time the NCDs will be checked for failures by running them in the rack with the NCD data acquisition system.

We will ship the remaining pre–deployment welding equipment to the SNO site in mid May 2002. After inspection, it will be taken underground for EMI tests as soon as possible. We anticipate completing the review in June 2002 so we can begin pre–deployment welding after the schedule maintenance shutdown, mid September 2002.

*Sudbury Neutrino Observatory, Lively, Ontario, Canada P3Y 1M3.

[1]CENPA Annual Report, University of Washington (2001) p. 37.

[2]Section No. 4.1.3, *Development and Approval Process for Technical Activities.*

2.14 NCD deployment equipment progress

J. F. Amsbaugh, M. Anaya,* T. A. Burritt, P. J. Doe, G. C. Harper, J. Wilhelmy* and J. Wouters*

The development of the equipment needed to deploy the neutral current detectors (NCDs) into the heavy water acrylic vessel (AV) of the Sudbury Neutrino Detector (SNO) is complete. A previous progress report[1] listed glove box glove mount revisions, laser welding fixture (WF), WF mount, pre–deployment welding bench, and hauldown mechanism redesign. Outstanding items were finishing the gantry crane, the neckview camera system and equipment leaching tests.

The gantry crane is a commercial[2] all-aluminum construction A-frame unit with 2000-lb capacity, equipped with an aluminum manual winch[3] with automatic brake. The crane cross beam and winch spool have been hard anodized. The completed assembly was load tested, shipped, taken underground at the SNO site. It has been assembled and verification that it can reach all required positions is expected soon.

The neck view camera system uses a remote focus, aperture, and zoom lens[4] coupled to a monochrome 1/2 inch CCD video camera.[5] The light source uses super bright LEDs, 3 white, 3 yellow and 6 green, which can be switched on or off in groups. The camera, lens and LEDs are in a sealed, suitably clean enclosure that can be mounted in one of seven positions during use. This mount also provides manual camera pan of 360° and tilt of 120°. Bench tests assure the system can read the NCD cable labels at the appropriate range of distances.

The equipment is well along for having the deployment occur in spring of 2003. We are working on the documentation, procedures, training materials, and so forth that will be required for the activity review in late summer or fall of 2002. Training at the LANL test pool in equipment use must start in fall 2002 to meet the deployment date. The only unresolved major issue at present is whether the radon emanation and leaching of the deployment equipment is sufficiently low to allow placing into the AV.

---

*Los Alamos National Laboratory, Los Alamos, NM 87545.

[1] CENPA Annual Report, University of Washington (2001) p. 37.

[2] Model 1ALU1208B, Spanco, Morgantown, PA 19543.

[3] Model CMA-1760, Jeamar Winches, Inc., Buffalo, NY, 14206.

[4] COMPUTAR Model H6Z0812M, Chugai Boyeki Corp., New York, NY.

[5] Model TM-200, Pulnix America, Inc., Sunnyvale, CA.

Neutrino Detectors

2.15 Lead perchlorate as a neutrino detection medium

M. K. Bacrania, P. J. Doe, S. R. Elliott and L. C. Stonehill

Due to its apparent transparency, large interaction cross section, and relatively low cost, lead perchlorate $Pb(ClO_4)_2$ is an attractive candidate for a Čerenkov neutrino detector. Neutrino interactions with lead may occur by either the charged-current (CC) or neutral-current (NC) reactions:

$$
\begin{array}{lcll}
\nu_e + {}^{208}\mathrm{Pb} & \Rightarrow & {}^{208}\mathrm{Bi}^* + e^- & \quad (\mathrm{CC}) \\
 & & \Downarrow & \\
 & & {}^{208-\mathrm{y}}\mathrm{Bi} + x\gamma + yn & \\
\nu_x + {}^{208}\mathrm{Pb} & \Rightarrow & {}^{208}\mathrm{Pb}^* + \nu_x' & \quad (\mathrm{NC}) \\
 & & \Downarrow & \\
 & & {}^{208-\mathrm{y}}\mathrm{Pb} + x\gamma + yn &
\end{array}
\tag{1}
$$

At 30 MeV the CC cross section with lead is about 600 times that of carbon and the NC cross section is about 100 times that of carbon. The signature of a CC interaction consists of a prompt electron followed by gamma rays and neutrons. The signature of a NC interaction consists only of gamma rays and neutrons with no prompt electron. The number of neutrons depends on the energy of the interacting neutrino. Because lead perchlorate solutions contain an appreciable amount of hydrogen, the neutrons quickly thermalize and are captured by the ^{35}Cl which then emits an 8.6 MeV gamma ray. The gamma ray is detected by subsequent Compton scattered electrons.

To determine if a lead perchlorate Čerenkov detector can be built we investigated the optical properties of the solution. Studies using a spectrophotometer revealed that there are no obvious absorption lines between wavelengths of 250 to 600 nm. We constructed a special apparatus to measure the attenuation of 460 nm light in lead perchlorate solution. Initial measurements yielded attenuation lengths of less than half a meter, which is insufficient to build a large lead perchlorate Čerenkov neutrino detector. Diluting the solution away from saturation while heating and stirring improved the attenuation length somewhat. To remove scattering particles we filtered the solution using a series of filter pore sizes from 5.0 microns down to 0.2 microns. This resulted in an attenuation length of just over 4 meters. This improvement is sufficient for a reasonably sized Čerenkov detector and suggests that additional filtering might further increase the attenuation length.

The work we have done with lead perchlorate solution has shown that it is a viable medium for a Čerenkov neutrino detector. The OMNIS collaboration, which is planning a next-generation lead-based neutrino detector, has chosen to incorporate lead perchlorate into their detector proposal. Thus, although no further work with lead perchlorate solution is planned at CENPA, we have made a valuable contribution to the field of neutrino physics. A report of our work has been submitted to Nuclear Instruments and Methods and can be found at xxx.lanl.gov under nucl-ex/0202013.

Double Beta Decay

2.16 Heat capacity and thermal conductivity of molybdenum at millikelvin temperatures for a molybdenum bolometer

P. J. Doe, S. R. Elliott, R. Hazama, R. G. H. Robertson, O. E. Vilches,* J. F. Wilkerson and D. I. Will

Molybdenum is in principle a good candidate for the high energy resolution bolometer[1] and this has been investigated further at UW. Recently in the context of an ultracryogenic resonant-mass gravitational wave detector, in the temperature range of 0.2 K to 1 K, the specific heat of commercial 99.5 % purity annealed polycrystalline molybdenum are reported.[2] We calculated the expected energy resolution of molybdenum at millikelvin temperature by using these recent experimental data of heat capacity. We extrapolated the specific heat below 0.2 K and this is fairly good agreement with the data in Fig. 2.16-1. For superconductors at low enough temperature the relevant heat capacity is the Debye(lattice) term, not the electronic term. Thus, this is also shown as dotted line in Fig. 2.16-1. The estimated specific heat of molybdenum at 5 mK by these two extrapolation is $1.2{\times}10^{-1}\mu$J/g/K and $3.0{\times}10^{-8}\mu$J/g/K for the electronic plus lattice term and the only lattice term, respectively. Now we can compare our estimation with the calculation of E. Fiorini and T. O. Niinikoski[3] at 5 mK. The estimated energy resolution at 5 mK for a mass of 1 kg is $\triangle E_{\mathrm{FWHM}}$ = 4.5 - 8900 eV, while their estimated energy resolution for a mass of 1 kg at 5 mK is 47 eV.

There are three available data for the thermal conductivity of molybdenum. The temperature dependence of the thermal conductivity of single crystal molybdenum in the superconducting state and in the normal state is measured[4] in the temperature range of 0.1 - 300 K. All data are summarized and compared in Fig. 2.16-2. You can see these are not consistent with each other and it shows roughly two order difference. In order to get the expected time constant at millikelvin temperature(T), we extrapolated the thermal conductivity(k) data using the assumption of a linear dependence of k on T and which give us a good agreement. (The linear coefficient $1/A$ is associated with electron-defect.) This is justified by the expectation that the effects of electron-phonon scattering to contribute less than 2 % to the normal metal thermal conductivity below 1 K. It is noted that the typical steeper falls can be seen with decreasing temperature below 0.5 K and 0.9 K for the full circles and the squares, respectively. The thermal conductivity exhibits this behavior in the superconducting state for the normal metal. Each extrapolation gives us the thermal conductivity at 5 mK and the results are summarized in Table. 1 with the time constant τ, which is obtained by the internal thermal resistance R and the heat capacity c.

---

*Department of Physics, University of Washington, Seattle, WA 98195.

[1] CENPA Annual Report, University of Washington (2001) p. 46.

[2] W. Duffy, Jr., J. Appl. Phys., **81**, 6675 (1997).

[3] E. Fiorini and T. O. Niinikoski, Nucl. Instr. Methods **224**, 83 (1984).

[4] A. Waleh and N. H. Zebouni, Phys. Rev. B **4**, 2977 (1971).

Reference	Form	Purity %	T_c K	Temp. range K	1/A W/cm/K^2	κ W/cm/K	τ sec/g
A. C. Mota	-	-	-	4-300	0.135	0.00068	0.0016-3.9e-10
Duffy et al.	polycrystalline	99.95	0.50	0.1-1.0	0.56	0.0028	0.00038-9.5e-11
Waleh et al.	single crystal	-	0.903	0.4-1.0	15.6	0.078	0.000014-3.4e-12

Table 2.16-1. Measurements of 1/A and κ and τ of Mo. The value of τ depends on the heat capacity(c) and crystal's size (in this case, bar of 1.2 cm diameter and 10 cm long.

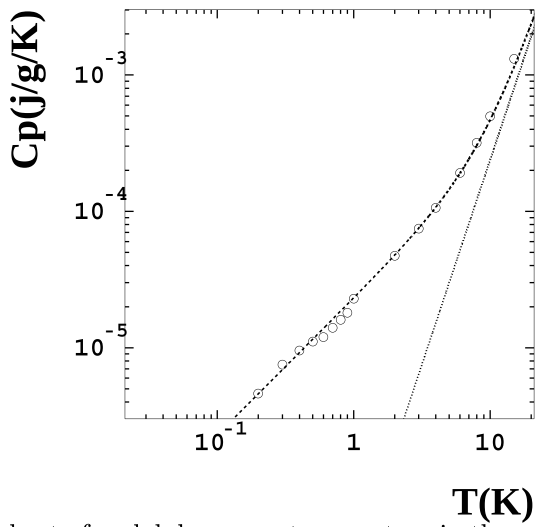

Figure 2.16-1. Specific heat of molybdenum vs temperature in the range of 0.2 K to 10 K. The dashed line is the Debye-Sommerfeld equation, which includes both the lattice (Debye) term and the electronic term. The dotted line is only the second (Debye) term.

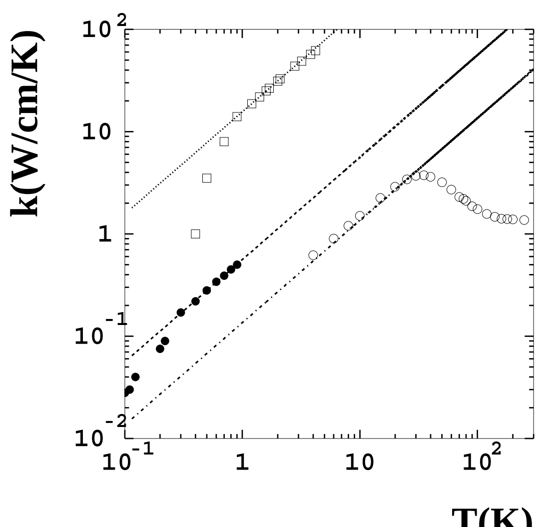

Figure 2.16-2. Results referring to the whole set of measurement of the thermal conductivity of molybdenum. Full circles: Duffy Jr. et al., squares: Waleh et al., open circles: A. C. Mota.

2.17 Cosmogenic backgrounds for MOON

P. J. Doe, S. R. Elliott, R. Hazama, R. G. H. Robertson, J. F. Wilkerson and D. I. Will

By using the program COSMO,[1] which calculates the production of all radionuclides by nucleon-induced reactions in a given target, we surveyed entire cosmogenic production for MOON detector[2] on the earth with a reference of Table of Isotopes.[3] The variation of spallation, evaporation, fission and peripheral reaction cross sections with nucleon energy, target and product charge and mass numbers, as well as the energy spectrum of cosmic ray nucleons near the Earth's surface are incorporated in this program. We can categorize the background as a correlated (delayed) one and an accidental one for solar neutrino and double beta decay studies, respectively in Table 2.17-1. As for solar neutrino backgrounds, ^{90}Sr will be the major cosmogenic backgrounds, but enrichment of ^{100}Mo is very effective for the reduction of an order of 3. We can apply a chemical purification, too. Considering the raw event rate, ^{88}Zr and ^{95}Zr will be much higher and by an accidental coincidence these backgrounds sneak into the energy window of solar neutrino signals. However, these radioactivities are short lived and enrichment of ^{100}Mo is quite effective about an order of 4 reduction. While, ^{91}Y is the major cosmogenic backgrounds for neutrinoless double beta decay ($0\nu\beta\beta$). The accidental sum of two beta-rays from ^{91}Y is 3088 keV and close to the Q-value of $0\nu\beta\beta$ (3034 keV). This can be reduced by a chemical purification. Enrichment is also effective. It is noted here the activity of ^{91}Y will be 10^{-2} after 1 year of storage at underground.

Signal	half-life $T_{1/2}$	Raw rate (/34 ton ^{n}Mo − 3 ton^{100}Mo/day)	Effective (/34ton ^{n}Mo − 3 ton^{100}Mo/day)
0ν, 0.05 eV		0.25	0.035
^{7}Be		0.33	0.12
pp		0.99	0.21
Correlated			
^{90}Sr	28.78 yr	1200 − 6.66	4.3e-4 − 2.4e-6
^{99}Nb	15 sec	398 − 363	0
Accidental			
^{95}Zr	64.0 day	8.0e+5 − 8500.	0.89 − 1e-4
^{88}Zr	83.4 day	4.9e+5 − 347.	0.80 − 0
^{91}Y	58.51 day	1.7e+5 − 201	0.001 − 0
^{60}Co	5.27 yr	166. − 1.9	0

Table 2.17-1. Expected rates for the major cosmogenic backgrounds for MOON. Prompt event rates of 1 year cosmic radiation on the earth.

[1] C. J. Martoff and P. D. Lewin, Comp. Phys. Comm. **72**, 96 (1992).
[2] R. Hazama *et al.*, AIP Conference Proceedings, Volume 610, page 959-963, ed by E. Norman *et al.*, New York, 2002, *International Nuclear Physics Conference (INPC2001)*, July 2001, Berkeley, CA.
[3] 8th ed., edited by R. B. Firestone and V. S. Shirley, Wiley, New York, NY 1996.

2.18 Search for a molybdenum-loaded liquid scintillator

P. J. Doe, S. R. Elliott, R. Hazama, R. G. H. Robertson, J. F. Wilkerson and D. I. Will

Liquid scintillators loaded with appropriate double beta decay candidates are attractive detector media for searching for neutrinoless double beta decay[1] and for detection of low energy solar neutrinos by inverse beta decay.[2] The full energy from beta decays is measurable when the isotope is dissolved directly in a liquid scintillator allowing accurate spectroscopy at the end point. ^{100}Mo is one excellent candidate.[3]

For use in a successful detector, an isotope must meet several criteria. Some chemical form must be sufficiently soluble in a liquid scintillator, yet not quench too strongly, so as to permit accurate scintillation spectroscopy. Solution attenuation length for blue light should exceed 5 meters, setting stringent limits on absorption and scattering. Events from radioactive impurities such as uranium and thorium can easily distort the spectrum, and effective purification techniques must separate these emitters from the element of interest. Finally, detectors which will operate for many years or decades require a stable compound in a stable solution.

Several techniques for dissolving molybdenum in liquid scintillator hold promise. Chemical suppliers offer a variety of molybdenum compounds, some of which might meet the criteria for solubility, clarity, purity, stability and lack of quenching. R. S. Raghavan[4] and colleagues in the LENS (Low Energy Neutrino Spectroscopy) collaboration have developed a successful, tested and refined recipe utilizing carboxylic acid chemistry[5] for the isotope ^{176}Yb. They have proven the same recipe[5] satisfactory for the isotope ^{115}In. A variation of this technique might work for molybdenum. Finally, as a transition metal, molybdenum exhibits substantial covalent organometallic chemistry and several monodentate ligands and chelating agents offer possibilities.

After selection, synthesis, and purification of the desired chemical form, testing consists of four main steps. A series of solutions (with concentration increasing until material remains undissolved) yield the solubility in the chosen liquid scintillator. Spectral absorption, 430-nm attenuation length, density and refractive index are found with a UV-Vis spectrophotometer, a meter-long cell, a pycnometer and a refractometer, respectively. The shift in the Compton edges of a ^{207}Bi source with increasing concentration permits determination of scintillation light output (relative to pure liquid scintillator) as a function of concentration. Observations of the solution and retests after a week and after longer intervals, reveal any instability. ICPAA (Inductively-Coupled Plasma Atomic Absorption spectroscopy) is available as a method of confirming per cent by weight molybdenum in the solutions.

Tests of $Mo(CO)_6$ directly dissolved in Bicron[6] BC-505 (a pseudocumene-based liquid

[1] CENPA Annual Report, University of Washington (2001) p. 46.
[2] H. Ejiri, J. Engel, R. Hazama, P. Krastev, N. Kudomi and R. G. H. Robertson, Phys. Rev. Lett. **85**, 2917 (2000).
[3] Nuclear Physics Laboratory Annual Report, University of Washington (2000) p. 31.
[4] Bell Labs division of Lucent Technologies, 600 Mountain Ave, Murray Hill, NJ 07974.
[5] R. S. Raghavan, Status Report on LENS- September 2001, and personal communication.
[6] Bicron, a subsidiary of Saint-Gobain Industrial Ceramics, Inc.

scintillator) are complete. Between 0.66 and 0.72 g of $Mo(CO)_6$ dissolve per 100 cc of solution at 20 C. In a 10-cm cell, BC-505 itself absorbs strongly below 420 nm and shows no measurable absorption ($\pm 1\%$) at longer wavelengths (to 800 nm). In the same cell the 98% saturated solution shows 1-2% ($\pm 1\%$) absorption at wavelengths longer than 420 nm. For this 98% saturated solution scintillation light output is reduced to 23.6% $\pm$ 7% of pure BC-505. While light output was stable over a week's time, a haze of blue precipitate formed on the bottom of our storage flask over several months. Fig. 2.18-1 shows this CENPA result superimposed upon a Bell Labs plot for comparison.[7] $Mo(CO)_6$ directly dissolved in BC-505 exhibits insufficient solubility and light output and unsatisfactory stability for use in a detector.

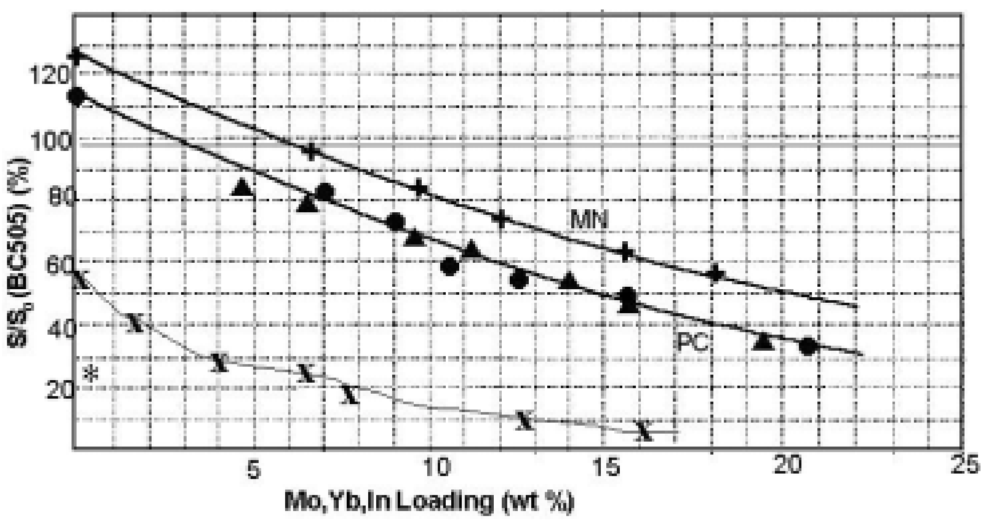

Figure 2.18-1. Scintillation yield relative to BC-505 standard (12000 photons/MeV). ($*$) $Mo(CO)_6$ in BC-505. (**X**) Indium loaded liquid scintillator pre-2000. (✚) Yb loaded liquid scintillator in methylnaphthalene. (●, ▲) Yb in pseudocumene. (In, Yb data: LENS Collaboration with % by weight using ICPAA.)

Ammonium isovalerate is a precursor to various organic compounds of molybdenum which might show adequate solubility in BC-505. Tests of ammonium isovalerate solubility in BC-505 are in progress. Ammonium isovalerate in BC-505 shows variable solubility (probably due to varying amounts of free isovaleric acid remaining in the ammonium isovalerate). Preliminary results show that the solubility of ammonium isovalerate in BC-505 increases with increasing acidity (provided by isovaleric acid and acetic acid). Values seem repeatable once the solution is sufficiently acidic to mask variations in the amount of stray isovaleric acid in the synthesized ammonium isovalerate. This behavior suggests that acetic acid, isovaleric acid and ammonium isovalerate (though principally ionic in character) exist in molecular form in pseudocumene, a largely nonpolar solvent (and the main component of BC-505). Presumably, various ammonium isovalerate/isovaleric acid/acetic acid complexes form, each with its own relatively independent solubility, permitting greater amounts of ammonium isovalerate to remain in solution.

[7] R.S. Raghavan, *op. cit.*

2.19 Majorana search for neutrinoless $\beta\beta$ decay

P. J. Doe, S. R. Elliott, K. Kazkaz, R. G. H. Robertson and J. F. Wilkerson

A group from the University of Washington has joined the Majorana collaboration.[1] Majorana[2] is a next-generation double beta decay experiment, and has two main goals: to determine whether the electron neutrino has a Majorana character (*i.e.*, whether the ν_e is its own antiparticle), and if so to measure the effective Majorana mass of the neutrino, $\langle m_\nu \rangle$. We use ^{76}Ge as both the decay and detector medium. The experiment will be installed in the anticipated National Underground Science Laboratory, provided the Laboratory is built. Alternate sites are being evaluated in case the creation of NUSL falls through.

For $0\nu\beta\beta$ decay to be possible, the ν_e must not only have a Majorana component, but it must also be massive to allow for a boost to a frame of reference where the ν_e helicity becomes right-handed. The more massive the ν_e, the more accessible such a frame becomes. Thus by measuring the rate of $0\nu\beta\beta$ decay, we put upper limits on the effective Majorana mass of the ν_e.

Extrapolation of data on the $0\nu\beta\beta$ decay rate by the IGEX experiment,[3] put a lower bound on the halflife of this process at 1.57×10^{25} years, corresponding to an upper limit[4] of $\langle m_\nu \rangle$ between 0.33 eV and 1.35 eV. The Majorana experiment seeks to increase the halflife lower limit by two orders of magnitude, to 4.2×10^{27} years, corresponding to a reduced upper limit on $\langle m_\nu \rangle$ of 20-70 meV. We will achieve this goal by using germanium isotopically purified to 86% ^{76}Ge. The Ge crystals will be produced over several years and continually added to the detector array until we reach our goal of 500 kg, with a target integrated lifetime of 5000 kg·years.

Current projects of the collaboration include detector simulation, identification and analysis of contributing backgrounds at 2039 keV (the endpoint energy of $\beta\beta$ decay from ^{76}Ge), and spectrum simulation. We use standard physics simulation and analysis packages available from CERN (Geant4, FLUKA, ROOT). Simulations run thus far predict a peak sensitivity to the $0\nu\beta\beta$ event rate of 1 to 2 per year averaged over the life of the experiment. Given such a low event rate, it is crucial to identify and reduce backgrounds. To this end, we are currently involved in identifying any process that may contaminate the spectrum at the endpoint energy. In addition to background identification, pulse shape discrimination, a large overburden, passive and active vetoes, and ultraclean manufacturing of the crystals, their support structure, and electronics are crucial to the success of the experiment.

[1] Pacific Northwest National Laboratory, University of Washington, University of South Carolina, Triangle Universities Nuclear Laboratory, New Mexico State University, Institute for Theoretical and Experimental Physics, Joint Institute for Nuclear Research.

[2] Information available at http://majorana.pnl.gov.

[3] Aalseth *et al.* The IGEX ^{76}Ge Neutrinoless Double-Beta Decay Experiment: Prospects for Next Generation Experiments, hep-ex/0202026.

[4] The spread in $\langle m_\nu \rangle$ derives from uncertainty in the matrix elements.

KATRIN

2.20 The KATRIN tritium beta decay experiment

P. J. Doe, S. R. Elliott, M. A. Howe, R. G. H. Robertson, J. F. Wilkerson and the KATRIN Collaborators

With the SNO discovery that electron neutrinos from the Sun are converted to other active flavors, the neutrino sector appears to be characterized by strong mixing between three active flavors. The atmospheric neutrino data indicate maximal mixing between two eigenstates with $\Delta m^2 = 3.5 \times 10^{-3}$ eV^2. The recent SNO neutral current results[1] combined in a global analysis with all solar data strongly favor the MSW large mixing angle region with a best fit mixing angle of about 30 degrees and a mass splitting on the order of $\Delta m^2 = 5 \times 10^{-5}$ eV^2.

Oscillation experiments yield values only for mass-squared differences. The mass itself can only be obtained from single and double beta decay. The oscillation experiments do, however, show that the mass eigenstates are close together, not more than 60 meV apart. Now, for the first time, a precise determination of or limit on the mass of ν_e from tritium beta decay constrains the masses of all three eigenstates. Currently the best limit on the weighted sum of mass eigenvalues squared,

$$\langle m_e \rangle^2 = \sum_{i=1}^{3} m_i^2 U_{ei}^2,$$

comes from the Mainz experiment, and is 2.2 eV at 95% CL.

A new experiment is underway to improve this limit greatly, down to approximately 0.4 eV on $\langle m_e \rangle^2$. The experiment, called "KATRIN" (KArlsruhe TRItium Neutrino project),[2] will be centered around a huge retarding-field magnetic-electrostatic analyzer and gaseous T_2 source to be built at Karlsruhe. The spectrometer will be 7 m in diameter and 20 m in length and will be capable of resolution close to 1 eV. The goal is to reach a limit or an observation down to 0.35 eV. Such a limit would match the sensitivity expected from the best future astrophysical measurements of MAP and SDSS, and would also constrain (or reveal) degenerate scenarios for the neutrino mass spectrum.

The UW group expects to apply to KATRIN our previous experiences gained in developing and building the LANL tritium beta decay experiment, which was the first experiment to utilize a gaseous T_2 source. In addition we have accepted the responsibility to design and develop the data acquisition system used in the experiment. This DAQ system will be based on our real-time object oriented DAQ system that has been used in SNO and emiT. We also plan to be involved in the development of the electronic readout of the segmented silicon detector, in particular working in collaboration with the Karlsruhe group on the design and construction of the analog front-end electronics. A successful DAQ and electronics working group meeting of the Karlsruhe and UW groups was held in Seattle in February 2002.

[1] Q. R. Ahmad *et al.*, LANL arXive, nucl-ex/0204008.

[2] KATRIN Letter of Intent, A. Osipowicz *et al.*,arXiv:hep-ex/0109033.

National Underground Science Laboratory

2.21 National Underground Science Laboratory at Homestake

P. J. Doe, S. R. Elliott, W. C. Haxton,* R. G. H. Robertson and J. F. Wilkerson

At the Neutrino pre-town Nuclear Physics Long Range Planning (LRP) meeting held in Seattle in September 2000, a strong consensus emerged from the participants that now is an ideal time to establish a National Underground Science Laboratory (NUSL) in the United States. In particular, given the revolutionary results coming out of neutrino physics, the coming decade promises to be exciting with the potential of continued scientific discoveries in the neutrino sector. Hence, there clearly is a need for a dedicated deep underground facility that can accommodate the planned next generation of double beta decay and solar neutrino experiments.

Since that meeting there has been truly remarkable progress. The LRP process culminated in late March 2001 with the following recommendation:

Recommendation 3 We strongly recommend immediate construction of the world's deepest underground science laboratory. This laboratory will provide a compelling opportunity for nuclear scientists to explore fundamental questions in neutrino physics and astrophysics.

Separately, a national committee,[1] was convened with membership from the nuclear, particle, and astrophysics communities. Chaired by John Bahcall, the committee was established to examine the science case for establishing a NUSL, to define the necessary characteristics of such a laboratory, and to consider potential sites. That committee completed its work in early March 2001 and issued the following recommendation:

The Committee unanimously recommends the establishment of a deep premier national underground scientific laboratory to enable US leadership and synergism in a broad array of scientific fields in the coming decades. The committee endorses a single primary site as the most effective method of realizing the anticipated scientific program.

At the time of this meeting the committee favors the Homestake site for the following reasons:
- *faster time scale to produce important scientific results,*
- *less initial capital outlay to produce world-class science,*
- *greater positive impact on the local population,*
- *lower inherent uncertainties.*

Turning these recommendations into reality will require major efforts from many groups within the US program. Our UW group decided that given our expertise in underground experiments and because of our interest in developing the next generation neutrino experiments, we should play an active role in the establishment of NUSL. Following the strong

*Institute for Nuclear Theory, University of Washington, Seattle, WA 98195.

[1] Wilkerson served on this committee and Doe on the technical subcommittee. Go to Bahcall's website http://www.sns.ias.edu/~jnb/toc.html for more information, including a report on the science case for the establishment of a NUSL.

recommendations from NSAC and the Bahcall committee, we assisted in the preparation of a proposal for a NUSL at Homestake[2] that was submitted in June to the National Science Foundation (NSF).[3] This proposal has been favorably reviewed by several NSF convened panels. At this time we continue to work with NSF to move the proposal forward through the complex review process.

Without question in many ways Homestake offers an ideal site for the NUSL. It has drifts at great depth, a critical requirement for many underground experiments and will thus provide the world's best shielded laboratory from the cosmic ray muon flux. The substantial infrastructure and underground drifts will allow for a full science program to start up within a very short time. The rock structure of the mine is extremely well characterized, and based on previous excavations and engineering studies, large cavities can be excavated at depths of up to 8000 feet. We anticipate several major modifications that will allow efficient direct access to the main deep laboratory, which is currently slated to be located on the 7400 foot level. The deep laboratory itself will be engineered specifically to support next generation experiments, which will likely have normally stringent requirements of being ultra clean while containing large amounts of flammable material or cryogens, that are normally problematic in operating mines. You can find much more information in the full proposal.

We are establishing a NUSL collaboration[4] that will help design and build the best possible laboratory. We are also soliciting feedback from the community as we craft the initial science program. As part of our process of involving the community we organized and held a conference on Underground Science in Lead, South Dakota in October.

During the past year we also assisted in setting up and directing a transition team that was based in Lead, that assisted in coordination issues with the Barrick Gold Corporation[5] and with other technical design issues.

[2]The proposal was submitted by Wick Haxton as PI, with J. Wilkerson, J. Conrad (Columbia Univ.), M. Marshak (U. Minn.), and S. Farwell (SD School of Mines and Tech.) as co-PIs.

[3]See our NUSL web site at: http://int.phys.washington.edu/NUSL/ to obtain a copy of the proposal.

[4]Again, visit our NUSL web site at: http://int.phys.washington.edu/NUSL/ for details.

[5]The Homestake Mining Corporation merged with Barrick in December 2001.

3 Nuclear and Particle Astrophysics

3.1 Astrophysical S-factor for ^{7}Be(p,γ)^{8}B

E. G. Adelberger, A. R. Junghans, E. C. Mohrmann, K. A. Snover, T. D. Steiger,*
H. E. Swanson and TRIUMF Collaborators†

The uncertainty in $S_{17}(0)$, the astrophysical S-factor for the ^{7}Be(p,γ)^{8}B reaction, has long been one of the main sources of error in calculations of the production rate of energetic solar neutrinos. An improved understanding of this production rate is desirable because of its importance in the determination of neutrino masses, mixing angles and the possible role of a sterile neutrino.

This past year we completed Phase I, an experiment designed to make a precision determination of $S_{17}(0)$.[1] A goal of this work was to measure all relevant systematic uncertainties. A sharply-focused beam was magnetically rastered over a large area in order to produce a uniform flux over the surface of a metallic ^{7}Be target[2] of 106-mCi initial activity. The activity was monitored frequently *in situ* with a calibrated Ge detector, and used to determine corrections for small sputtering losses. Corrections for the energy loss of the beam in the target become appreciable at low proton bombarding energies and require a knowledge of the target energy thickness, which we measured directly using the narrow resonance in ^{7}Be(α,γ)^{11}C at E_α = 1.376 MeV. A clean vacuum was maintained with cryopumps and large LN_2 cold traps. Repeat measurements of the ^{7}Be(α,γ)^{11}C resonance showed no change, indicating no significant contaminant buildup or other target degradation during the experiment. The correction due to backscattering loss of ^{8}B was measured for the first time, using a fixed target and plates mounted on the water-cooled rotating arm to catch the backscattered ions.

We began our Phase II measurements in early 2002 with a new ^{7}Be target together with several improvements to our experimental apparatus. Our initial goal is to make a semi-independent check of the absolute normalization of our published result. A new absorber was machined for use with the Ge detector to reduce the (small) pile-up and dead time from counting the high γ-intensity from the ^{7}Be target. A ^{148}Gd α-source was fabricated on a backing of the same design as that used for the ^{7}Be target, and used to determine the α-detector solid angle. The α-detector was located on a translation stage to permit precision detector-to-target distance changes as part of the solid-angle determination. Preliminary results indicate a different value for the solid angle compared to the value inferred previously using the ^{7}Li(d,p)^{8}Li reaction. New cross section measurements were made near and above E_p = 1 MeV and are being analyzed.

With improvements that have been made in the accelerator beam intensity and stability at low voltage, we plan additional detailed cross section measurements at low E_p in the near future with a new higher activity target.

*Presently at Cymer Lasers, San Diego, CA 92127.

†L. Buchmann, S. Park and A. Zyuzin, TRIUMF, Vancouver, BC, Canada.

[1] A. R. Junghans et. al., Phys. Rev. Lett. **88**, 041101-1(2002); see also CENPA Annual Report, University of Washington (2001) pp. 49-52.

[2] A. Zyuzin et. al., Nucl. Instrum. Methods B **187**, 264 (2002).

3.2 e^+e^- pair emission and the $^3He+^4He\rightarrow^7Be$ S-factor

A. Hurd,* K. A. Snover and R. G. H. Robertson

The astrophysical S-factor for ^{3}He+^{4}He→^{7}Be is very important for determining the flux of solar neutrinos from decay of ^{7}Be and ^{8}B in the Sun. The presently recommended value is $S_{34}(0) = 0.53 \pm 0.05$ keV-b[1] based on measurements of the capture cross section at low energies by detection of the capture γ-rays and by detection of the residual ^{7}Be activity. The relatively large uncertainty stems from an apparent difference in the results of the two types of experiments, with activation experiments yielding a mean value for $S_{34}(0)$ that is ∼13% larger than the value determined from the capture γ-ray experiments.[1] This has raised the question whether there might be some other capture reaction mechanism that could explain this difference, such as E0 pair emission.

We have determined the cross section for direct E0 pair emission by relating it to the cross section for direct E2 photon emission. This is possible since the operators (in nucleon coordinates) for E0 and E2 emission, $O_{E0} \sim r^2$ and $O_{E2} \sim r^2 Y_{lm}$, have the same radial dependence in the long wavelength limit. As a result, E0 and E2 direct capture amplitudes for specific partial wave transitions may be numerically related. At low bombarding energies, this leads to a simple relation between the cross sections for direct E0 pair emission and direct E2 photon emission.

We find for center-of-mass energies less than 5 MeV and p-wave direct capture in ^{3}He + ^{4}He →^{7}Be, the E0 pair emission cross section is less than 1% of the E2 photon emission cross section. This reduction occurs because E0 pair emission involves an additional electromagnetic vertex, in which the virtual E0 photon converts into an e^+e^- pair - hence this rate is smaller than the E2 photon emission rate by an additional power of the fine-structure constant. From the literature, one finds in this same energy range that the p-wave direct E2 photon emission cross section is calculated to be less than 0.3% of the total cross section, which is primarily direct E1 photon emission. Thus the direct E0 pair emission cross section is less than a few parts in 10^5 of the total capture cross section and hence is completely negligible.

Pair emission may occur for any electromagnetic multipolarity. The unique aspect of E0 emission is that it cannot occur by single photon emission, and hence pair emission is relatively much more important for this multipole. For other multipoles, the pair emission coefficients (ratio of pair emission and single photon emission strengths) are of similar magnitude.[2] Since the total cross section is predominantly direct E1 photon emission, E1 pair emission will dominate over E2 and M1 pair emission. The E1 pair emission coefficient rises with energy and is roughly 0.13% at E = 3 MeV for Z = 4.[2] Hence pair emission is predominantly E1 in ^{3}He+^{4}He→^{7}Be and makes a negligible contribution to the total cross section. Internal conversion is also unimportant in this reaction. We conclude that electromagnetic emission processes other than single photon emission are much too weak to explain the apparent difference between direct photon detection experiments and ^{7}Be activation experiments.

*Department of Physics, University of Washington, Seattle, WA 98195.

[1] E. G. Adelberger *et al.*, Rev. Mod. Phys. **70**, (1998) 1265.

[2] P. Schluter, G. Soff and W. Greiner, Phys. Rep. **75**, (1981) 327.

3.3 Search for the ^{8}B$(2^+) \rightarrow {}^8$Be(0^+) transition

M. K. Bacrania, M. W. Gohl, R. G. H. Robertson, K. A. Snover and D. W. Storm

The high-energy solar neutrino spectrum predicted by the standard solar model consists of neutrinos arising from two mechanisms, the *hep* reaction ($^3\mathrm{He}(\mathrm{p}, \mathrm{e}^+\nu_\mathrm{e})^4\mathrm{He}$), and ^{8}B decay ($^8\mathrm{B} \rightarrow^8 \mathrm{Be}^* + \beta^+ + \nu_\mathrm{e}$). The *hep* reaction has a predicted flux of order $10^3\,\mathrm{cm}^{-2}\mathrm{s}^{-1}$, with an endpoint energy of 19.7 MeV. The ^{8}B decay reaction has a measured neutrino flux of order $10^6\,\mathrm{cm}^{-2}\mathrm{s}^{-1}$, and takes place primarily through the allowed $2^+ \rightarrow 2^+$ transition to the 3.04 MeV broad excited state in ^{8}Be, with an endpoint energy of approximately 14 MeV. It is also possible for ^{8}B to decay to the ground state of ^{8}Be, through a second forbidden transition ($2^+ \rightarrow 0^+$) with an endpoint of approximately 17 MeV. While this second forbidden decay is predicted to have an extremely small branching ratio, the actual branching ratio has never been measured experimentally. The standard solar model does not account for ^{8}B neutrinos above 14 MeV, and thus neutrinos produced by the second-forbidden decay branch would appear as a background to measurements of the *hep* neutrino spectrum.

We are working to measure the branching ratio of the ^{8}B ($2^+ \rightarrow 0^+$) reaction to an accuracy of 10^{-4} of the main branch. ^{8}B will be produced by bombarding a ^{6}LiF target with a 5.5-MeV ^{3}He ion beam produced with the UW CENPA Tandem Van de Graaff accelerator. The resulting 3-MeV ^{8}B will be separated and transported to a 24” scattering chamber and implanted into a 300μm solid-state Si detector at a depth of $\approx 3\mu$m. The resulting ^{8}B decay ($t_{1/2}$ = 770ms) will produce a β^+, and the prompt decay of ^{8}Be will produce a pair of α particles. A decay via the $2^+ \rightarrow 0^+$ branch will result in two 45 keV α particles, each traveling a distance $< 1\mu$m in the Si detector. We will detect the β^+ in an annular scintillator upstream of the Si detector. ^{8}B decays will be identified by a coincidence between the scintillator and the Si detector.

In 2001 we completed preliminary calculations of rates and other relevant experimental quantities. Our expected ^{8}B deposition rate into the Si detector is approximately 10 particles per second per μA. We also built holders for the detector and LiF targets. As the magnetic rigidity of 2 MeV $^3\mathrm{He}^{2+}$ is identical to that of 3 MeV $^8\mathrm{B}^{4+}$, $^3\mathrm{He}^{2+}$ which has lost energy through scattering is a potentially large background. We conducted beam tests in order to determine the amount of ^{3}He scattering and energy loss in the ^{8}B production region, and the corresponding background rate at the 24” scattering chamber.

As a result of these tests, we found that by 1) using GVM rather than slit control of the terminal voltage, and 2) by making a very thin (1/8 mm) target holder with a large diameter (16 mm) hole, we were able to obtain a counting rate, in an Si detector placed on the beam line in the scattering chamber, of approximately 200 counts per sec per μA of ^{3}He. This figure was for our anticipated running conditions, with a 5.5 MeV $^3\mathrm{He}^{1+}$ beam incident on the target and the downstream beam transport set for the ^{8}B as described above.

3.4 Reanalysis of $\alpha+\alpha$ scattering and β-delayed α spectra from ^{8}Li and ^{8}B decays.

E. G. Adelberger and M. Bhattacharya

We have completed the reanalysis of $\alpha+\alpha$ scattering and β-delayed α decay from ^{8}Li and ^{8}B[1] taking into account the important recoil broadening effect that was ignored in all previous analyzes. We find that the difference in the ^{8}Be continuum inferred from the β-decay data and phase-shift data are substantially smaller than that concluded by previous authors. We also speculate that the residual discrepancy in the extracted width of the lowest L=2 level from the phase-shift data and that extracted from the delayed-α data could be due to the simplifying assumption that the Gamow-Teller matrix elements to the broad levels in ^{8}Be are strictly energy independent. We also found excellent agreement between the old Wilkinson-Alburger singles data and the recent coincidence measurement of Ortiz *et al.*[2] Our work has been accepted for publication in Phys. Rev. C.

3.5 β-delayed α spectra from ^{8}Li and ^{8}B decays and the shape of the neutrino spectrum in ^{8}B decay

E. G. Adelberger, M. Bhattacharya and H. E. Swanson

We finished data taking for our high precision measurement of the β-delayed α spectra from ^{8}Li and ^{8}B decays.[3] Our data runs were stable ($< \pm 2$ keV gain drifts over one week long periods of data taking) and we achieved an energy calibration accuracy of ± 5 keV over a 5.5 MeV α energy range. We have good statistics (> 1 million counts per detector for the ^{8}B run and > 2 million counts per detector for the ^{8}Li run) and are currently in the process of analyzing our data.

[1] CENPA Annual Report, University of Washington (2001) p. 47.
[2] C. E. Ortiz *et al.*, Phys. Rev. Lett. **85**, 2909 (2000).
[3] CENPA Annual Report, University of Washington (2001) p. 48.

3.6 WALTA: The Washington Large-area Time-coincidence Array

T. A. Anderson,* H. Berns,* T. Burnett,* R. Corn,* J. G. Cramer, S. R. Elliott, T. Haft,† M. Lautenschlager,* M. Lemagie,* E. Muhs,‡ M. Roddy,§ J. Wilkes,* E. Zager* and <u>H. M. Zorn</u>

Ultra-high energy cosmic rays are of particular interest to many physicists. Where do these particles come from and what could possibly accelerate the particles to such high energies are just two of the questions scientists would really like to answer. WALTA (Washington Area Large-scale Time-coincidence Array) is a project to study ultra-high energy cosmic rays through a distributed network of detectors. These particle detectors will be placed on the roofs of high schools and middle schools in the Seattle-metro area, and students and teachers will be an integral part of the research.

Over the past year, we have been dedicated to getting teachers and students involved in the project. Last summer, at the Snowmass 2001 conference, we worked with the University of Nebraska and the University of Alberta to run a week-long workshop for teachers and students from both the Aspen area and an Illinois high school near Fermilab. The workshop included lectures where the teachers and students learned about the physics of cosmic rays and the physics of our detector system. In addition, half of the time was devoted to refurbishing the detectors, learning how to use NIM electronics and then running basic calibration measurements.

We also ran a similar workshop at the University of Washington for 10 high-school teachers from the Seattle area, in collaboration with QuarkNet, an outreach program through Fermilab. Throughout the school year, we have had continued contact with the WALTA teachers through two workshops held specifically for the teachers, and weekly group meetings that the teachers are invited to attend. Currently, two teachers have been running experiments using their school's four detectors and a basic collection of NIM electronics. The other eight teachers are just about ready to start conducting their own tests. At the end of the school year, students will be presenting their research findings to the entire WALTA group. This summer we will be running another week-long workshop for both the current WALTA teachers and new teachers.

We have continued research on a data-acquisition electronics system. Two basic ideas were pursued. One involved using a National Instruments counting board to measure the size of the pulses and the relative timing. We have also been collaborating with Fermilab and the University of Nebraska to build a custom data-acquisition electronics package. A prototype of the custom electronics board will be tested early this summer and delivered to the teachers soon after.

In collaboration with the University of Nebraska, approximately 1600 scintillators, 1600 photomultiplier tubes, and 400 low to high voltage converters were retrieved from Dugway,

*Physics Department, University of Washington, Seattle, WA 98195.
†Issaquah High School, Issaquah, WA.
‡Shorewood High School, Shoreline, WA.
§Education Department, Seattle University, Seattle, WA.

Utah and are being stored at the University of Nebraska. This equipment was used in the Chicago Air Shower Array (CASA),[1] an experiment to study cosmic rays that was in operation from 1990 - 1998. With a portion of this supply and equipment that was collected last year, we have enough scintillators and PMTs to outfit all of the schools in the initial WALTA array. Each school will have four detectors. Throughout the year, research was conducted on the efficiency of the CASA detectors and on ways to improve this efficiency, both by University members of the WALTA team and the high school teachers and students.

[1]M. A. K. Glasmacher *et al.* Astroparticle Phys. **10**, 291 (1999).

4 Ultra-Relativistic Heavy Ion Physics

HBT Physics at STAR

4.1 Overview of HBT physics at STAR

J. G. Cramer, J. M. S. Wu and the STAR HBT Physics Working Group*

The STAR HBT[1] Physics Working Group (HBT PWG), active membership about 20 physicists led by convenor Sergei Panitkin, has made very significant progress in the past year in analyzing data from the first two years of operation of the STAR detector at RHIC. A paper reporting the initial HBT results for pion data at 130 GeV per nucleon from the first year of RHIC operation has now been published in Physical Review Letters.[2] Several additional papers about aspects of STAR HBT physics are in various stages of preparation. Analysis of RHIC Year-2 data at 200 GeV per nucleon is in progress.

The impact of our initial STAR HBT results has been very strong. In particular, the relatively small increase in R_{long}, the longitudinal radius of the pion-emitting source, has called into question the conventional assumption of boost invariance, the approximation that the longitudinal source can be treated as infinitely long because of the kinematic cutoff arising from the gradient in longitudinal velocity along the source.

An even larger impact has come from the observation from the HBT analysis that the ratio $R_{out}/R_{side} \approx 1$ is inconsistent with essentially all of the models of 130-GeV/A Au+Au collisions that existed before initial RHIC operation. The large increases in source size and emission duration that most models predicted for the RHIC regime are not observed, and in some sense the models have been falsified. In the theoretical community, this failure of model predictions has been named "The HBT Puzzle." Several unsatisfactory solutions to the HBT Puzzle have been discussed in recent seminars and other discussions. They involve the "freezeout" process, the point at which emitted pions undergo their last scattering and proceed to the detector as free particles. The scenarios are:
(1) One can assume that the transition from quark-gluon plasma occurs at the same time as chemical and kinematic freezeout, instead of these transitions being separated in time by 2-10 fm/c.
(2) One can assume that the pion freezeout does not start at the cooler outside of the collision fireball and proceed inward, as has been universally assumed, but instead, by some unknown energy-loss mechanism freezes out first in the hot central region of the source and proceeds outward.
(3) One can assume that the source is opaque, so that pion emission can take place only from source regions having a relatively short path length to traverse before freezeout.

Each of these scenarios has problems. Scenario (1) would probably predict source sizes

*See the HBT PWG web site at http://connery.star.bnl.gov/STAR/html/hbt_l.

[1] HBT is a widely used abbreviation for Hanbury-Brown Twiss interferometry.

[2] C. Adler *et al.*, Phys. Rev. Lett. **87**, 082301 (2001).

much smaller than those observed and would require some unknown physics to produce the rapid succession of transitions. Scenario (2) requires an unknown and probably unphysical energy-loss mechanism. Scenario (3) requires absorption that is consistent with rough estimates of the pion mean free path, but it strongly reduces the number of pions emitted, leading to inconsistencies with the observed number of emitted pions.

We are attempting to investigate the HBT Puzzle by establishing an intermediate reference point, an empirical source model (See Section 4.4). Based on the work of Tomasik and Heinz,[3] we are developing a numerical model of the pion emitting source that is relatively free of simplifying approximations and can predict the experimental observables, the pion momentum spectrum, HBT radii, and phase space density. This numerical model, which is now operating in a preliminary form, will allow us to provide one or more descriptions of the pion-emitting source that are consistent with the STAR data and analysis. Such descriptions can then serve as targets for collision models that probe the underlying physics of RHIC collisions.

In summary, the STAR HBT Physics Working group has made considerable progress in analyzing the data from the first two years of RHIC operation. The initial HBT analysis has presented several theoretical puzzles that are now being addressed. We look forward in the coming year to further progress in data analysis and in theoretical understanding.

[3] B. Tomasik and U. Heinz, preprint nucl-th/0108051.

4.2 Pion phase space density and "bump volume"

J. G. Cramer, J. M. S. Wu and the STAR HBT Physics Working Group*

The average 6-dimensional phase space density $< f >$ of pions emitted from an ultra-relativistic heavy-ion collision is a Lorentz scalar that has the form:

$$< f >= \left[\frac{1}{E_\pi}\right]\left[\frac{d^2N}{2\pi m_T dm_T dy}\right]\left[\frac{1}{\sqrt{\lambda}}\right][V_p] \text{ where } V_P = \left[\frac{\lambda(\hbar c\sqrt{\pi})^3}{R_S\sqrt{R_O^2 R_L^2 - R_{OL}^4}}\right].$$

Here the first term in brackets is the Jacobian that preserves Lorentz invariance, the second term is the momentum spectrum, and the third term corrects for the "purity" of the observed pions. The term V_p is the momentum-space volume occupied by the three-dimensional Bose-Einstein "bump" $C_2(q_O, q_S, q_L)-1$ where O, S, L refers to the Bertsch-Pratt out, side, and long momentum directions. This factor is critical for the determination of the phase-space density. It can be estimated using measured HBT parameters, as indicated in the second equation, or can be obtained directly from the 3-dimensional correlation histogram by directly summing histogram channel contents $C_2(\vec{p}) - 1$.

For the first momentum bin of our analysis (p_T=0.125-0.225 GeV/c), we have determined V_p by both methods using Coulomb-corrected 3-dimensional histograms from the published HBT analysis of STAR data.[1] For the direct sum method, because of the tall "grass" at large q_O, we have used direct summation only within a momentum sphere with a radius of q=0.080 GeV/c (about the point where the bump dies away) and have used the HBT fits to estimate the additional volume present in the "tail" region outside this spherical cutoff. The results are shown in Table 4.2-1.

Mom. Bin GeV/c	$< Npart >$	V_p(HBT) $\times 10^{-5}$	dV_p $\times 10^{-5}$	V_p(Sum) $\times 10^{-5}$	dV_p $\times 10^{-5}$	Diff. %
0.125-0.225	345	9.136	0.100	12.436	0.006	36.11
0.125-0.225	286	9.644	0.096	13.536	0.006	40.36
0.125-0.225	221	11.829	0.142	15.262	0.014	29.03
0.125-0.225	149	14.361	0.227	17.186	0.029	19.67
0.125-0.225	97	20.627	0.392	22.790	0.107	10.49
0.125-0.225	61	27.196	0.746	30.559	0.238	12.37
0.125-0.225	18.4	47.385	2.235	50.547	1.253	6.67

Table 4.2-1. "Bump Volume" V_p in $(GeV/c)^3$ (statistical errors only)

We see that the statistical errors are around 1 to 4% for the HBT determination and 0.05 to 2% using the direct sum method. However, there is a very significant difference ranging from 36% to 7% in the values of V_p measured by the two methods. This difference is well outside the statistical errors of the determinations. We attribute the difference to a

*See HBT PWG web site at http://connery.star.bnl.gov/STAR/html/hbt_l.

[1]C. Adler et al., Phys. Rev. Lett. **87**, 082301 (2001).

systematic error that comes from the assumption in the HBT analysis that the correlation function is a 3-dimensional Gaussian. There is evidence that the source has an enhancement at low q-values that significantly deviates from Gaussian behavior. The deviation may arise from incorrect correction for Coulomb effects, but attempts to modify the Coulomb correction have not been found to significantly modify the effect shown here. Fig. 4.2-1 below shows sample correlation data and fits, illustrating this deviation.

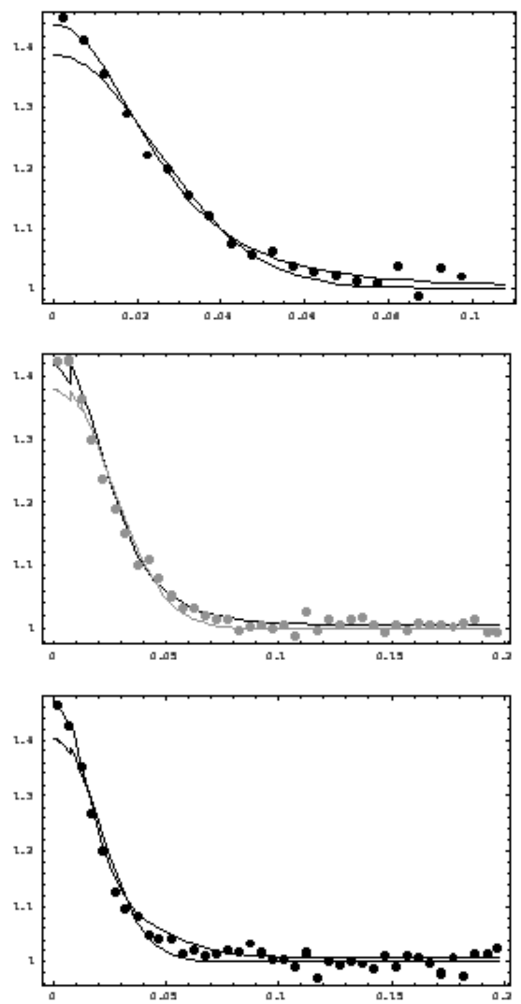

Figure 4.2-1. Fits with one Gaussian (gray) and with two Gaussians (black), for the q_O (top), q_S (mid), and q_L (bottom) projections of the 3D correlation histogram.

Shown are projections averaging from 0 to 0.0175 GeV/c in the other momenta for q_O (top), q_S (center) and q_L (bottom). Horizontal scale is the momentum difference q in GeV/c. We conclude from this analysis that estimating the correlation volume from derived HBT parameters is unreliable, and that the preferred method of deriving the correlation volume and extracting the phase space density should be to directly sum the three dimensional HBT histogram out to some cutoff momentum, and to correct this sum with an estimate of the volume in the tail region derived from a 3D Gaussian fit to the histogram.

4.3 Moment analysis of 3D HBT histograms and the R_{out}/R_{side} ratio

J. G. Cramer, J. M. S. Wu and the STAR HBT Physics Working Group*

The "HBT Puzzle" discussed above makes it important to establish the robustness of the result that the HBT analysis ratio R_{out}/R_{side} is very close to 1, independent of the various assumptions implicit in the analysis. A less model-dependent alternative to fitting 3D HBT histograms with a Gaussian distribution is computing the 0th and 2nd moments of the distribution along the three momentum axes and using these to infer "moment-based" HBT parameters. In addition, one can use the 2nd and 4th moments along the three axes to calculate the kurtosis (or non-Gaussian-ness) of the distribution, with a positive kurtosis indicating an over-peaked distribution, a negative kurtosis indicating a flat-topped distribution, and zero kurtosis indicating a perfect Gaussian distribution.

Wiedemann and Heinz[1] have laid out the formalism for this kind of analysis and have used it to investigate flow and resonance effects.[2] The principal problem with the moment procedure, as they point out, is that it does a weighted sum over the correlation histogram that de-emphasizes the correlation bump region and gives large weight to the statistics-poor tail region. Therefore, the data set used in this kind of analysis needs to have very good statistics, particularly in the tail region, to give reliable results. Nevertheless, it's interesting to see what can be accomplished with the 3D histograms that we have available from STAR data.

Basically, the procedure we have used in this analysis is to define a general moment function: $\mathbf{M}_x[q_{cut}, m] \equiv \sum[q_x^m(C[q_{out}, q_{side}, q_{long}] - 1)]$ where $x = out, side, long$. The sum is taken over all histogram bins having an non-zero "signal" and that fall inside the momentum sphere $q_{out}^2 + q_{side}^2 + q_{long}^2 < q_{cut}^2$. Using this moment function, the moment-based estimates of the HBT parameters are:

$$\begin{aligned}
\langle\lambda\rangle(q_{cut}) &= \sqrt{\mathbf{M}_{side}^5(0, q_{cut})/[(2\pi)^3\mathbf{M}_{out}(2, q_{cut})\mathbf{M}_{side}(2, q_{cut})\mathbf{M}_{long}(2, q_{cut})]} && (1)\\
\langle R_{out}\rangle(q_{cut}) &= \hbar c\sqrt{\mathbf{M}_{out}(0, q_{cut})/[2\,\mathbf{M}_{out}(2, q_{cut})]} && (2)\\
\langle R_{side}\rangle(q_{cut}) &= \hbar c\sqrt{\mathbf{M}_{side}(0, q_{cut})/[2\,\mathbf{M}_{side}(2, q_{cut})]} && (3)\\
\langle R_{long}\rangle(q_{cut}) &= \hbar c\sqrt{\mathbf{M}_{long}(0, q_{cut})/[2\,\mathbf{M}_{long}(2, q_{cut})]} && (4)\\
\langle\frac{R_{out}}{R_{side}}\rangle(q_{cut}) &= \sqrt{\mathbf{M}_{side}(2, q_{cut})/\mathbf{M}_{out}(2, q_{cut})} && (5)\\
\langle K_{out}\rangle(q_{cut}) &= \mathbf{M}_{out}(0, q_{cut})\,\mathbf{M}_{out}(4, q_{cut})/[3\,\mathbf{M}_{out}^2(2, q_{cut})] - 1 && (6)\\
\langle K_{side}\rangle(q_{cut}) &= \mathbf{M}_{side}(0, q_{cut})\,\mathbf{M}_{side}(4, q_{cut})/[3\,\mathbf{M}_{side}^2(2, q_{cut})] - 1 && (7)\\
\langle K_{long}\rangle(q_{cut}) &= \mathbf{M}_{long}(0, q_{cut})\,\mathbf{M}_{long}(4, q_{cut})/[3\,\mathbf{M}_{long}^2(2, q_{cut})] - 1 && (8)
\end{aligned}$$

Here is a table of the estimates of λ, R_{side}, R_{out}, and R_{long} over a range of q_{cut} values,

*see http://connery.star.bnl.gov/STAR/html/hbt_l.

[1] U. A. Wiedemann and U. Heinz, Phys. Rev. C **56**, R610 (1997).

[2] U. A. Wiedemann and U. Heinz, nucl-th/9611031.

calculated using the 3D histogram for most central events (0-5% of total reaction cross section) and the lowest p_T bin (0.125 to 0.225 GeV/c):

Table 1 – HBT Radii from Moment Analysis

q_{cut}	λ	R_{side}	R_{out}	R_{long}
0.02	**1.57244**	**16.4336**	**15.7039**	**16.2915**
0.03	**1.18497**	**11.0832**	**10.9730**	**11.7297**
0.04	**0.91339**	**8.5015**	**8.6429**	**9.3760**
0.05	**0.70711**	**7.0438**	**7.1061**	**7.8167**
0.06	**0.56690**	**6.1484**	**6.1771**	**6.7130**
0.07	**0.46275**	**5.4038**	**5.4573**	**6.0224**
0.08	**0.38699**	**4.9564**	**5.0078**	**5.3932**
0.09	**0.32490**	**4.5211**	**4.6752**	**4.8616**
0.10	**0.27025**	**4.0435**	**4.4505**	**4.3533**

We observe HBT parameters, when estimated in this way, have an unacceptable "walk" that depends on the value used for q_{cut}. However, it is of interest to observe the value of the R_{out}/R_{side} ratio estimated in the same way. Here is a table of the estimates of R_{out}/R_{side}, K_{side}, K_{out}, and K_{long} over a range of q_{cut} values, calculated using the same 3D histogram:

Table 1 – HBT Radii from Moment Analysis

q_{cut}	R_{out}/R_{side}	K_{side}	K_{out}	K_{long}
0.02	**0.95660**	**-0.2475**	**-0.2660**	**-0.2333**
0.03	**0.99006**	**-0.2234**	**-0.2476**	**-0.2012**
0.04	**1.01663**	**-0.2052**	**-0.2038**	**-0.1457**
0.05	**1.00884**	**-0.1921**	**-0.1644**	**-0.1077**
0.06	**1.00468**	**-0.1728**	**-0.1423**	**-0.0797**
0.07	**1.00991**	**-0.1346**	**-0.1220**	**-0.0766**
0.08	**1.01039**	**-0.1164**	**-0.0681**	**-0.0035**
0.09	**1.03410**	**-0.0801**	**-0.0296**	**-0.0330**
0.10	**1.10066**	**-0.0240**	**-0.0138**	**-0.0633**

We see that the R_{out}/R_{side} ratio is quite stable. This provides a more model-independent case for the robustness of the result that the R_{out}/R_{side} is very close to 1. We note that the moment-derived HBT parameters are closest to the Gaussian-fit HBT parameters for q_{cut} values between 60 and 80 MeV/c.

4.4 Simulation of opacity effects in HBT sources

J. G. Cramer, F. L. Ray,* J. M. S. Wu and the STAR HBT Physics Working Group†

As mentioned in Section 4.1, we wish to develop a source model that predicts our observed pion spectra and momentum-dependent HBT radii, to serve as a "middle-ground" between the basic data from STAR and other RHIC experiments and the various QCD or hydrodynamics-based theoretical models. We wish to make as few simplifying assumptions as possible, so we employ a fairly general hydrodynamically-inspired thermal Bose-Einstein emission function,[1,2] which has the form:

$$\begin{aligned} S(x,p) &= \frac{m_T \cosh(y-\eta_L)}{(2\pi\hbar)^3} G(r, R_{RMS}) \\ &\times\{\exp(\frac{\mathbf{p}\cdot\mathbf{u}(x)-\mu(r)}{T})-1\}^{-1} \\ &\times \exp(-(\eta_L-\eta_0)^2/2\delta\eta^2) \\ &\times \exp(-(\tau-\tau_0)^2/2\delta\tau^2)/(\delta\tau\sqrt{2\pi}) \\ &\times \exp(-L_{eff}/\lambda_{MFP}) \end{aligned} \quad (1)$$

Here, the pion momentum four-vector is $\mathbf{p} = \{m_T \cosh(y),\, p_T \cos(\Phi),\, p_T \sin(\Phi),\, m_T \sinh(y)\}$, the transverse momentum of an emitted pion is p_T, $m_T = \sqrt{p_T^2 + m_\pi^2}$ is its transverse mass, and y is its longitudinal rapidity. The source expansion velocity four-vector is $\mathbf{u}(x) = \{\cosh[\eta_T(r)]\cosh(\eta_L),\, \cos(\phi)\sinh[\eta_T(r)],\, \sin(\phi)\sinh[\eta_T(r)],\, \cosh[\eta_T(r)]\sinh(\eta_L)\}$. The transverse flow rapidity η_T(r) is related to the transverse flow velocity $\beta_T = p_T/mT$ by $beta_T = \tanh(\eta_T)$, and η_L is the longitudinal source rapidity. We assume that the pion emission is observed in the longitudinal center of mass frame of the source ($\eta_0 = 0$) at midrapidity ($y = 0$) along the x axis ($\Phi = 0$).

The source is assumed to have a transverse density profile given by $G(r, R_{RMS})$. In the present work we consider four alternative transverse density profiles, a "box" function $\theta(R-r)$, a Gaussian $\exp[-(r/R)^2/2]$, a surface peaked Gaussian $(r/R)^2\exp[-(r/R)^2/2]$, and a Woods-Saxon distribution $\{\exp[(r-R)/\delta]+1\}^{-1}$, with R chosen in each case to match the specified RMS radius of the distribution. The transverse source rapidity η_T has a maximum value η_f and is assumed to start from 0 at r=0 and to increase in proportion to the local density of the source, i.e., $d\eta_T/dr \sim G(r, R_{RMS})$, so that for a box profile it grows linearly to η_f. The chemical potential is assumed have the radial dependence $\mu(r) = \mu_0 G(r, R_{RMS})$. The quantity $L_{eff}(r,\phi)$ is the effective path length from the pion emission point at $\{r,\phi\}$ to infinity, as the pion passes through the source medium on its way to the detector, and depends on the transverse distribution shape.[3] The nine adjustable parameters that characterize the

*Department of Physics, University of Texas, Austin, TX 78712.

†see *http : //connery.star.bnl.gov/STAR/html/hbt_l*.

[1] B. Tomasik, U. A. Wiedemann, and U. Heinz, nucl-th/9907096.

[2] B. Tomasik and U. Heinz, nucl-th/0108051.

[3] H. Heiselberg and A. P. Vischer, nucl-th/9609022.

emission function are: the local temperature T, the source rapidity width $\delta\eta$, the mean emission time τ_0, the pion emission duration $\delta\tau$, the transverse source RMS radius R_{RMS}, the Woods-Saxon skin thickness δ, the maximum transverse rapidity η_f, the maximum chemical potential μ_0, and the mean free path of pions in the source medium λ_{MFP}.

We have written a FORTRAN program to perform appropriate integrals of this source emission function over a plausible freezeout surface to calculate the momentum spectrum of emitted pions, the HBT radii, and the pion phase space density. The code has been debugged, and we are beginning to test its predictions. Even though it must perform four-dimensional numerical integrals and evaluate an infinite series, it can perform a calculation for a given set of parameters and predict the spectrum and HBT observables over a range of pion momenta in around 10 to 20 seconds.

We find that with a mean free path around $\lambda_{MFP} = 10R_{RMS}$ there are significant regions of the parameter space in which the HBT radius ratio R_{out}/R_{side} can be made approximately unity. We note that a mean free path of this approximate size is expected from rough estimates of the pi-pi scattering cross section in a medium of nuclear density. However, we have not found a plausible set of conditions for which the R_{out}/R_{side} ratio stays close to unity over a wide range of pion momenta, as observed in the data. These investigations are continuing. We plan to attach a fitting program to the source-function code, so that we can efficiently fit the available experimental spectra and HBT parameters from STAR.

We are also investigating extensions of the code that would allow time and radial dependence for the temperature, momentum dependence for the absorption mean free path, and integration over a more general freezeout surface.

Event-by-Event Physics

4.5 Event-by-event analysis overview

T.A. Trainor

On one side of the QCD phase boundary at some asymptotic distance lies the idealization of perturbative or p-QCD, an uncorrelated Stefan-Boltzmann gas of colored quarks and gluons. On the other side lies the highly-correlated hadronic regime: a resonance gas of colorless hadrons and broken symmetries described approximately by strong-interaction phenomenology. During a relativistic heavy ion collision of sufficient energy a small system, far from equilibrium, approaches this boundary from the p-QCD side, expanding, cooling and traversing the phase boundary in a complex way. Only the hadronic final state is accessible to observation. In event-by-event analysis we search for remnants of the deconfined system and phase-boundary traversal embedded in the correlation structure of the final state. We have recently found these remnants at small amplitudes whose detection and study require precision techniques. Progress has been made along several paths. An understanding of the relation between fluctuation and correlation measures is established, and between two-particle mixed-pair correlation references and central-limit fluctuation references. Systematic biases in fluctuation measures have been identified and reduced. The structure of the two-particle momentum space has been surveyed, and lower-dimensional joint autocorrelations have resulted in visualizable spaces which retain almost all correlations.

Centrality dependence of nonstatistical p_t fluctuations indicates that initial-state scattering is the dominant source of these fluctuations at RHIC, leading to the possibility that ISS provides a probe of a dissipative medium that depends strongly on collision centrality. We compare centrality dependence of p_t fluctuations with that of particle production and inclusive p_t production to obtain a more complete picture of measure transport from axial to transverse phase space and the evolution of correlations throughout the collision. Study of two-particle correlations has been complemented by a re-examination of single-particle spectra and their correlation structure. The recent introduction of the Lévy distribution as a reference for partially-equilibrated dissipative systems adds a new dimension to these studies, to distinguish between structure arising from QCD hard parton scattering and from incomplete equilibration. The evolution of the single-particle p_t spectrum with centrality complements studies of dissipation with two-particle correlations.

Until recently, the analysis of heavy-ion collisions has been dominated by classical many-body concepts: a multiparticle phase space admitting different chemical species and described by cascade Monte Carlos, equilibrium statistical models and hydrodynamic continuum models. These asymptotic cases provide essential guidance but are not valid in general. As precision results appear these models must fail. Event-by-event analysis has emerged as an alternative model-independent approach in which the collision final state is characterized phenomenologically by its correlation content. For complex systems this may be the ultimate approach, a broader context in which particles and continua are limiting cases. First RHIC heavy-ion collisions have shown a wealth of correlation detail in the initial stages of analysis whose interpretation is just beginning, as described further in the accompanying articles.

4.6 P_t fluctuations

Non-statistical $< p_t >$ fluctuations in STAR data

J. G. Reid and T. A. Trainor

One of the most powerful tools that probes event-scale physics is measurement of excess (non-statistical) fluctuations in global event variables. We have two basic methods for measuring the excess fluctuations in the $< p_t >$ distribution. The first is a graphical method. The central limit theorem (CLT)[1] tells us that purely statistical fluctuations would yield a distribution which has the form of a gamma distribution.[2] We can compare the $< p_t >$ data distribution to this gamma distribution to see if there are any excess fluctuations. An increase in fluctuations

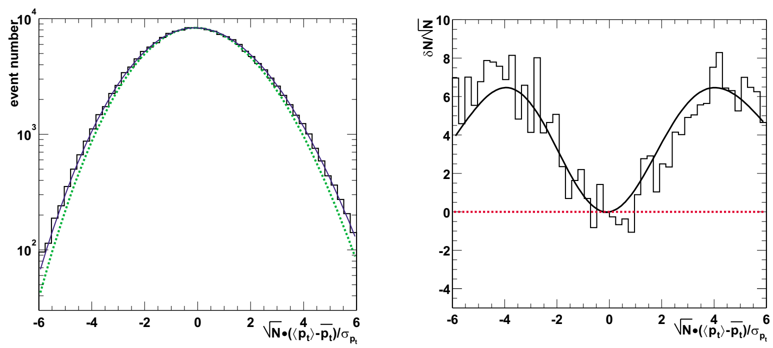

Figure 4.6-1. Normalized $< p_t >$ distribution compared to a gamma reference (dotted line, right panel). The solid line is the reference gamma with a 10% *rms* width excess. The difference between the data and reference is also plotted with the 10% *rms* width scaled gamma difference (solid line, left panel).

beyond the statistical baseline appears as an increase in the width of the data distribution over the reference. We can model this as an increase in *rms* width. These results are consistent with excess fluctuations at the 10% level for Au-Au collision at $\sqrt{s_{NN}} = 130$ GeV.

The second method for measuring fluctuation excess is an algebraic analog to the graphical method. We can do a direct algebraic width comparison between the data and the CLT expectation with the $\Delta\sigma_{p_t}$ measure.

$$\Delta\sigma^2_{p_t} = \overline{n(< p_t > -\hat{p}_t)^2} - \sigma^2_{p_t} \tag{1}$$

Corrected results for central events are $\Delta\sigma_{++} = 14$ MeV/c, $\Delta\sigma_{--} = 14$ MeV/c, and $\Delta\sigma_{+-} = 14$ MeV/c, where we have considered different charge combinations separately. Charge-independent and charge-dependent results are $\Delta\sigma_{\Sigma} = 27 \pm 3$ MeV/c and $\Delta\sigma_{\Delta} = 0 \pm 1$ MeV/c respectively. These results are in close agreement to the results from the graphical method. The charge-independent centrality dependence for minbias data are shown and discussed in Section 4.8.

[1] T. A. Trainor, Event-by-Event Analysis and the Central Limit Theorem, hep-ph/0001148.

[2] M. J. Tannenbaum, Phys. Lett. B **498**, 29 (2001).

Systematic error analysis for $< p_t >$ fluctuations

J. G. Reid and T. A. Trainor

The sensitivity of event-scale fluctuation analysis makes it particularly prone to experimental and systematic errors. To insure robust results an analysis effort has been made to understand and minimize systematic error effects. The first order of business in generating robust results is to minimize contamination of the data sample. To do this we apply a series of track and event cuts. At the event scale we remove all events that do not have a reconstructible vertex within 75 cm of the center of the detector ($v_z < 75$), if an event's primary vertex is off-center it biases the η measurements and can create significant problems with track matching and reconstruction at the TPC's central membrane.

At the track level a variety of cuts are applied, mostly to insure only well reconstructed primary tracks are used. We only use tracks which pass within 3 cm of the primary vertex (dca < 3) and have been fit with the requirement that this vertex lies at the start of each track. Any tracks that cannot be satisfactorily fit with the primary vertex on the track are rejected. To avoid double counting tracks which may have been inadvertently split in the reconstruction process we require the length of each accepted track to be at least half of the possible length ($\frac{n_{fit}}{n_{max}} > 0.5$). Also, the p_t of accepted tracks is restricted to $0.15 < p_t < 2$ GeV. This removes abnormally high momentum tracks and cuts out the low p_t region where the reconstruction process is most vulnerable to error. This also serves to limit the scope of our analysis to the soft-physics regime in which we are interested.

We would also like to be able to cut out tracks which are reconstructed poorly. This requires us to examine carefully the χ^2 goodness-of-fit parameter. Applying a simple cut to reject tracks with $\chi^2 > 2$ was tried, but after further investigation its validity was called into question. The χ^2 distribution was peaked below one, suggesting the errors on track cluster point positions had been underestimated. Also, the χ^2 distribution did not exhibit the expected P_χ behavior, suggesting that it does not properly measure the goodness-of-fit. Also, upon further investigation we found that there is a non-uniform p_t dependence of the χ^2 distribution. Thus, application of a χ^2 cut is equivalent to changing our p_t acceptance in an unpredictable way. Since it is impossible to deconvolute the χ^2 distribution and its p_t dependence a χ^2 cut had to be abandoned.

A great deal of effort has been made to utilize the least biased possible measure (see Section 4.11). We have found this to be the $\Delta\sigma_{p_t}$ measure which is unbiased, but requires acceptance correction. To make this correction a study was done in which particles were randomly removed from the data sample. Fortunately, we found a simple, linear relationship between the number of particles included in the analysis and $\Delta\sigma_{p_t}$. This was true for both charge-dependent and -independent results. Thus, we can trivially extrapolate our results to the full acceptance of the detector after quality cuts have been made.

4.7 Multiplicity fluctuations

Scale-dependent shape analysis of the minimum-bias terminus and multiplicity fluctuations at b = 0

Q. J. Liu, D. J. Prindle, J. G. Reid and T. A. Trainor

The average number of produced particles in a A-A collision increases monotonically as the impact parameter decreases. Selecting a finite range of impact parameters will thus lead to produced particle fluctuations. The number of nucleons participating in a collision approaches a limit as the impact parameter approaches 0, leading to a sharp edge at the terminus of the minimum-bias multiplicity distribution. The observed shape at the terminus is primarily determined by fluctuations in particle production and by sampling with finite acceptance. By analyzing the shape of the terminus we can exclude variation in impact parameter as the source of event to event particle fluctuation. Repeating this shape analysis for multiple bin sizes in η and ϕ we can probe for fluctuations occurring at different scales as well as cross check our acceptance corrections.

To analyze the shape of the terminus we start with a reference distribution calculated using a Glauber model. (See Section 4.11.) We incorporate fluctuations by convoluting the Glauber calculation with a distribution characterized by $\sigma = \sigma_0 \times \sqrt{N}$. The distribution is

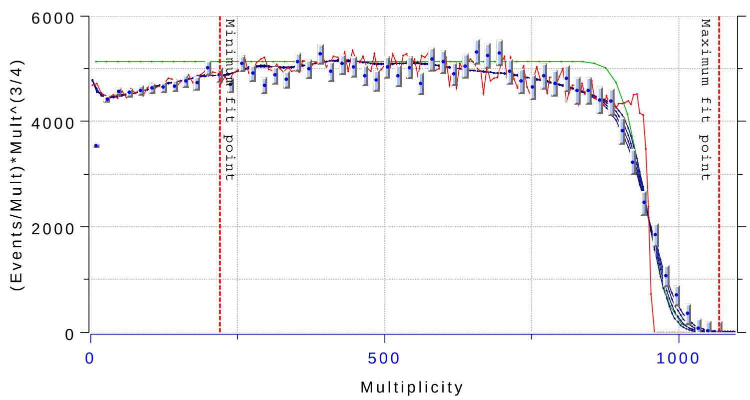

Figure 4.7-1. Minimum-bias multiplicity distribution. The multiplicity is restricted to tracks with $|\eta| < 1.0$. The points with the error bars are the data. The lines shows a Glauber calculation with the track finding efficiency applied and convoluted with various variances.

binomial, Poisson or negative binomial if σ_0 is less than, equal to or greater than 1 respectively. Next we multiply the convoluted Glauber calculation by our track-finding efficiency. Using Monte-Carlo tracks embedded in real events we find $\epsilon = 0.89 - 0.14 \times N_{tracks}$ for tracks passing our quality cuts and falling within our largest acceptance. A sample comparison of data to our reference is shown in Fig. 4.7-1. We have three fit parameters. Two of them, the number of produced particles per participant and the number of events, scale the Glauber calculation in the horizontal and vertical directions to match the data. We find these parameters are independent of the η and ϕ bin sizes. The third parameter, σ_0, characterizes the shape of the terminus and does depend on the η and ϕ bin sizes. In all cases $\sigma_0 > 1$. We can do this terminus shape analysis for any particle species. In practice we are interested in positive, negative and all charged hadrons.

Net charge fluctuations as a function of scale and centrality

Q.J. Liu, D. J. Prindle, J. G. Reid and T. A. Trainor

Last year we reported our progress on measuring charge fluctuations in heavy-ion collisions in STAR.[1] Briefly, our measure of charge difference fluctuations is

$$\Delta\sigma^2_{N_\Delta} = \overline{(\delta N_+ - \delta N_-)^2/(N_+ + N_-)}$$

where δN is a deviation from the mean and N_+ and N_- are the numbers of positive and negative charged particles measured in an event.

Our measurements are shown in Fig. 4.7-2. In this figure the solid line shows what we expect due to charge conservation; as our bin size approaches 4π we expect no fluctuations because total charge is conserved. We expect our measurements to be below this line because the decays of neutral particles correlate N_+ and N_-. As the bin size increases we should see all the charged products of the neutral decays within a bin and this correlation reduction should saturate. There also appears to be a small dependence of $\Delta\sigma^2_{N_\Delta}$ on impact parameter. This dependence seems to be larger when we bin in ϕ than when we bin in η.

We will combine the results of the most central impact parameter events with the results of the terminus shape analysis (see previous part of this section) to determine the positive-negative covariances as well as the variances.

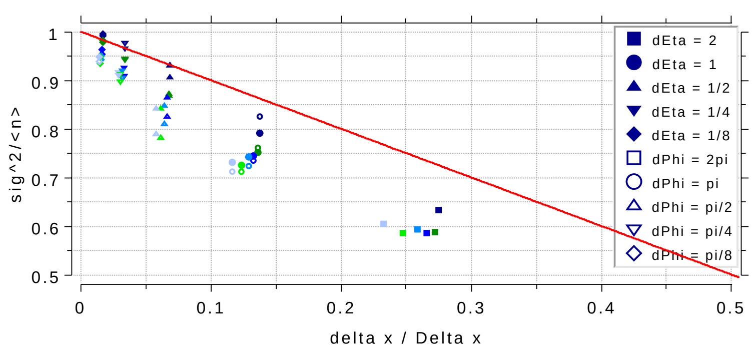

Figure 4.7-2. $\Delta\sigma^2_{N_\Delta}$ as a function of normalized bin size. Δx is the largest possible bin size (4π acceptance). We have binned in ϕ (open symbols) and η (closed symbols). For each bin size we measure $\Delta\sigma^2_{N_\Delta}$ at six different centralities. (Each centrality bin is slightly spread in $\delta x/\Delta x$ due to the track-finding efficiency dependence on track density.)

From Fig. 4.7-2 we see that there is a small reduction in $\Delta\sigma^2_{N_\Delta}$ beyond charge conservation. There are claims[2] that a Quark-Gluon Plasma should result in dramatically smaller net charge fluctuations. Our measurements are inconsistent with those claims but are consistent with a hadronic gas scenario.

[1] CENPA Annual Report, University of Washington (2001) p. 67.

[2] S. Jeon, V. Koch, Phys. Rev. Lett. **85**, 2076 (2000).

4.8 Centrality dependence

Initial state scattering, Glauber model and p_t fluctuations

Q. J. Liu, J. G. Reid and T. A. Trainor

The assumption that high-energy nucleus-nucleus collisions achieve substantial equilibration before chemical and kinetic freezeout is built into conventional hadrochemical statistical models in the form of exponential Boltzmann factors such as the fugacity. How true is this assumption, and how complete is equilibration according to the data? A high-energy nucleus-nucleus collision begins with a complex momentum exchange over a range of scales - the initial condition. The subsequent equilibration cascade (dissipation) is dominated by transport of initial-state flow-field correlations to smaller scales - toward a scale-invariant state consistent with the central limit theorem (thermal equilibrium). Residual inhomogeneities in the final state measure the dissipation provided one can estimate the initial state.

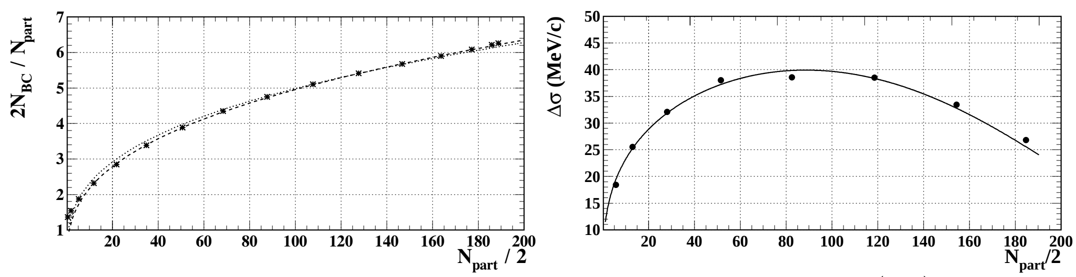

Figure 4.8-1. Glauber calculation of binary collisions *per* participant pair (left) and measured nonstatistical p_t fluctuations (right), both *vs* centrality in Au-Au collisions.

In pA collisions the Cronin effect is observed as an increase of the inclusive p_t distribution width proportional to the effective mean path length of the projectile nucleon in the target nucleus ($\propto A^{1/3}$). This effect can be explained by a stochastic multiple-scattering process (initial-state scattering or ISS) which generates additional p_t beyond soft-QCD thermal radiation. In AA collisions we should expect similar ISS scaling to some extent, but with the path length related to participant number by the Glauber model. In the left panel of Fig. 4.8-1 is plotted the Glauber-model prediction for number of binary collisions *per* participant pair as a function of the participant pair number (centrality).[1] This estimates the average path length of a participant nucleon in its passage through the other nucleus, which varies with centrality approximately as $N_{part}^{1/3}$. In a stochastic multiple scattering process additional inclusive p_t and p_t fluctuations should be simply proportional to this path length. In the right panel we show a measure of nonstatistical p_t fluctuations *vs* participant number in Au-Au collisions measured with the STAR detector at $\sqrt{s_{NN}} = 130$ GeV, which is described in more detail in Section 4.6. For more peripheral collisions (smaller N_{part}) the centrality dependence is comparable with the Glauber result, suggesting that ISS multiple scattering effects survive to the final state as a fluctuation excess. For more central events there is a significant reduction from the Glauber expectation, perhaps caused by growth of a dissipative medium. These data thus offer the possibility to measure the growth and properties of this dissipative medium - and the extent of equilibration with varying centrality.

[1] D. Kharzeev and M. Nardi, nucl-th/0012025, M. Miller (Yale) private communication.

Hijing Inclusive p_t distributions and the 1D Lévy reference

Q.J. Liu and T.A. Trainor

The 1D Lévy distribution was introduced[2] to describe *correlated* continuous measures sampled by random partition, for example a partially-equilibrated many-body system in which residual correlations remain. The sample distribution then deviates from its expected exponential Boltzmann form to that of a Lévy distribution. The exponent parameter n of the Lévy distribution represents fluctuations with relative variance given by $1/n \approx \sigma_m^2/\bar{m}^2$.

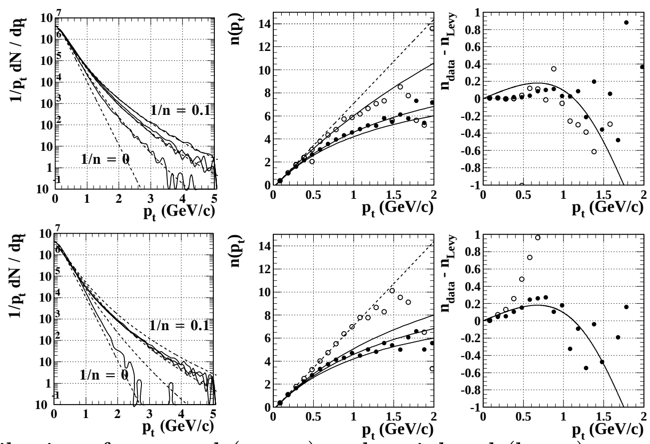

Figure 4.8-2. Distributions for central (upper) and peripheral (lower) events are shown for p_t distributions (left), exponents (middle) and deviations from Lévy (right).

p_t distributions for high-energy collisions are well described by

$$1/p_t\, dN/dp_t = C/\left(1 + \beta_0\sqrt{m_0^2 + p_t^2}/n(p_t, \sqrt{s})\right)^{n(p_t,\sqrt{s})} \tag{1}$$

which is a Lévy distribution if the exponent parameter n is independent of p_t. If $1/n \to 0$ the equilibrium exponential Boltzmann factor results. More generally, a p_t distribution may require a p_t- and $\sqrt{s}$-dependent exponent as in Eq. (1). Fig. 4.8-2 shows in the left panels Hijing p_t distributions[3] for central and peripheral Au-Au collisions at $\sqrt{s_{NN}} = 130$ GeV. The Hijing results for central events are well described by Lévy distributions, but there are significant deviations for peripheral events. This is seen more clearly in center and right panels. The center panels show p_t-dependent exponents derived from data on the left (points) relative to Lévy expectations (curves). The right panels show deviations from the Lévy expectations in greater detail. Peripheral events show little dissipation (significant deviations), whereas central events show good agreement with the Lévy distribution. Note that $1/n \approx 0.1 \Rightarrow \sigma_T/\bar{T} \approx 0.3$: relative temperature variation within each central event is roughly 30 *percent*! According to the Hijing model heavy-ion collisions at RHIC energies are fluctuation dominated, but with substantial dissipation for the more central events.

[2] G. Wilk and Z. Wlodarczyk, hep-ph/0002145, Phys. Rev. Lett. **84**, 2770 (2000)and references therein.
[3] X. N. Wang and M. Gyulassy, nucl-th/9502021, Phys. Rev. D **44**, 3501 (1991).

Centrality dependence of inclusive p_t distribution parameters

Q. J. Liu and T. A. Trainor

The centrality dependence of particle production is of basic interest in heavy ion collisions,[4] especially the relative yield from the 'binary collision' production mechanism associated with hard QCD processes and its $\sqrt{s}$ dependence. Particle production is discussed in the next subsection of this report. Equally important is the mechanism of p_t production, one aspect of which - p_t fluctuations - is also discussed in Section 4.6. In this article we discuss centrality dependence of *inclusive* p_t distribution moments.

In Fig. 4.8-3 is shown the centrality dependence of *rms* width and mean of the inclusive p_t distribution (left and center) plotted *vs* $N_{part}^{1/3}$, which estimates the participant mean path length λ according to the Glauber model. We observe that to a good approximation both quantities scale linearly with path length, suggesting that stochastic multiple scattering (binary collisions) is generating up to 12% additional p_t for the most central events, and that multiple scattering is manifested by a simple dilation of the p_t distribution with little distortion of the shape (with a possible exception in the least central point). We note that this trend of increasing dilation with path length appears to break down for the most central events, which could indicate the onset of a dissipative medium, or breakdown of the stochastic multiple scattering mechanism for central events.

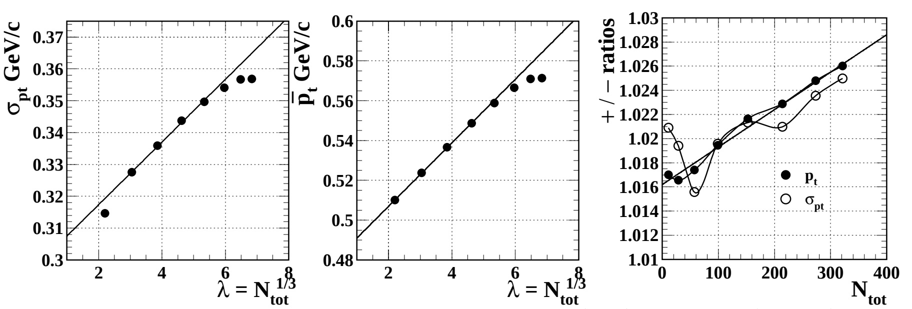

Figure 4.8-3. Centrality dependence of standard deviation (left), mean p_t (center), and ratio of positive to negative statistics (right).

These trends seem to be consistent with those for $< p_t >$ fluctuations, where we observe a linear increase in the AA/pp ratio of nonstatistical p_t fluctuations for less-central events, but a dramatic reduction from this trend for more-central events. Comparison of inclusive and fluctuation p_t trends may help to discriminate between increased dissipation and reduced initial-state scattering as possible mechanisms in the observed deviation from linearity for more central events. The right panel shows the ratios of positive to negative values for each inclusive quantity, which exhibit a *linear* dependence on N_{part}. This result suggests a 1% Coulomb energy shift in positive relative to negative particle spectra proportional to net nuclear charge contained in the participants.

[4] D. Kharzeev and M. Nardi, nucl-th/0012025.

Centrality dependence of particle production

Q. J. Liu and T. A. Trainor

If excess fluctuations are generated by stochastic initial-state binary collisions there are specific implications for centrality dependence. An expectation for initial-state scattering (ISS) can be derived from the Glauber model where one observes that the number of binary collisions varies approximately as the 1/3 power of the participant number (actually $\approx N_{part}^{0.355}$). (See Section 4.8.) Thus, a component of nonstatistical fluctuations with this centrality dependence would suggest stochastic initial-state binary collisions as one source of final-state correlations.

This argument is already implemented in the description of particle production in nucleus-nucleus collisions in terms of relative contributions from a 'wounded nucleon' mechanism (particles per participant pair independent of centrality) and a 'binary collisions' mechanism (particles per participant pair $\propto N_{part}^{1/3}$). Relative contributions to particle production from these two mechanisms are expected and observed to be $\sqrt{s_{NN}}$ dependent, reflecting the increase of hard parton scattering with increasing collision energy. Any hypothesis of *correlation* production by ISS should therefore be coordinated with a study of particle production.

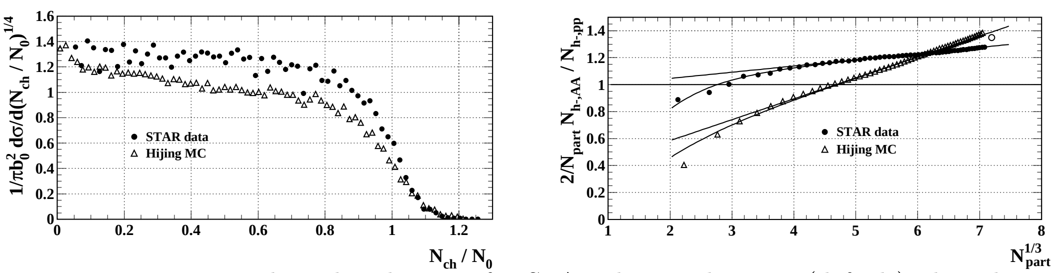

Figure 4.8-4. Minimum-bias distributions for STAR data and Hijing (default) plotted as $d\sigma/dN^{1/4}$ (left) and hadrons *per* participant pair (right) *vs* average path length $\propto N_{part}^{1/3}$.

Fig. 4.8-4 shows in the left panel minimum bias distributions in the form $d\sigma/dN^{1/4}$ for STAR data and Hijing (default) for $\sqrt{s_{NN}} = 130$ Gev. This compact plotting format provides better visual access to relatively small but significant differences. In the right panel is shown the yield per participant pair relative to p-p collisions, derived by integrating the minimum-bias distributions, *vs* $N_{part}^{1/3}$ ($\propto$ average path length or number of binary collisions) illustrating (straight lines) the trend of a constant component (wounded nucleons) and a linear component (binary collisions). Curves sketch trigger inefficiency for peripheral events. These results can be compared with the centrality trends for inclusive p_t parameters (previous subsection) and p_t fluctuations (Section 4.6). Particle production and p_t production have in common the trend of a constant offset (WN) plus a linear increase (BC) which, for p_t production only, seems to flatten out for the most central events. p_t fluctuations increase linearly with the number of binary collisions for peripheral events, but show a major reduction from this trend for more central events.

4.9 Scaling analysis

Scaling analysis of $<p_t>$ fluctuations

Q. J. Liu and T. A. Trainor

Preliminary results regarding measurement of scaling of $<p_t>$ (event-wise average transverse momentum) fluctuations are shown in Fig. 4.9-1 for Au - Au collisions at $\sqrt{s_{NN}} = 130$ GeV. The data sample we analyzed is the top 12% most central events selected from minimum-biased trigger events recorded by the STAR Collaboration. Detailed event selection and track quality cuts can be found in the footnoted reference.[1]

The scaling is done in pseudo-rapidity (η) space, and the scale $\delta\eta$ is defined as the bin width of a binning of acceptance $\Delta\eta$, e.g., $\delta\eta = \Delta\eta/M$. Here M is the total number of bins for each binning of the full acceptance $\Delta\eta$ ($|\eta| < 1$). The p_t acceptance is 0.15 GeV/c $< p_t <$2 GeV/c. At each scale, $<p_t>$ fluctuations are measured through the calculation of $\Delta\sigma_{p_t}$ (Section 4.6) and $\Delta\sigma_{<p_t>}$ formulated as:

$$\Delta\sigma_{p_t} = \frac{\overline{n(<p_t> - \hat{p}_t)^2} - \sigma^2_{\hat{p}_t}}{2\sigma_{\hat{p}_t}}, \quad and \quad \Delta\sigma_{<p_t>} = \frac{\bar{n}\,\overline{(<p_t> - \hat{p}_t)^2} - \sigma^2_{\hat{p}_t}}{2\sigma_{\hat{p}_t}} \tag{1}$$

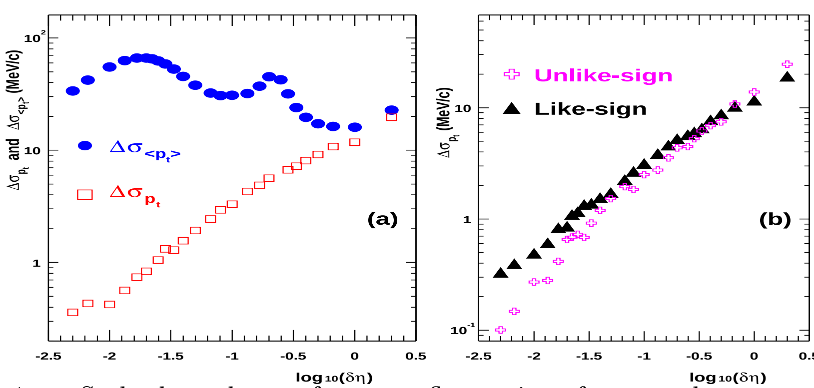

Figure 4.9-1. Scale dependence of $< p_t >$ fluctuations for central events of Au - Au at $\sqrt{s_{NN}} = 130$ GeV. In (a), results for $\Delta\sigma_{p_t}$ and $\Delta\sigma_{<p_t>}$ are compared for negatively charged particles; in (b), $\Delta\sigma_{p_t}$ for like-sign and unlike-sign particles are presented.

The difference between $\Delta\sigma_{<p_t>}(\delta\eta)$ and $\Delta\sigma_{p_t}(\delta\eta)$ as shown in Fig. 4.9-1(a) results from the fact that multiplicity fluctuations, which can be measured via $\Delta\sigma^2_n = \sigma^2_n/\bar{n} - 1$, are included in $\Delta\sigma_{<p_t>}$. This inclusion can be seen more clearly from an expansion of $\sigma^2_{<p_t>}$:

$$\sigma^2_{<p_t>} = \overline{(<p_t> - \hat{p}_t)^2} \approx \sigma^2_{\hat{p}_t} \quad \overline{1/n} \approx \frac{\sigma^2_{\hat{p}_t}}{\bar{n}} \quad (1 + \frac{\sigma^2_n}{\bar{n}^2}) \tag{2}$$

$\Delta\sigma_{<p_t>}$ is thus a more biased measure in this sense. Fig. 4.9-1(b) demonstrates that $<p_t>$ fluctuations for like-sign and unlike-sign charged particles follow different scaling behavior in η.

[1]STAR Collaboration, K. H. Ackermann et al., Phys. Rev. Lett. **86**, 402 (2001).

Scaling analysis of multiplicity fluctuations

Q. J. Liu and T. A. Trainor

In this report we present scaling analysis results for the global observable event multiplicity N. The variable $\Delta\sigma_N^2$ used in this analysis is defined in the following:

$$\Delta\sigma_N^2 = \frac{\overline{(N-\bar{N})^2}}{\bar{N}} - 1 = \frac{\sigma_N^2}{\bar{N}} - 1 \tag{3}$$

Applying the procedure, together with the various event cuts and track quality cuts used in the previous subsection, $\Delta\sigma_N^2$ as a function of scale ($\delta\eta$) in pseudo-rapidity (η) space was measured for top 5% most central Au -Au collisions (selected using ZDC coincidence[2]) at $\sqrt{s_{NN}} = 130$ GeV. This preliminary result is compared with Hijing1.37 predictions,[3] as shown in Fig. 4.9-2.

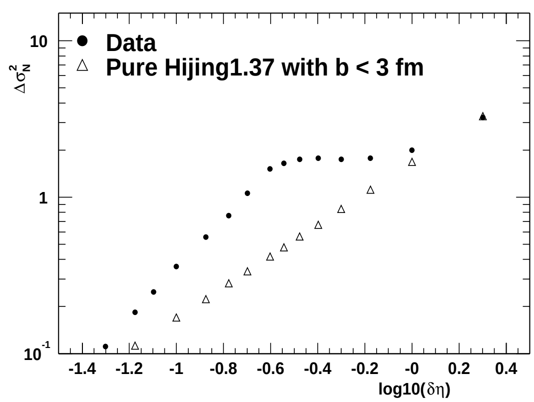

Figure 4.9-2. Scale dependence of multiplicity fluctuations for negatively charged particles in central Au - Au collisions at $\sqrt{s_{NN}}$=130 GeV.

Fig. 4.9-2 shows that minijet production as modeled in the Hijing1.37 contributes non-trivially to multiplicity fluctuations. However Hijing1.37 cannot reproduce the scale dependence of multiplicity fluctuations observed. Fluctuations have their origins in two-point correlations. Among the two-point correlations are flow-induced correlations, Bose-Einstein correlations in addition to minijet-induced correlations. We examined how flow-induced correlations and Bose-Einstein correlations contribute to the scale dependence of multiplicity fluctuations by using the event generator Mevsim,[4] in which the two types of correlations are simulated optionally. We found that flow contributes little while Bose-Einstein correlations contribute as significantly as minijet production modeled in Hijing1.37.

[2] C. Adler *et. al.*, Nucl. Instrum. Methods Phys. Res., Sect. A **461**, 337 (2001).

[3] M. Gyulassy and X. N. Wang, Comp. Phys. Comm. **83**, 307 (1994); X. N. Wang and M. Gyulassy, Phys. Rev. D **44**, 3501 (1991).

[4] R. L. Ray and R. S. Longacre, STAR Note SN0419, 1999, e-print nucl-ex/0008009.

4.10 Two-point correlations

Two-point correlations on (η, ϕ) and source opacity

A. Ishihara* and T.A. Trainor

In a related article (Section 4.11), we describe formation of joint autocorrelation densities as a method for visualizing two-particle correlation structure as differentially but compactly as possible. Given that most of the two-particle correlation information for each momentum component is retained in a 1D autocorrelation density, we can form 2D *joint* autocorrelations taking momentum components in pairs: $\eta \otimes \phi$, $\eta \otimes p_t$ and $p_t \otimes \phi$. These joint autocorrelations for CI (charge independent) and CD (charge dependent) charge combinations maximize the dispersion of different physical sources of correlation within the practical limitations of visualization and numerical analysis. Examples are shown in the first two panels of Fig. 4.10-1 for CD and CI combinations of the $\eta \otimes \phi$ joint autocorrelation. Difference variable ϕ_Δ is the vertical variable in each panel and η_Δ is the horizontal variable. New correlation structures appear in these 2D joint distributions which are not visible in the individual autocorrelations for single momentum components.

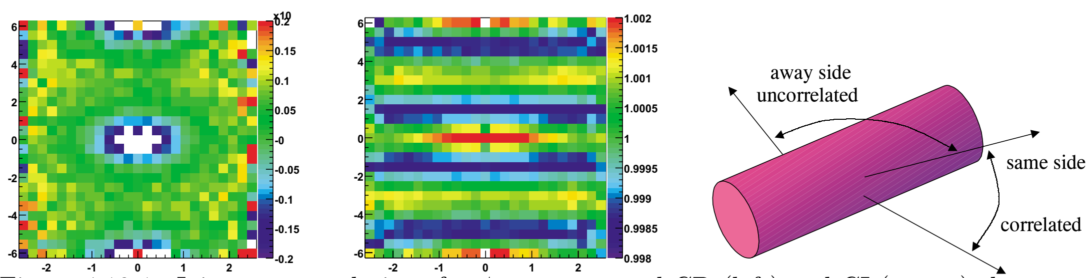

Figure 4.10-1. Joint autocorrelations for $\phi \otimes \eta$ space and CD (left) and CI (center) charge combinations. The vertical axis is ϕ_Δ and the horizontal axis is η_Δ. The right panel shows a cartoon defining same-side and away-side pairs relative to a boost-invariant section of the collision volume.

Detailed study of the correlation structures in Fig. 4.10-1 indicates that there is qualitatively different behavior for away-side pairs and same-side pairs as defined by the relative azimuthal emission angle ϕ_Δ of the pair. As illustrated in the right panel of this figure, same-side pairs fall in the interval $|\phi_\Delta| \leq \pi/2$, while away-side pairs fall in the complementary interval $\pi/2 < |\phi_\Delta| \leq \pi$. We note in Fig. 4.10-1 that there is little CD or CI correlation structure for away-side pairs in central Au-Au collisions, whereas there are substantial structures evident for same-side pairs. This trend depends only weakly or not at all on the pseudorapidity difference η_Δ. It appears to be a global property of central collisions over a pseudorapidity difference interval of at least two units. This result suggests the presence of *source opacity* during a substantial part of the kinetic freezeout interval. The observed trends in two-particle angular correlations near mid rapidity (more or less correlation for same-side or away-side pairs) can be explained by a combination of local ($\approx$ 1 fm) structure in particle-pair configuration space as the correlation source and scattering of at least one of two potential away-side local pair partners in the interior of the approximately boost-invariant collision volume.

---

*University of Texas, Austin, TX.

Two-point correlations on $m_t \otimes m_t$ and 2D Lévy distributions

A. Ishihara,* J. G. Reid and T. A. Trainor

The assumption in hadrochemical statistical models that nucleus-nucleus collisions achieve substantial equilibration remains open to question. Two-point correlations on $m_t \otimes m_t$ provide information on temperature correlations within events as well as true event-wise temperature variation. We have developed a method to study temperature correlations based on a newly-defined 2D Lévy distribution. The 1D Lévy distribution on m_t describes a single-particle distribution which may reflect substantial temperature fluctuations due to incomplete equilibration

The 1D m_t distribution for a partially equilibrated system is a conditional distribution derived from a 2D joint distribution on space (β, m_t). The condition is defined by a peaked distribution on $\beta = 1/T$ representing temperature fluctuations or thermal heterogeneity. If the 2D joint distribution $e^{-\beta\, m_t}$ is folded with the condition on β represented by a gamma distribution $g_n(\beta;\beta_0) = \frac{n}{\beta_0 \Gamma(n)}(n\beta/\beta_0)^{n-1} e^{-n\beta/\beta_0}$ there results the conditional 1D Lévy distribution on m_t[1]

$$
\begin{aligned}
< e^{-\beta\, m_t} >_n &= \int_0^\infty d\beta g_n(\beta;\beta_0) e^{-\beta\, m_t} \\
&= 1/(1 + \beta_0\, m_t/n)^n \qquad (1)
\end{aligned}
$$

The gamma- and Lévy-distribution parameter n measures temperature fluctuations as $1/n = \sigma_\beta^2/\beta_0^2$.

The 2D (m_{t1}, m_{t2}) distribution for a heterogeneous system is in turn derived by generalization to a 4D joint distribution $e^{-\beta_1\, m_{t1} - \beta_2\, m_{t2}}$ on space $(m_{t1}, m_{t2}; \beta_1, \beta_2)$. The condition on space (β_1, β_2) is now a 2D gamma distribution, and the resulting conditional distribution is a 2D Lévy distribution. Defining $m_{t,\Sigma} \equiv m_{t1} + m_{t2}$, $m_{t,\Delta} \equiv m_{t1} - m_{t2}$ and $\beta_\Sigma \equiv \beta_1 + \beta_2$, $\beta_\Delta \equiv \beta_1 - \beta_{s2}$ we obtain $e^{-\beta_1\, m_{t1} - \beta_2\, m_{t2}} \rightarrow e^{-(m_{t,\Sigma}\beta_\Sigma + m_{t,\Delta}\beta_\Delta)/2}$, and the 2D gamma distribution for uncorrelated fluctuations is a simple product of two 1D distributions which can be rearranged as

$$
\begin{aligned}
g_n(\beta_1, \beta_2; \beta_0) &= \left(\frac{2n}{\beta_0 \Gamma(2n)}\right)\left(\frac{n\beta_\Sigma}{\beta_0}\right)^{2n-1} e^{-n\beta_\Sigma/\beta_0} \cdot \frac{\Gamma(2n)}{4^n \Gamma(n)^2} \cdot \frac{2\beta_0}{n\beta_\Sigma}(1 - \beta_\Delta^2/\beta_\Sigma^2)^{n-1} \\
&\equiv g_{2n}(\beta_\Sigma/2;\beta_0) \cdot g'_{2n}(\beta_\Delta/2;\beta_0) \qquad (2)
\end{aligned}
$$

to yield the product of a gamma distribution on sum variable $\beta_\Sigma/2$ and a symmetric distribution on difference variable $\beta_\Delta/2$, the latter typically depending weakly on $\beta_\Sigma/2 \approx \beta_0$, with $|\beta_\Delta| \leq \beta_\Sigma$. If n is the same for both factors we obtain the $reference$ 2D Lévy distribution - a simple product of two 1D distributions

$$
f_n(m_{t1}, m_{t2}; \beta_0) = \int_0^\infty d\beta_\Sigma\; g_{2n}(\beta_\Sigma/2;\beta_0) \int_{-\beta_\Sigma}^{\beta_\Sigma} d\beta_\Delta\; g'_{2n}(\beta_\Delta/2;\beta_0)\; e^{-(m_{t,\Sigma}\beta_\Sigma + m_{t,\Delta}\beta_\Delta)/2}
$$

*University of Texas, Austin, TX.

[1] G. Wilk and Z. Wlodarczyk, hep-ph/0002145, Phys. Rev. Lett. **84**, 2770 (2000) and references therein.

$$= \frac{1}{\{1+\beta_0 m_{t,\Sigma}/2n\}^{2n}} \cdot \frac{1}{\{1-\beta_0^2 m_{t,\Delta}^2/(2n+\beta_0 m_{t,\Sigma})^2\}^n} \tag{3}$$

If we allow the 2D distribution on (β_1, β_2) to have different widths on sum and difference variables (a nonzero covariance reflecting correlated temperature fluctuations) characterized by exponents n_Σ and n_Δ then the *object* 2 D Lévy distribution is

$$\begin{aligned} f_{n_\Sigma n_\Delta}(m_{t1}, m_{t2}; \beta_0) &\equiv \int_0^\infty d\beta_\Sigma \; g_{2n_\Sigma}(\beta_\Sigma/2; \beta_0) \int_{-\beta_\Sigma}^{\beta_\Sigma} d\beta_\Delta \; g'_{2n_\Delta}(\beta_\Delta/2; \beta_0) \; e^{-(m_{t,\Sigma}\beta_\Sigma + m_{t,\Delta}\beta_\Delta)/2} \\ &\approx \frac{1}{\{1+\beta_0 m_{t,\Sigma}/2n_\Sigma\}^{2n_\Sigma}} \cdot \frac{1}{\{1-\beta_0^2 m_{t,\Delta}^2/(2n_\Delta+\beta_0 m_{t,\Sigma})^2\}^{n_\Delta}} \end{aligned} \tag{4}$$

A two-point *object* distribution is constructed from sibling (same event) pairs and a *reference* distribution from mixed pairs (different events). A ratio is then formed from these distributions, with typical deviations from unity at the *permil* level for heavy ion central collisions. The *object*/*reference* density ratios for STAR data (left), a Monte Carlo simulation (right) and the analytic Lévy ratio $f_{n_\Sigma n_\Delta}(m_{t1}, m_{t2}; \beta_0)/f_n(m_{t1}, m_{t2}; \beta_0)$ (center) are plotted in Fig. 4.10-2. For correlated temperature fluctuations the density ratio has a characteristic saddle shape. Curvatures on $m_{t,\Sigma}$ and $m_{t,\Delta}$ measure exponent differences $1/n_\Sigma - 1/n$ and $1/n_\Delta - 1/n$ respectively ($1/n$ is derived from the single-particle m_t distribution). The two-temperature linear correlation coefficient is $\kappa(1,2) \approx n/4 \cdot (1/n_\Sigma - 1/n_\Delta)$. If $\kappa(1,2) = 1$ temperature variations are completely correlated at all points within each event - *extramural* or true event-by-event temperature fluctuations dominate. If $\kappa(1,2) = 0$ temperature variations are completely uncorrelated within each event - *intramural* fluctuations dominate and successive events are not statistically distinguishable.

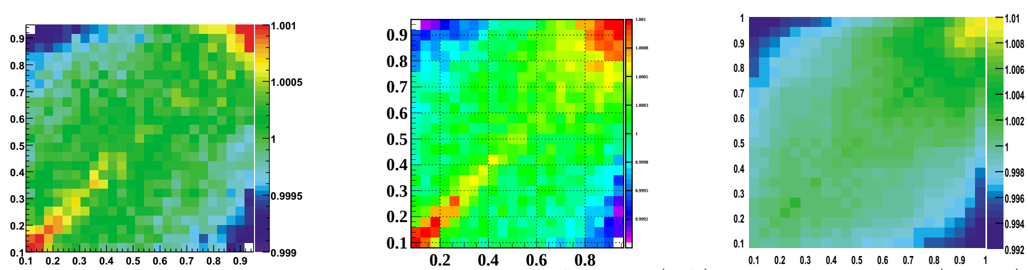

Figure 4.10-2. Two-point density ratios on $m_t \otimes m_t$ for data (left), Lévy distribution (center) and Monte Carlo simulation (right).

The simulation on the right represents a 5% purely extramural relative temperature fluctuation (each event formed with a single temperature drawn from a gaussian distribution). This corresponds to $1/n = 0.0025$, $1/n_\Sigma = 0.01$, $1/n_\Delta = 0$ and $\kappa(1,2) = 1$. The data on the left show a correlation amplitude about 1/10 of the simulation, implying $1/n_\Sigma - 1/n_\Delta = 0.001$. Since $1/n \approx 0.11$ from the 1D m_t spectrum (see Section 4.8), we obtain $\kappa \approx 0.002$. There is a significant two-point temperature correlation, but this is a small fraction of the temperature heterogeneity inferred from the 1D m_t distribution. The center plot is a ratio of 2D Lévy distributions consistent with the exponent numbers above which agrees well with the data distribution (statistical fluctuations and a simple model of quantum correlations have been added to the analytical Lévy ratio for better visual comparison with the data).

4.11 Analysis Techniques

Glauber model and minimum-bias distribution shape

D. J. Prindle and T. A. Trainor

The shape of the minimum-bias distribution in a heavy ion collision is dominated by the geometry of the colliding nuclei. This can be quantified by calculating the overlap (for the participant number) or product (for binary collisions) of the nuclear densities using the Glauber model. Our primary goal is to determine a reference shape for the minimum-bias multiplicity data enabling us to extract particle fluctuations at the terminus.

The nuclear density is approximated using a Wood-Saxon potential,

$$\rho(\mathrm{r}) = \frac{\rho_0}{1 + \exp(\frac{\mathrm{r}-\mathrm{R_A}}{\mathrm{a}})}$$

where $\mathrm{R_A}$ is the radius, a is the skin depth and ρ_0 is the density. Most nuclei have static deformations and all have ground state shape oscillations. The radius is described as a sum of spherical harmonics. For Au only the lowest order correction is important and we have

$$\mathrm{R_A} = \mathrm{R_0} \times (1 + \beta_2 \times \left[3\cos^2(\theta) - 1\right]/2).$$

A reasonable value for Au is $\beta_2 \approx -0.15$, including the shape oscillations.

To average over nuclear orientation we use Monte-Carlo techniques, picking random nuclear orientations and impact parameter for each event. The numbers of participants and binary collisions are shown in Fig. 4.11-1. The participant distribution has a very sharp terminus. In contrast, the binary collision terminus has a visible dependence on β_2.

To connect this Glauber calculation with our minimum-bias distribution we assume[1]

$$\mathrm{M(b)} = (1-\mathrm{x})\mathrm{N_{pp}N_{part}(b)}/2 + \mathrm{xN_{pp}N_{bc}(b)}$$

where $\mathrm{N_{pp}}$ is the number of produced particles per elementary interaction and x determines the mixture of hard and soft particle production. In Fig. 4.11-1 we include an example with x = 0.05, where about 25% of the particle production is due to binary collisions.

Accessing a two-particle momentum space with joint autocorrelations

A. Ishihara* and T.A. Trainor

Two-particle correlations in p-p axial phase space studied in CERN ISR and Fermilab fixed-target experiments[2] provide limiting cases for the centrality dependence of A-A collisions. We have initiated similar studies in A-A collisions at RHIC and SPS. On the basic two-particle momentum subspaces $m_t \otimes m_t$, $\eta \otimes \eta$ and $\phi \otimes \phi$ we construct sibling- and mixed-pair densities for each particle charge combination using event ordering[3] (mixed pairs are formed

[1] D. Karzeev and M. Nardi, Phys. Lett. B **507**, 121 (2001).

*University of Texas, Austin, TX.

[2] T. Kafka *et al.*, Phys. Rev. D **16**, 1261 (1977); J. Whitmore, Phys. Repts. **27**, 187 (1976).

[3] J. G. Reid and T. A. Trainor, Nucl. Instrum. Methods A **457**, 378 (2001).

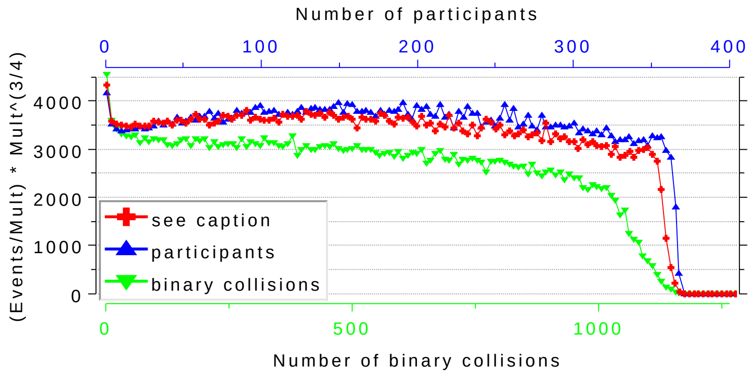

Figure 4.11-1. Participant (upper scale) and binary collision (lower scale) minimum-bias distributions calculated using the Glauber model. The intermediate curve is an admixture of participant and binary collisions as explained in the text.

from 'nearest-neighbor' event pairs in a space spanned by several global event variables). The density ratios of sibling to mixed pairs are then formed. Assuming approximate charge symmetry ($++ = --$ and $+- = -+$) we then form like-sign (LS) and unlike-sign (US) pair combinations. This facilitates comparison with previous p-p analyses. We then form charge-independent ($CI \equiv LS + US$) and charge-dependent ($CD \equiv LS - US$) combinations, which serve to isolate certain physics mechanisms.

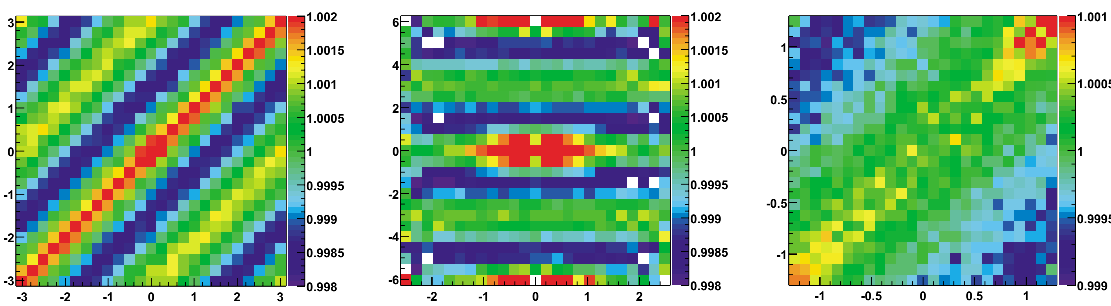

Figure 4.11-2. Spaces $\phi \otimes \phi$ and $\eta \otimes \eta$ (left, right) and joint autocorrelation on $\eta \otimes \phi$ (center)

The left and right panels in Fig. 4.11-2 represent the LS charge combination for $\phi \otimes \phi$ and the US combination for $\eta \otimes \eta$ spaces respectively for central Au-Au collisions in the STAR detector. The $\phi \otimes \phi$ distribution clearly shows the dominant $cos(2\phi_\Delta)$ contribution from elliptic flow[4] Most of the structure in these distributions appears on the difference variables $\phi_\Delta \equiv \phi_2 - \phi_1$ and $\eta_\Delta \equiv \eta_2 - \eta_1$, with negligible structure on sum variables $\phi_\Sigma \equiv \phi_2 + \phi_1$ and $\eta_\Sigma \equiv \eta_2 + \eta_1$. Thus, projection onto the difference variables retains most of the correlation information, improves statistical S/N and provides dimension reduction required for further visualization. Such projections are called autocorrelation densities, which thus contain most if not all two-point correlation information reduced to a 1D space for each momentum component. We then form *joint* autocorrelation densities on *pairs* of momentum components which offer more differential access to correlation information. The center panel of Fig. 4.11-2

[4]K. H. Ackermann *et al.* [STAR Collaboration], nucl-ex/0009011, Phys. Rev. Lett. **86**, 402 (2001).

shows the joint autocorrelation density for $\eta \otimes \phi$ space and the CI charge combination exhibiting substantial correlation structure. The individual and joint autocorrelation densities are then directly related to scaling studies of fluctuations.

Statistical measure bias

J. G. Reid and T. A. Trainor

Much of the information in heavy ion collisions is carried by fluctuations at the few *percent* level or less. One limitation to measurement precision is *measure bias*: the mean value of a random variable deviates systematically from the parent parameter it is intended to estimate. The basic reference for fluctuation measurements is shown in the left panel in Fig. 4.11-3: the random partition of a space containing a uniform measure density and a random point set ('particles'). Contours represent the frequency distribution of partition-element contents on $(m/\hat{m}, n)$, where $\hat{m}$ is a single-particle ensemble mean. If partition elements with a specific point number are selected, the 1D conditional distribution on measure m is a gamma distribution. Alternatively, if partition elements with a fixed amount of measure m are specified, the 1D conditional distribution on point number n is a Poisson distribution.

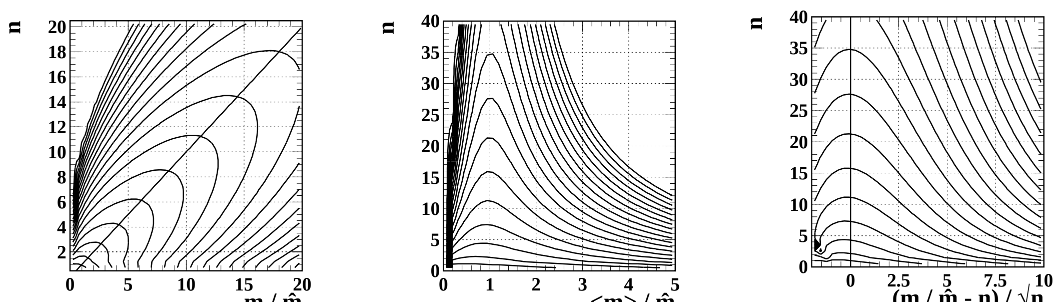

Figure 4.11-3. Bin-contents distributions for a general central-limit reference (left), a ratio of random variables (center) and a minimally-biased variable (right).

If the continuous measure $m \to p_t$, the event-wise mean $< p_t > \equiv p_t/n$ serves as a temperature estimator. It is then conventional to transform the CLT reference distribution (left panel) to the space $(<p_t>, n)$ (center panel) as a reference for event-by-event 'temperature' fluctuations. However, *ratios* of random variables exhibit measure bias. The bias mechanism depends on variation of the distribution width with multiplicity n and consequent dependence of the $<p_t>$ variance on multiplicity fluctuations.[5] In contrast, the *difference* variable $(m/\hat{m} - n)/\sqrt{n}$ with corresponding reference distribution shown in the right panel of Fig. Fig. 4.11-3 is *minimally biased*. The additional factor $\sqrt{n}$ reduces sensitivity to multiplicity fluctuations: the distribution width in the right panel is by construction independent of n. The variance comparison measure in this case is

$$\Delta\sigma^2_{p_t,n} \equiv \overline{n(<p_t> - \hat{p}_t)^2} - \sigma^2_{\hat{p}_t} \tag{1}$$

[5]An example of large measure bias for $<p_t>$ fluctuations is given in Fig. 4.9-1, left panel.

which is minimally biased for heavy-ion collisions. Other variance comparisons with the same structure are: $\Delta\sigma^2_n \equiv \overline{(n-\bar{n})^2/n} - 1$, $\Delta\sigma^2_{n_+,n_-} \equiv \overline{(n_+ - n_-)^2/(n_+ + n_-)} - 1$ and $\Delta\sigma^2_{p_t} \equiv \overline{(p_t - \bar{n}\hat{p}_t)^2/n} - \sigma^2_{\hat{p}_t}$. The overlines in these expressions indicate averages over all bins in an event ensemble, where a bin may be the entire detector acceptance, or fractions of the acceptance at smaller scale. A bin-based rather than event-based approach provides a more general analysis framework compatible with scaling studies.

4.12 Comparison of measured and calculated Landau functions for STAR-TPC

H. Bichsel

The distribution function $g(I; x, pc)$ resulting from the ionization I in TPCs ("Landau function," thickness of gas x) can be approximated by the distribution function $f(\Delta; x, pc, r)$ for the energy loss Δ of the charged particles (momentum pc) traversing the gas. Comparison of measured $g(I; x, pc)$ with calculated functions $f(\Delta; x, pc, r)$ have been made. For a large set of data, the shapes of the functions agree well. Because of the stochastic nature of $g(I)$, two parameters, viz. the value I_p of the most probable ionization and the full-width-at-half maximum w_I are used to characterize $g(I)$. These parameters are compared with the corresponding ones, Δ_p and w, for $f(\Delta)$. The $f(\Delta; x, pc, r)$ are calculated with the convolution method and r is a resolution parameter. The present determination of I_p and w_I is made graphically with data from ROOT and results in an uncertainty estimated to be $\pm 0.3\%$ for I_p and $\pm 0.6\%$ for w_I. The quoted absolute values if I_p are based on the use of the Bethe-Bloch expression for dE/dx and are thus too large. Results are shown in figure Fig. 4.12-4.

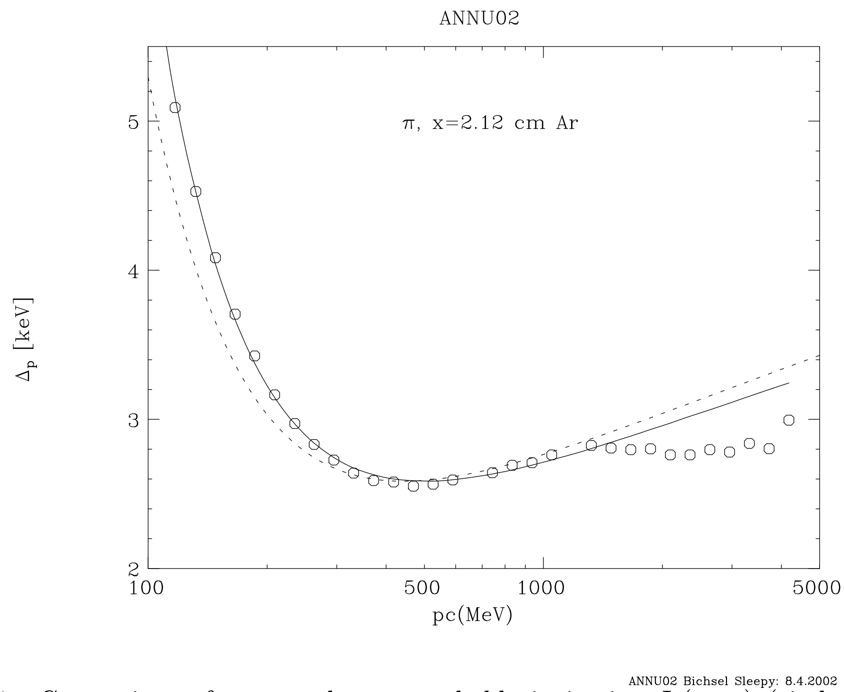

Figure 4.12-4. Comparison of measured most probable ionization $I_p(pc, x)$ (circles) for $x = (2.12 \pm 0.05)$ cm as a function of pion momentum pc with the calculated function $\Delta_p(pc, x, r)$, solid line. The Bethe-Bloch dE/dx function is shown by the dotted line. For $pc < 1500$ MeV, the RMS value of the ratio Δ_p/I_p is $0.679 \pm 0.7\%$, and I_p is reduced by this amount. The Bethe-Bloch function is scaled to Δ_p at minimum ionization The increasing difference between Δ_p and I_p for $pc > 1500$ MeV indicates problems with the current evaluation of the data.

5 Atomic and Molecular Clusters

5.1 Structure of anions containing B and N

R. Vandenbosch

Clusters of B and N with an equal number of atoms of each element are isoelectronic with C clusters with the same number of total atoms. C_n clusters with n less than about 10 are primarily linear chains. When produced by sputtering or laser desorption from graphite the yields of the different anions exhibit a striking odd-even pattern, with the even-numbered clusters being produced with much larger yields. This pattern correlates with an alternation in the electron affinities with n, which in turn can be traced back to the filling of delocalized pi electron subshells. For mixed clusters of B and N with more than two atoms there are a number of geometrical isomers possible. The most stable isomer for a $B_xN_y{}^-$ anion may be different than for the neutral cluster with the same values of x and y. It is of interest to determine which isomers are produced in different processes and to understand the factors governing the relative yields of different structures.

There has been very little if any experimental work on $B_xN_y{}^-$ anions with more than two atoms. In this work mixed cluster anions are produced by Rb^- or Cs^- sputtering of boron nitride. The mass-selected anions are collisionally fragmented in a gas cell and both the negative and positive fragment distributions are examined. This enables a deduction of the dominant geometrical structure assuming a linear anion. It is expected that in the "hot" sputtering environment entropy considerations will favor formation of the linear isomer even if a cyclical configuration is close-lying in energy.

As an example of the deduction of the structure, consider the results for B_3N_2. The positive ion fragmentation spectrum exhibits large yields of B, B_2 and B_3, as well as mixed species such as BN, B_2N, B_2N_2. It also exhibits significant yields of N and N_2. The presence of both B_3 and N_2 implies a geometry of BBBNN. It is interesting to note that although B_2 and B_3 appear in the negative ion spectrum, N and N_2 do not. This is because neither N or N_2 binds an electron. This illustrates the importance of looking at both the positive and negative ion spectra. Our preliminary results for other anions are B_2N: BBN, BN_2: BNN, B_3N: BBBN, B_4N: BBBBN, B_2N_2: BBNN, and B_3N_2: BBBNN. Thus we see that mixed clusters with like atoms adjacent to each other are prominent anion species produced by sputtering.

In an attempt to understand these results, *ab initio* quantum chemical calculations have been performed. These calculations suggest that although alternating B and N structures are the most stable structures for anions, the electron affinities of neutral species with like atoms adjacent to each other are often larger than for alternating B and N structures. This is consistent with a mechanism where Rb or Cs transfers an electron to a neutral species produced by sputtering.

6 Electronics, Computing and Detector Infrastructure

6.1 Status of an advanced object oriented real-time data acquisition system

M. A. Howe, F. McGirt,* L. P. Parazzoli† and J. F. Wilkerson

The Object oriented Real-time Control and Acquisition (ORCA) software system has been described in past CENPA annual reports,[1] so only a brief overview is provided here. The goal of the ORCA project is to produce an advanced software application that can be used for quickly building scalable, distributed, and flexible data acquisition systems. Unfortunately, due to a number of problems, progress on the development of the ORCA code has been substantially delayed during the last year. Linux version and update problems, hardware failures, hacker attacks, and limited manpower all contributed to the lack of progress.

The failure of a disk drive on one of the development machines caused some delay, because of the time required to reinstall and rebuild the numerous third-party, open-source development tools. A more serious setback was caused when one of the development machines was broken into and vandalized by a hacker. The hacker managed to erase most of the development machine's disk and some unbacked-up work was lost.

For most of the last year work on ORCA was deferred due to the extreme time constraints on the programming staff, which was busy preparing data acquisition systems for the NCD (see Section 2.8) and emiT (see Section 1.1) projects and so little time was left for ORCA development.

The biggest problem has been the operating system that was initially chosen for ORCA development. Major problems have occurred and much time has been lost each and every time that the Linux kernel or any of the numerous development tools have been updated to new versions. It is becoming clear that the open source Linux operating system is not mature enough to fully support the development of ORCA to its specified design.

Some work has been done exploring the possibility of moving ORCA development to MacOS X and the advanced development tools that are available under that operating system. McGirt has written a driver for using the SBS 617 PCI to VME hardware. It has been tested and functions well under MacOS X.

*Los Alamos National Laboratory, Los Alamos, NM 87545.
†Presently at Los Alamos National Laboratory, Los Alamos, NM 87545.
[1] CENPA Annual Report, University of Washington (2001) p. 83.

6.2 Electronic equipment

G. C. Harper, A. W. Myers and T. D. Van Wechel

Along with the normal maintenance and repair of the laboratory's electronic equipment, projects undertaken by the electronics shop included the following:

1. A scope summing board for the SNO NCD system. This board has four sections. Each section sums the outputs from two of the NCD MUX boxes and produces two outputs, providing a single channel input for each of the two scopes.

2. A NCD Global Trigger ID card was designed and constructed. This VME card provides the timing interface between the NCD data acquisition electronics and the SNO Trigger system. It also has a local VME clock counter to simulate the function of the SNO Master Trigger Card when it is not available.

3. A time base NIM module was designed and constructed for the ^{7}Be experiment. This module produces a negative NIM level pulse at switch selected frequencies from .001 Hz to 100 kHz.

4. A Scope isolation board was constructed for the SNO NCD system. This breaks the ground loop on the scope trigger and scope busy signals.

5. A preamp bias interlock system was designed and constructed for the emiT experiment. The detector bias current is monitored and if a setable threshold is exceeded, the bias power is turned off. Also an optical fiber telemetry system for the bias voltage and current was constructed.

6. An optical fiber based telemetry system for monitoring the temperature of the proton detector paddles in the emiT experiment was developed and constructed. Also, a multi-channel fiber optic receiver/transmitter board was constructed for transmitting the test pulser signals for the emiT preamps and receiving the digital telemetry signals for the emiT system.

7. An interface board for the C.A.E.N. Model V862 32 channel QDC VME module was constructed. This interfaces the multi-channel flat cable inputs of the QDC to provide individual LEMO connector inputs.

8. A prototype for the SNO NCD pulser distribution system has been designed. It will provide individually switched test pulse signals to each of the 96 NCD preamps.

6.3 Laboratory computer systems

M. A. Howe, R. J. Seymour and J. F. Wilkerson

This year saw slower growth in numbers of systems than previous years. We were forced to devote more time and resources to network and system security as scans and outright attacks on our systems increased in frequency and sophistication. The existing Linux systems were upgraded frequently to track security improvements. A "logical firewall" has been implemented to allow nodes on our network to be moved from fully "visible" to fully protected from outside access.

Our computing and analysis facility consists of:

- Our principal central computer-server base, now a mix of Linux and Compaq Unix-based systems, with the number of Linux systems increasing. Many people still rely on our five VMS/Vaxes and two VMS Alpha systems for email and "legacy" computing.
- The Ultra-Relativistic Heavy Ion group's Hewlett Packard Unix systems, sited both here in Seattle and at STAR at Brookhaven. One of the HP's serves as the lab's principal World Wide Web server (www.npl.washington.edu).
- The SNO and emiT groups, relying upon Macintosh systems. As systems are placed on-site in Sudbury, newer G4 systems fill their slots in Seattle. An original iMac serves as the EWI web and file server. Our seven-year-old Sun Sparcstation 20 has been joined by a new pair of ten-times-faster SunBlade 100 workstations for CADENCE circuit design, analysis and layout duties.
- Three MBD-11 equipped VMS VAXstation 3200s still serve as the Lab's primary data acquisition systems and are running acquisition software based upon TUNL's XSYS, with a number of local modifications to their DISPLAY program. A VAXstation is the Linac and Vacuum systems' control and display system. Some third-party components are dying with age, and are proving difficult or impossible to repair or replace. These include Parallax-brand Qbus graphics cards, and "traditional" (15 years ago) slow-phosphor video monitors.
- Co-location services for the Institute for Nuclear Theory and the Physics Nuclear Theory group in the form of two VMS VAXstation 3200s, although not directly used by Lab personnel. The Astronomy Department has located a 64-processor Xeon-based Beowulf cluster in our machine room.
- The Lab's general internal network, a mixture of 100baseTX and 10baseT ethernet ports, and our existing legacy 10base2 net. Continuing our cooperative relationship with the campus network division, a gigabit ethernet line was provided to the laboratory without charge, based upon the expected needs of the Astronomy cluster.

6.4 An alternative data acquisition system

M. Bhattacharya and H. E. Swanson

JAM is a data acquisition and analysis package authored by Ken Swartz, Dale Visser, and John Baris at the Wright Nuclear Structure Lab at Yale University and is available for download from their web site.[1] Taking real-time CAMAC data requires a separate VME system to host the CAMAC controller which communicates with the JAM package through a private ethernet connection. In addition to the VME event stream JAM can be easily configured to sort event files using other formats such as XSYS or from data acquisition systems used at other labs. Except for the VME code itself, JAM is written in Java and is reasonably platform independent. With the availability of a PCI CAMAC controller such as the Wiener PCI_CC32, the VME host for a CAMAC controller is no longer necessary. It is therefore possible to make a stand alone PC based data acquisition system with JAM.

We have developed code for a PC running Windows 2000 that interfaces the JAM application to a PCI_CC32 CAMAC controller using the internal IP address 127.0.0.1. It consists of a thread to listen for commands and requests from JAM and another to intercept LAM generated interrupts from the controller. When the run is setup in JAM, a sequence of CAMAC operations for the event is downloaded to the program. This sequence is executed in response to each LAM and the resulting CAMAC data are buffered and periodically uploaded to JAM through the same internal IP address. No changes to the JAM code are required as we have emulated their VME system's communication protocol. The code was written in C# taking full advantage of its built in threading and Internet capabilities. This system will replace a MicroVax running XSYS on the Mass-8 beam line.

[1] http://jam.physics.yale.edu.

7 Accelerator and Ion Sources

7.1 Van de Graaff accelerator operations and development

J. F. Amsbaugh, G. C. Harper, T. L. McGonagle,* A. W. Myers, P. N. Peplowski, D. W. Storm, T. D. VanWechel and D. I. Will

The tandem was entered 36 times this year. Four of these tank openings were to remove the #3 spiral inclined field tube and install the modified KN beam tube or the reverse.

The following openings were for development or repair of the Terminal Ion Source (TIS). These are discussed in more detail in section 7.2. Seventeen openings were for diagnosing a problem with vertical steering while running the ^{3}He beam under a variety of conditions. Four tank openings were for the purpose of ascertaining the optimum distribution of ball bearing column section shorts to allow operation with ultra-low terminal voltages. Four openings were to change the gas and magnet for the production of different ion species. Power supplies for the TIS were repaired during four of the tank openings.

There was one tank opening for each of the following:
1) To install a shortened version of the 5 cm diameter TIS einzel lens.
2) To install check valves in the TIS gas manifold.
3) To install and test the 2 mm canal in the TIS for use with protons.

We replaced no chain idlers or pick-up pulleys this year. After decades of reliable operation, our Ingersoll-Rand compressor blew one of the copper valve seals in the high pressure cylinder. We spent three days cleaning the cylinder, machining a new seal, and reassembling the compressor cylinder.

During the 12 months from April 1, 2001 to March 31, 2002 the tandem pellet chains operated 988 hours and the SpIS 282 hours. The DEIS was not operated this year. Additional statistics of accelerator operations are given in Table 7.1-1.

ACTIVITY	DAYS SCHEDULED	PERCENT
Molecular research, deck ion sources only	36	10
Nuclear physics research, TIS	67	18
Subtotal, molecular or nuclear physics research	103	28
Machine development, maintenance, or crew training	151	41
Grand total	254	69

Table 7.1-1. Tandem Accelerator Operations April 1, 2001 to March 31, 2002.

*No longer at CENPA.

7.2 Tandem terminal ion source

G. C. Harper, A. W. Myers, P. N. Peplowski and T. D. Van Wechel

The terminal ion source (TIS) was used for the ^{7}Be(p,γ)^{8}B, ^{7}Li(d,p)^{8}Li, and ^{6}Li(^{3}He,n)^{8}B experiments during this reporting period. The ions used were $^1H^+$ at terminal voltages from 0.16 MV to 1.5 MV, $^2H^+$ at terminal voltages from 0.77 MV to 1.4 MV, $^3He^+$ at a terminal voltages from 5.0 MV to 6.0 MV, and $^4He^+$ at a terminal voltage of 1.37 MV. The list of experiments run with the TIS to date is given in Table 7.2-1 below.

This is the first year that we used a 2-mm diameter source canal in an attempt to increase the beam current for very low energy proton runs. We have produced currents as high as 70 μamps at terminal voltages of 500 kV and higher. We can regularly produce 35 μamps at the high energy cup and 10 μamps on the image cup at terminal voltages as low as 140 kV. Gas load at the accelerator tube ends increases by a factor of about four with the larger canal.

Maintenance for this year was dominated by a troubling vertical steering component introduced somewhere in the $^3He^+$ beam. Seventeen tank openings were devoted to diagnosing this problem. During these openings the einzel lens assembly was changed, the einzel lens feedthru electrode was shielded, the mass-3 dipole magnet was installed in place of the electrostatic deflector, the solenoidal plasma compression magnets were replaced, the TIS steerers were moved downstream, all of the source components were replaced, the entire TIS and associated optics were aligned, the spiral inclined field tubes were aligned, and a variety of gradient shorting schemes were tested to resteer the beam. None of these attempts were successful but the gradient alteration allowed running the experiment with 70% of the available beam current with stable regulation.

Other maintenance included upgrading the transient suppression for the power supplies used for the electrostatic deflector. Also, three check valves were installed in the gas manifold to eliminate cross contamination of the gas bottles during tank sparks and computer turn on transients.

We continue to use the KN van de Graaff tube procured from the Wright Nuclear Structure Lab at Yale University and modified to replace our spiral tube #3. We have observed the onset of x-rays from the backstreaming of electrons in the tube produced from ions striking the first plane of spiral tube #4 when the KN tube is supporting 1 MV or more. The electron loading becomes significant enough that it is difficult to maintain charge on the terminal when the KN tube is supporting 1.4 MV and transporting a beam. We added magnetic electron suppression in the bellows section between the KN tube and spiral tube #4 to try to eliminate this problem for an upcoming run requiring 5.5 MeV $^3He^+$ for ^{6}Li(^{3}He,n)^{8}B. This reduced the x-ray generation substantially but not enough to take the terminal to the 5.5 MV required and still maintain regulation. We also added a collection of 70 permanent magnets that we attached to the tube planes in a rotating-field configuration but were still unable to reduce x-ray emission to an acceptable level. We had to install the spiral inclined field tube to avoid this problem.

ION	ENERGY RANGE (kev)	EXPERIMENT	BEAM CURRENT (μamps)
$^1H^+$	160-1400	$^7Be(p,\gamma)$	10-40
$^2H^+$	770-1400	$^7Li(d,p)$	15-20
$^3He^+$	5000-6000	$^6Li(^3He,n)$	28
$^4He^+$	1370	$^7Be(\alpha,\gamma)$	15

Table 7.2-1. Table of Ion Species and TIS Experiments.

8 The Career Development Organization for Physicists and Astronomers

T. V. Bullard, K. Kazkaz, J. L. Orrell and L. C. Stonehill

The Career Development Organization for physicists and astronomers (CDO) is a Registered Student Organization at the University of Washington. CDO was founded in June 2000 by Hans Vija, a recent Ph.D. graduate of the UW Department of Physics. For its two years of operation, a number of physics graduate students who are research assistants at CENPA have participated in CDO (including this year's president Theresa Bullard and next year's president John L. Orrell). Because of this high level of CENPA student involvement in CDO, we felt it was appropriate to include a description of it in this Annual Report.

CDO's goal is to inform physics and astronomy students of the broad array of career options available and to help them plan and prepare their future career paths. To do this, CDO takes a two-fold approach that both informs the students of how to prepare for career transitions and increases the visibility of the students and the Department to post-degree employers. Some of the services CDO provides include: career seminars and workshops, a web site with helpful information for career preparation, a posting of relevant statistics and trends related to the employment of physics graduates, and opportunities for networking and meeting potential employers.

In the 2001-2002 academic year, CDO organized several events. These events included a career seminar featuring a panel of physics teachers from all levels of educational instruction, a workshop on what to expect and how to prepare for career fairs and interviews, a workshop on how to present your physics research to a broader audience of employers, and the First Annual UW Physics Networking Day. The Networking Day was the biggest event that CDO has organized thus far. This event, held on March 29th, 2002, brought representatives from industry and national laboratories to the Department of Physics to interact with the students and learn about the scientific research that is taking place at the University of Washington. The day was composed of an introduction to CDO and to the Department of Physics, followed by student oral and poster presentations. There was also a recruiting session where employers passed out information about their organizations, as is done at many job fairs. All the events of the Networking Day were designed to give the students exposure for their work and to encourage an atmosphere of intermingling, networking, and contact building. We feel that the Networking Day was a success and has left a lasting, positive impression on the attendees. It has led to a number of potential job offers for students and some possible collaborative research efforts between groups in the Department and industry. As a result of its success, the UW Physics Department has committed to the institutionalization of this event and will continue to fund it in the years to come.

CDO intends to further develop its breadth of career-related services and events. We are confident that we will continue to have a successful program of connecting physics and astronomy students with the resources they need to actively create the careers that they desire.

9 Center for Experimental Nuclear Physics and Astrophysics Personnel

9.1 Faculty

Eric G. Adelberger	Professor	
Hans Bichsel	Affiliate Professor	
John G. Cramer	Professor	
Peter J. Doe	Research Professor	
Steven R. Elliott	Research Assistant Professor	
George W. Farwell	Professor Emeritus	
Jens H. Gundlach	Research Associate Professor	
Isaac Halpern	Professor Emeritus	
Blayne R. Heckel	Professor	
Arnd R. Junghans	Research Assistant Professor	
Michael V. Romalis[1]	Assistant Professor	
R.G. Hamish Robertson	Professor;	Scientific Director
Kurt A. Snover	Research Professor	
Derek W. Storm	Research Professor;	Executive Director
Thomas A. Trainor	Research Professor	
Robert Vandenbosch	Professor Emeritus	
William G. Weitkamp	Professor Emeritus	
John F. Wilkerson	Professor	

9.2 Postdoctoral Research Associates

Manojeet Bhattacharya
Joseph Formaggio
Alice Araz Hamian[2]
Ryuta Hazama
Qingjun Liu

[1]Presently at Department of Physics, Princeton University, Princeton, NJ 08544.
[2]Presently at Avocent Corporation, 9911 Willows Road NE, Redmond, WA 98052.

9.3 Predoctoral Research Associates

Minesh Bacrania
Theresa Bullard
Thomas Butler
Ki-Young Choi
G. Adam Cox
Charles Duba
Matthew Feig
Karsten Heeger
Charles David Hoyle[1]
Anne Hurd[2]
William Clark Griffith
Dan Kapner
Kareem Kazkaz
Jeffrey Manor
Erik Mohrmann
Hans Pieter Mumm
Christian Neumann[3]
John Orrell
Jeffrey Reid
Kathryn Schaffer
Miles Smith
Laura Stonehill
Jackson Wu
Heather Zorn[2]

9.4 Research Experience for Undergraduates participants

Sara Beckman[4]
Carolyn Johnson[5]
Rafael Jaramillo[6]
Laura Melling[7]

[1]Presently at Dipartimento di Fisica, Universita di Trento, Via Sommarive, 14, 38050 Povo(TN), Italy.
[2]Physics Dept, University of Washington, Seattle, WA 98195.
[3]Physikalisches Institut, Justus-Liebig Universitaet Giessen, Heinrich-Buff-Ring 16, 35392, Giessen, Germany.
[4]Department of Physics, University of California, Berkeley, CA.
[5]Department of Physics, Amherst College, Amherst, MA, 01002.
[6]Department of Physics, Cornell University, Ithaca, NY.
[7]Department of Physics, University of Oregon, Eugene, OR.

9.5 Professional staff

The professional staff are listed with a description of their recent major efforts.

John F. Amsbaugh	Research Engineer	Mechanical design, Vacuum systems
Thomas H. Burritt	Research Engineer	Construction SNO NCD's
Gregory C. Harper	Research Engineer	Electronic and mechanical design Accelerator upgrades and operation
Mark A. Howe	Research Engineer	Software for DAQ, control systems
Christopher Morgan[1]	Research Engineer	
Duncan J. Prindle, Ph.D.	Research Scientist	Heavy Ion software
Richard J. Seymour	Computer Systems Manager	
H. Erik Swanson, Ph.D.	Research Physicist	Precision experimental equipment
Timothy D. Van Wechel	Electronics Engineer	Electronic design, construction, maintenance
Douglas I. Will	Research Engineer	Cryogenics, Ion sources

9.6 Technical staff

James Elms	Instrument Maker
David Hyde	Instrument Maker
Allan Myers	Electronics Technician
Hendrik Simons	Instrument Maker, Shop Supervisor

9.7 Administrative staff

Barbara J. Fulton	Administrator
Kate J. Higgins	Fiscal Specialist

[1]Computer Science and Engineering, University of Washington, Seatttle, WA 98195.

9.8 Part time staff

Tuesday Anderson[1]
Paul Duffell[1]
Adam Elias[1]
Mikel Grezner[1]
Robert Kyle
Tami McGonagle[1]
Lambert Paul Parazolli[1]
Ehren Reich
Tina Stremick[1]
Derek Viita
Mark Wehrenberg
Matthew White
Ryan Bressler
Clara Eberhardy[1]
Matthias Gohl
Laura Grout[1]
Mara Lemagie
Christy McKinley
Patrick Peplowski
Susanna Simons[1]
Kyle Sundqvist[1]
Lincoln Webbeking[1]
Jeff West[1]

[1]Left during 2001.

10 List of Publications from 2001-2002

Published papers:

"New tests of Einstein's Equivalence Principle and Newton's Inverse Square Law," E. G. Adelberger, Classical and Quantum Gravity **18**, 2397 (2001).

"Resolving the solar neutrino problem: evidence for massive neutrinos in the Sudbury Neutrino Observatory," K. M. Heeger and the SNO Collaborators, Europhysics News **32**, 5 (2001).

"Statistical fluctuations and pair mixing in two-point correlation analysis," J. G. Reid and T. A. Trainor, Nucl. Instrum. Methods A **457**, 378 (2001).

"Scintillation efficiency of nuclear recoils in a CaF_2(Eu) crystal for dark matter search," R. Hazama, S. Ajmura, H. Hayakawa, K. Matsuoka, H. Miyawaki, K. Morikubo, N. Suzuki and T. Kishimoto, Nucl. Instrum. Methods A **482**, 297 (2002).

"The fabrication of metallic ^{7}Be targets with a small diameter for ^{7}Be$(p,\gamma)^8$B measurements," A. Zyuzin, S.H. Park, L. Buchmann, K.R. Buckley, A.R. Junghans, E.C. Mohrmann, K.A. Snover, T.D. Steiger and J. Vincent, Nucl. Instru. Methods B **187**, 264 (2002).

"New results on structure effects in nuclear fission," K.-H. Schmidt, J. Benlliure, C. Böckstiegel, H. G. Clerc, A. Grewe, A. Heinz, A. V. Ignatyuk, A. R. Junghans, M. de-Jong, J. Müller, M. Pfützner, F. Rejmund, S. Steinhäuser and B. Voss, Nucl. Phys A **685**, 60 (2001).

"Fission of nuclei far from stability," K.-H. Schmidt, J. Benlliure and A. R. Junghans, Nucl. Phys. A **693**, 169 (2001).

"Star event-by-event fluctuations," J. G. Reid and the STAR Collaborators (including H. Bichsel, J. G. Cramer, Q. J. Liu, D. J. Prindle, J. G. Reid, T. A. Trainor and J. M. S. Wu), Nucl. Phys. A **698**; 611c (2002), *Proceedings of Quark Matter 01*, Brookhaven, NY, January (2001).

"Spectroscopy of ^{23}Al and ^{27}P using (^{7}Li,^{8}He) reaction and the implications for ^{22}Na and ^{26}Al nucleosynthesis in explosive hydrogen burning," J. A. Caggiano, D. Bazin, W. Benenson, B. Davids, R. Ibbotson, H. Scheit, B. M. Sherril, M. Steiner, J. Yurkon, A. F. Zeller, B. Blank. M. Chartier, J. Greene, J. A. Nolen Jr., A. H. Wousmaa, M. Bhattacharya, A. Garcia and M. Wiescher, Phys. Rev. C **64**, 025802-1 (2001).

"Mid-rapidity phi production in Au + Au collisions at $\sqrt{s_{NN}} = 130$ GeV," C. Adler and the STAR Collaborators (including H. Bichsel, J. G. Cramer, Q. J. Liu, D. J. Prindle, J. G. Reid, T. A. Trainor and J. M. S. Wu), Phys. Rev. C **65**, 041901(R) (2002).

"Midrapidity antiproton-to-proton ratio from Au+Au $\sqrt{s_{NN}} = 130$ GeV," C. Adler and the STAR Collaborators (including H. Bichsel, J. G. Cramer, Q. J. Liu, D. J. Prindle, J. G. Reid, T. A. Trainor and J. M. S. Wu), Phys. Rev. Lett. **86**, 4778 (2001).

"Measurement of the rate of $\nu_e + d \rightarrow p + p + e^-$ interactions produced by ^{8}B solar neu-

trinos at the Sudbury Neutrino Observatory," Q. R. Ahmad and the SNO Collaborators, Phys. Rev. Lett. **87**, 7, 071301 (2001).

"Pion interferometry of $\sqrt{s_{NN}}$ = 130 GeV Au+Au collisions at RHIC," C. Adler and the STAR Collaborators (including H. Bichsel, J. G. Cramer, Q. J. Liu, D. J. Prindle, J. G. Reid, T. A. Trainor and J. M. S. Wu), Phys. Rev. Lett. **87**, 082301 (2001).

"Multiplicity distribution and spectra of negatively charged hadrons in Au + Au collisions at $\sqrt{s_{NN}}$ = 130 GeV," C. Adler and the STAR Collaborators (including H. Bichsel, J. G. Cramer, Q. J. Liu, D. J. Prindle, J. G. Reid, T. A. Trainor and J. M. S. Wu), Phys. Rev. Lett. **87**, 112303 (2001).

"Identified particle elliptic flow in Au+Au collisions at $\sqrt{s_{NN}}$ = 130 GeV," C. Adler and the STAR Collaborators (including H. Bichsel, J. G. Cramer, Q. J. Liu, D. J. Prindle, J. G. Reid, T. A. Trainor and J. M. S. Wu), Phys. Rev. Lett. **87**, 182301 (2001).

"Antideuteron and antihelium production in Au+Au collisions at $\sqrt{s_{NN}}$ = 130 GeV," C. Adler and the STAR Collaborators (including H. Bichsel, J. G. Cramer, Q. J. Liu, D. J. Prindle, J. G. Reid, T. A. Trainor and J. M. S. Wu), Phys. Rev. Lett. **87**, 262301-1 (2001).

"Measurement of inclusive antiprotons from Au+Au collisions at $\sqrt{s_{NN}}$ = 130 GeV," C. Adler and the STAR Collaborators (including H. Bichsel, J. G. Cramer, Q. J. Liu, D. J. Prindle, J. G. Reid, T. A. Trainor and J. M. S. Wu), Phys. Rev. Lett. **87**, 262302-1 (2001).

"^{7}Be(p,γ)^{8}B astrophysical S factor from precision cross section measurements," A. R. Junghans, E. C. Mohrmann, K. A. Snover, T. D. Steiger, E. G. Adelberger, J. M. Casandjian, H. E. Swanson, L. Buchmann, S. H. Park and A. Zyuzin, Phys. Rev. Lett. **88**, 041101-1 (2002).

"Collisionally induced multifragmentation of C_{60}," R. Vandenbosch, Phys. Rev. A **64**, 033201-1 (2001).

"Direct measurements of neutrino mass," J. F. Wilkerson and R. G. H. Robertson, in *Current Aspects of Neutrino Physics*, ed. by D. O. Caldwell, Springer-Verlag, Heidelberg, Germany (2001).

"First results from STAR EbyE analysis at RHIC," T. A. Trainor, *Proceedings of the 17th Winter Workshop on Nuclear Dynamics*, Park City, UT, March 2001, eds. W. Bauer and G. Westfall, Kluwer Academic (New York).

"The Calculus of Passion," T. A. Trainor, book review of 'The Bride of Science' by B. Wooley, published in American Scientist, July 2001.

Papers submitted, to be published or letter of intent:

"Double beta decay," S. R. Elliott and P. Vogel, submitted to Ann. Rev. Nucl Part. Sci.

"Comment on evidence for neutrinoless double beta decay," C. E. Aalseth and SNO (including P. J. Doe, S. R. Elliott, R. G. H. Robertson and J. F. Wilkerson), Mod. Phys. Lett. A 0202018 (2002).

"Lead percholate as a neutrino detection medium," M. K. Bacrania, P. J. Doe, S. R. Elliott, C. E. Paul, L. C. Stonehill and D. I. Will, submitted to Nucl. Instrum. Methods.

"Reanalyses of α+α scattering and β-delayed α spectra from ^{8}Li and ^{8}B decays," M. Bhattacharya and E. G. Adelberger, accepted for publication, Phys. Rev. C.

"Direct evidence for neutrino flavor transformation from neutral-current interactions in the Sudbury Neutrino Observatory," Q .R. Ahmad and the SNO Collaborators, Phys. Rev. Lett. in press.

"Measurement of day and night neutrino energy spectra at SNO and constraints on neutrino mixing parameters," Q. R. Ahmad and the SNO Collaborators, Phys. Rev. Lett. in press.

"Mid-rapidity lambda and lambda bar production in Au + Au collisions at $\sqrt{s_{NN}} = 130$ GeV," C. Adler and the STAR Collaborators (including H. Bichsel, J. G. Cramer, Q. J. Liu, D. J. Prindle, J. G. Reid, T. A. Trainor and J. M. S. Wu), submitted to Phys. Rev. Lett.

"Azimuthal anisotrophy of K0s and lamda + lambdabar production at mid-rapidity from Au+Au collisions at $\sqrt{s_{NN}} = 130$ GeV," C. Adler and the STAR Collaborators (including H. Bichsel, J. G. Cramer, Q. J. Liu, D. J. Prindle, J. G. Reid, T. A. Trainor and J. M. S. Wu), submitted to Phys. Rev. Lett.

"Lead perchlorate as a neutrino detection medium," S. R. Elliott, P. J. Doe, R. G. H. Robertson and C. Paul, *Proceeding of the Carolina Symposium on Neutrino Physics*, Columbia, SC, March 2000, (World Scientific), to be published, presented by P. J. Doe.

"Double beta decay," P. Vogel and S. Elliott, section of white paper, to appear in *Science, Education, and Outreach Opportunities at the National Underground Science Laboratory*, Lead, SD, October 2001, to be published.

"Sub-millimeter tests of the gravitational inverse square law," E. G. Adelberger, to appear in the *Proceedings of the CPT01 Conference*, World Scientific (2002), hep-ex/0202008+.

"KATRIN: A next generation tritium beta decay experiment with sub-eV sensitivity for the electron neutrino mass," A. Osipowicz and the KATRIN Collaborators (including P. J. Doe, S. R. Elliott, R. G. H. Robertson and J. F. Wilkerson), arXiv:hep-ex/0109033 v1, Sept. 2001.

"New tests of the strong equivalence principle and of the inverse square law," E. G. Adelberger, *Proceedings of XXV Johns Hopkins Workshop 'A Relativistic Spacetime Odyssey,'* to be published.

Invited talks, abstracts and other conference presentations:

"Neutrino detection using lead perchlorate," S. R. Elliott, Presented to *Physics Potential of Supernova II Neutrino Detection*, Marina del Rey, CA, February 2001.

"The future of neutrino physics and the detection of dark matter," R. G. H. Robertson, Invited presentation at the *Nuclear Science Advisory Committee Long Range Planning Resolution Meeting*, Santa Fe, NM, March 2001.

"Science underground," J. F. Wilkerson, Invited Talk at the *Nuclear Science Advisory Committee Long Range Planning Resolution Meeting*, Santa Fe, NM, March 2001.

'Recent results from STAR EbyE analysis at RHIC," T. A. Trainor, Contributed workshop talk, *17th Winter Workshop on Nuclear Dynamics*, Park City, UT, March 2001.

"Double beta decay: experimental potential at the National Underground Scientific Laboratory," S. R. Elliott, Presented to the *Committee on the Physics of the Universe*, Washington, DC, May 2001.

"Lead percholate as a neutrino detection medium," M. Bacrania, *Northwest Chapter of the APS*, Seattle, WA, May, 2001.

"Muon induced spallation neutrons in the Sudbury Neutrino Observatory" J. L. Orrell and the SNO Collaborators, *Northwest Chapter of the APS*, Seattle, WA, May, 2001.

"The Sudbury Neutrino Observatory and the solar neutrino problem," R. G. H. Robertson, Invited presentation *Northwest Chapter of the APS*, Seattle, WA, May, 2001.

"The WALTA Project: Engaging students and teachers in forefront high energy research," H. M. Zorn, *Northwest Chapter of the APS*, Seattle, WA, May, 2001.

"First results from the Sudbury Neutrino Observatory (SNO)," K. M. Heeger, *Plenary Talk at the Euroconference on Neutrino Masses and Mixing*, Les Houches, France, June 2001.

"Neutrino physics," J. F. Wilkerson, Invited three lecture series given at the *Nuclear Physics Summer School*, Bay Harbor, ME, June 2001.

"First results from SNO," J. F. Wilkerson, P. J. Doe and R. G. H. Robertson, Special UW Physics Seminar, Seattle, WA, June 2001.

"EbyE theory and experiment at RHIC and SPS," T. A. Trainor, Invited lecture in two-day session on event-by-event physics, *CERN Heavy Ion Forum*, Cern, Switzerland, June 2001,

"Event-by-event analysis of ultrarelativistic heavy ion collisions," T. A. Trainor, Colloquium, University of Stellenbosch, South Africa, July 2001.

"Sub-millimeter tests of gravitational $1/\mathrm{r}^2$ law," C. D. Hoyle, Invited talk at Snowmass, *Future of Particle Physics Conference*, Snowmass, CO, July 2001.

"Double beta decay: new experimental approaches - present status," S. R. Elliott, Presentation at Snowmass, *Future of Particle Physics Conference*, Snowmass, CO, July 2001.

"Solar and atmospheric neutrinos," R. G. H. Robertson, Invited Plenary Talk, P4 Working Group, *Future of Particle Physics Conference*, Snowmass, CO, July 2001.

"Low energy solar neutrinos" R. G. H. Robertson, Invited Presentation, NAS-NRC Committee on the Physics of the Universe, *Future of Particle Physics Conference*, Snowmass, CO, July 2001.

"Science underground," J. F. Wilkerson, Invited talk at Snowmass, *Future of Particle Physics Conference*, Snowmass, CO, July 2001.

"Moon (Mo Observatory Of Neutrinos) for neutrino studies in ^{100}Mo by double beta decays and solar-neutrino capture reactions," R. Hazama, H. Ejiri, J. Engel, P Krastev, N. Kudomi, M. Nomachi and R. G. H. Robertson, *Proceedings of the International Nuclear Physics Conference*, (INPC2001), Berkeley, CA, July 2001, AIP Conference Proceedings, **610**, 959 (2002), eds. E. Norman *et al.*, New York, NY.

"A new determination of the astrophysical S factor for the ^{7}Be(p,γ)^{8}B reaction from direct cross section measurements," A. R. Junghans, E. C. Mohrmann, K. A. Snover, T. D. Steiger, E. G. Adelberger, J. M. Casandjian, H. E. Swanson, L. Buchmann, S. H. Park and A. Zyuzin, Contributed talk, *Proceedings of the International Nuclear Physics Conference*, Berkeley, CA, July 2001, AIP Conference Proceedings, **610**, 461 (2002); GSI Darmstadt, Germany, August, 2001.

"First event-by-event results from RHIC: summary and interpretation, T. A. Trainor, Invited talk, *meeting of the American Chemical Society*, Chicago, IL, August 2001.

"National Underground Science Laboratory," J. F. Wilkerson, Invited talk, *SNO Collaboration Meeting*, Sudbury, Ontario, Canada, August 2001.

"Neutrinos - A snapshot and some sketches," R. G. H. Robertson, Seminar, University of Illinois at Urbana-Champaign, Illinois, September 2001.

"SNO flies: The solar neutrino problem resolved," R. G. H. Robertson, Peter Axel Memorial Lecture, University of Illinois at Urbana-Champaign, September, 2001; Colloquium Fermilab, September 2001; Argonne National Laboratory, September 2001; University of Kentucky, October 2001; University of Chicago, November 2001; University of Dortmund, December 2001; University of Illinois at Chicago, April 2002.

"Neutral-current detection in the Sudbury Neutrino Observatory using ultra-low-background ^{3}He proportional counters," K. M. Heeger, *EuroConference on Neutrinos in the Universe: Frontiers in Astroparticle Physics and Cosmology*, Lenggries, Germany, September 2001.

"Sub-millimeter tests of gravitational $1/r^2$ law," C. D. Hoyle, Invited talk at University of Trento, Trento, Italy, October, 2001.

"Underground laboratories," P. D. Doe, *Conference for Underground Science*, Lead, SD, October 2001.

"Double beta decay," C. Aalseth and S. Elliott, section of white paper *Science, Education, and Outreach Opportunities at the National Underground Science Laboratory*, Lead, SD, October 2001.

"Moon: Hybrid solar-neutrino and double beta decay experiments," R. Hazama, *Conference on Underground Science*, Lead, SD, October 2001.

"The envisioned National Underground Science Laboratory at Homestake," J. F. Wilkerson, Invited talk, *Conference on Underground Science*, Lead, SD, October 2001. "The Sudbury Neutrino Observatory," R. G. H. Robertson, University of Washington Science Forum, October 2001.

"Backscattering of ^{8}B and other systematic effects in the determination of the ^{7}Be(p,γ)^{8}B cross section," E. C. Mohrmann and the ^{7}Be(p,γ)^{8}B Collaborators (including A. R. Junghans, K. A. Snover, E. G. Adelberger and H. E. Swanson), *First Joint Meeting of the Nuclear Physicists of the American and Japanese Physical Societies*, Maui, Hawaii, October, 2001, Bull. Am. Phys. Soc. **46**, no. 7, 63 (2001).

"Astrophysical S-factor for the ^{7}Be(p,γ)^{8}B from precision cross section measurements," Contributed talk, A. R. Junghans and the ^{7}Be(p,γ)^{8}B Collaborators (including E. C. Mohrmann, K. A. Snover, E. G. Adelberger and H. E. Swanson), *First Joint Meeting of the Nuclear Physicists of the American and Japanese Physical Societies*, Maui, Hawaii, October, 2001, Bull. Am. Phys. Soc. **46**, no. 7, 64 (2001).

"MOON (MO Observatory Of Neutrinos) detector for ν studies in ^{100}Mo," R. Hazama and the MOON Collaborators (including S. R. Elliott and R. G. H. Robertson), *First Joint Meeting of the Nuclear Physicists of the American and Japanese Physical Societies*, American Physical Society, Maui, Hawaii, October, 2001, Bull. Am. Phys. Soc. **46**, no. 7, 77 (2001).

"Preparations for a second run of the emiT detector," H. P. Mumm and the emiT Collaborators (including R. G. H. Robertson and J. F. Wilkerson), *First Joint Meeting of the Nuclear Physicists of the American and Japanese Physical Societies*, Maui, Hawaii, October, 2001, Bull. Am. Phys. Soc. **46**, no. 7, 93 (2001).

"Improvements to the emiT Experiment," K. Sundqvist and the emiT Collaborators (including J. F. Wilkerson, H. P. Mumm and R.G.H. Robertson), *First Joint Meeting of the Nuclear Physicists of the American and Japanese Physical Societies*, Maui, Hawaii, October, 2001, Bull. Am. Phys. Soc. **46**, no. 7, 107 (2001).

"Determination of the charged-current rate and energy scale in SNO by means of a calibration source-independent analysis of the energy spectrum," K. M. Heeger and the SNO Collaborators (including R. G. H. Robertson), *First Joint Meeting of the Nuclear Physicists of the American and Japanese Physical Societies*, Maui, Hawaii, October, 2001, Bull. Am. Phys. Soc. **46**, no. 7, 114 (2001).

"When does the Sun shine brightest in Sudbury? The day-night effect at SNO," M. Smith and the SNO Collaborators, *First Joint Meeting of the Nuclear Physicists of the American and Japanese Physical Societies*, Maui, Hawaii, October, 2001, Bull. Am. Phys. Soc. **46**, no. 7, 114 (2001).

"Muon induced spallation neutrons in the SNO," R. Hazama and the SNO Collaborators, *1st Joint Meeting of the Nuclear Physicists of the American and Japanese Physical Societies*, American Physical Society, Maui, Hawaii, October, 2001, Bull. Am. Phys. Soc. **46**, no. 7, 115 (2001).

"National Underground Science Laboratory - status and update," J. F. Wilkerson, Invited talk, *SNO Collaboration meeting*, Sudbury, Ontario, Canada, November 2001.

"SNO flies: The solar neutrino problem resolved," R. G. H. Robertson, Invited Presentation, NAS-NRC Board on Physics and Astronomy, Irving, CA, November 2001.

"Low-energy solar neutrinos," R. G. H. Robertson, Invited talk, *Workshop on the Future of Neutrino Physics*, Victoria, BC, November 2001.

"The solar neutrino mystery - solved!" J. F. Wilkerson, Physics Colloquium, University of Arizona, Tucson, AZ, September 2001; Brown University, Providence, RI, November 2001.

"The solar neutrino mystery - solved!" J. F. Wilkerson, *Joint Karlsruhe-Tuebingen-Heidelberg Seminar in Nuclear and Particle Physics*, Karlsruhe, Germany, December 2001.

"Fluctuations, correlations and scale," T. A. Trainor, Invited talk, *RHIC-INT workshop on correlations and EbyE physics*, University of Washington, Seattle, WA, January 2002.

"Purpose and physics of event-by-event analysis," T. A. Trainor, Invited lecture, *Pan American Advanced Studies Institute (summer school)*, *Proceedings of the Pan American Advanced Studies Institute*, Sao Paulo, Brazil, January 2002, Eds. Johann Rafelski and Robert L. Thews, to be published by American Institute of Physics.

"Going deep - discovery opportunities at a National Underground Science Laboratory," J. F. Wilkerson, Physics Colloquium, University of Washington, Seattle, WA, January 2002.

"The Sudbury Neutrino Observatory," R. G. H. Robertson, Invited Plenary Talk, *International Conference On Weak Interactions and Neutrinos*, Christchurch, New Zealand, January 2002.

"Beta-decay endpoint experiments: past, present, and future," J. F. Wilkerson, Invited talk, *Weak Interactions and Neutrinos Workshop*, Christchurch, New Zealand, January 2002.

"National Underground Science Laboratory at Homestake," J. F. Wilkerson, Invited talk, *Dark Matter 2002*, Marina del Rey, CA, February 2002.

Conference presentations by collaborators of NPL personnel:

"Results from the STAR experiment," J. W. Harris and the STAR Collaborators (including H. Bichsel, J. G. Cramer, Q. J. Liu, D. J. Prindle, J. G. Reid, T. A. Trainor and J. M. S. Wu), Nucl. Phys. A **698**, 64c (2002); *Proceedings of Quark Matter 01*, Brookhaven, NY, January (2001).

"Strangeness production at RHIC," H. Caines and the STAR Collaborators (including H. Bichsel, J. G. Cramer, Q. J. Liu, D. J. Prindle, J. G. Reid, T. A. Trainor and J. M. S. Wu), Nucl. Phys. A **698**, 112c (2002); *Proceedings of Quark Matter 01*, Brookhaven, NY, January (2001).

"Negatively charged hadron spectra in Au+ Au collisions," M. Calderon de la Barca Sanchez and the STAR Collaborators (including H. Bichsel, J. G. Cramer, Q. J. Liu, D. J. Prindle, J. G. Reid, T. A. Trainor and J. M. S. Wu), Nucl. Phys. A **698**, 503c (2002); *Proceedings of Quark Matter 01*, Brookhaven, NY, January (2001).

"High p hadron spectra in Au + Au collisions," J. C. Dunlop and the STAR Collaborators (including H. Bichsel, J. G. Cramer, Q. J. Liu, D. J. Prindle, J. G. Reid, T. A. Trainor and J. M. S. Wu), Nucl. Phys. A **698**, 515c (2002); *Proceedings of Quark Matter 01*, Brookhaven, NY, January (2001).

"Antinucleus production at RHIC," Hardtke and the STAR Collaborators (including H. Bichsel, J. G. Cramer, Q. J. Liu, D. J. Prindle, J. G. Reid, T. A. Trainor and J. M. S. Wu), Nucl. Phys. A **698**, 671c (2002); *Proceedings of Quark Matter 01*, Brookhaven, NY, January (2001).

"Anti-baryon to baryon ratios in Au + Au collisions," H. Z. Huang and the STAR Collaborators (including H. Bichsel, J. G. Cramer, Q. J. Liu, D. J. Prindle, J. G. Reid, T. A. Trainor and J. M. S. Wu), Nucl. Phys. A **698**, 663c (2002); *Proceedings of Quark Matter 01*, Brookhaven, NY, January (2001).

"The STAR-RHIC detector," B. Lasiuk and the STAR Collaborators (including H. Bichsel, J. G. Cramer, Q. J. Liu, D. J. Prindle, J. G. Reid, T. A. Trainor and J. M. S. Wu), Nucl. Phys. A **698**, 452c (2002); *Proceedings of Quark Matter 01*, Brookhaven, NY, January (2001).

"Elliptic flow in Au + Au collisions," R. J. M. Snellings and the STAR Collaborators (including H. Bichsel, J. G. Cramer, Q. J. Liu, D. J. Prindle, J. G. Reid, T. A. Trainor and J. M. S. Wu), Nucl. Phys. A **698**, 193c (2002); *Proceedings of Quark Matter 01*, Brookhaven, NY, January (2001).

"Resonance studies at STAR," Z. Xu and the STAR Collaborators (including H. Bichsel, J. G. Cramer, Q. J. Liu, D. J. Prindle, J. G. Reid, T. A. Trainor and J. M. S. Wu), Nucl. Phys. A **698**, 607c (2002); *Proceedings of Quark Matter 01*, Brookhaven, NY, January (2001).

"K*(892)^0 production in relativistic heavy ion collisions at $\sqrt{s_{NN}} = 130$ GeV," P. Fachini and the STAR Collaborators (including H. Bichsel, J. G. Cramer, Q. J. Liu, D. J. Prindle, J. G. Reid, T. A. Trainor and J. M. S. Wu), *Proceedings of Strange Quarks in Matter (SQM2001)*, Frankfurt am Main, Germany, to be published in J. Phys. G.

"Ultraperipheral collisions in STAR," P. Yepes and the STAR Collaborators (including H. Bichsel, J. G. Cramer, Q. J. Liu, D. J. Prindle, J. G. Reid, T. A. Trainor and J. M. S. Wu), Presented at *the Workshop on Electromagnetic Probes of Fundamental Physics*, Erice, Sicily, Italy, October 2001.

"STAR strangeness results from $\sqrt{s_{NN}} = 130$ GeV Au+Au collisions (and first results from 200 GeV)," G. van Buren and the STAR Collaborators (including H. Bichsel, J. G. Cramer, Q. J. Liu, D. J. Prindle, J. G. Reid, T. A. Trainor and J. M. S. Wu), *Proceedings of Strange Quarks in Matter (SQM2001)*, Frankfurt am Main, Germany, to be published in J. Phys. G.

"Strangeness production in STAR at RHIC," C. Roy, and the STAR Collaborators (including H. Bichsel, J. G. Cramer, Q. J. Liu, D. J. Prindle, J. G. Reid, T. A. Trainor and J. M. S. Wu), *Proceedings of the International Workshop on the Physics of the Quark-Gluon Plasma*, Palaiseau, France, September 2001.

"Multiplicity and mean transverse momentum fluctuations in Au + Au collisions at RHIC," S. A. Voloshin and the STAR Collaborators (including H. Bichsel, J. G. Cramer, Q. J. Liu, D. J. Prindle, J. G. Reid, T. A. Trainor and J. M. S. Wu), Talk at *the International Nuclear Physics Conference INPC2001*, Berkeley, CA, July/August 2001.

"Ultra-peripheral collisions of relativistic heavy ions," S. Klein and the STAR Collaborators (including H. Bichsel, J. G. Cramer, Q. J. Liu, D. J. Prindle, J. G. Reid, T. A. Trainor and J. M. S. Wu), Presented at *the International Nuclear Physics Conference INPC2001*, Berkeley, CA, July/August 2001.

"Observation of Au + Au $\rightarrow$ Au + Au + ρ^0 and Au + Au $\rightarrow$ Au* + Au* + ρ^0 with STAR," S. Klein and the STAR Collaborators (including H. Bichsel, J. G. Cramer, Q. J. Liu, D. J. Prindle, J. G. Reid, T. A. Trainor and J. M. S. Wu), *Presented at the 17th Winter Workshop on Nuclear Dynamics*, Park City, UT, March 2001.

"Majorana ^{76}Ge double beta decay project," C. E. Aalseth and the Majorana Collaborators, *Proceedings of the 3rd International Conference on Non-Accelerator New Physics*, Dubna Russia, June 2001, to be published.

"Nuclear responses of ^{100}Mo for low energy ν's, and the MOON project," H. Ejiri and the MOON Collaborators, *First Joint Meeting of the Nuclear Physicists of the American and Japanese Physical Societies*, Maui, Hawaii, October, 2001, Bull. Am. Phys. Soc. **46**, no. 7, 77 (2001).

"Search for time reversal violation in neutron beta decay," J. Nico and the emiT Collaborators, *First Joint Meeting of the Nuclear Physicists of the American and Japanese Physical Societies*, Maui, Hawaii, October, 2001, Bull. Am. Phys. Soc. **46**, no. 7, 148 (2001).

11 Degrees Granted, Academic Year, 2001-2002

Sub-millimeter Tests of the Gravitational Inverse-Square Law, Charles David (C.D.) Hoyle, University of Washington (2001).

Muon Correlated Background at the Sudbury Neutrino Observatory, Q. Rushdy Ahmad, Brown University and University of Washington (2002).